1-5-2017

Sequence Specific DNA Damage on P53 Gene Fragments for Determination of Tissue Specific Cancers Using LC-MS/MS & Biosensors for Multiple Prostate Cancer Biomarker Detection

Spundana Malla
University of Connecticut, spundana.malla@uconn.edu

Sequence Specific DNA Damage on P53 Gene Fragments for Determination of Tissue Specific Cancers Using LC-MS/MS

&

Biosensors for Multiple Prostate Cancer Biomarker Detection

Spundana Malla

University of Connecticut, 2017

Cancer is the second leading cause of deaths in the United States. This thesis focuses on two research project (1) development of novel LC-MS/MS methodology to screen chemicals and their metabolites for DNA damaging effects which might eventually lead to cancer and (2) development of automated and 3D printed elecrochemical biosensors to detect panels of prostate cancer biomarkers for early diagnosis and to differentiate aggressive and non-aggressive versions of prostate cancer.

Chapter 1 gives a brief introduction and describes goals and significance of the thesis. It also gives an overview of genotoxicity, DNA damaging events, xenobiotics, and cytochrome P450 enzymes and their role in reactive metabolite formation. A brief description of P53 tumor suppressor gene and its role in cancer and organ specific cancer is also included.

Chapter 2 describes the first ever restriction enzyme-assisted LC-MS/MS methodology for sequence specific DNA damage by chemical metabolites on exon 7 fragment of P53 gene. It describes the importance of structural integrity of large ds-DNA vs small ss-DNA for codon specific DNA damage in co-relation tissue specific cancer.

Chapter 3 shows the effect of cytosine methylation on sequence specificity and rate of metabolite adduction on exon 7 fragment of P53 gene. Kinetics of BPDE adduction was validated using both LC-MS/MS methodology and molecular modelling.

Chapter 4 describes the development of magnetic biocolloid technology in a 96 well platform to feed DNA damage products to LC-MS/MS to screen multiple cyt P450 enzymes on bioactivation of drugs or chemicals and resulting DNA damaging events on P53 gene and correlation of results to tissue specific cancer.

Chapter 5 involves brief overview of prostate cancer and the need for automated low cost biosensor in cancer diagnostics. It also describes the developed automated reagent/sample cassette and 3D printed user friendly microfluidic devices for protein-based point of care diagnostics.

Sequence Specific DNA Damage on P53 Gene Fragments for Determination of Tissue Specific Cancers Using LC-MS/MS

&

Biosensors for Multiple Prostate Cancer Biomarkers Detection

Spundana Malla

B. Pharmacy Andhra University, 2009

M.S. Chemistry Lamar University, 2011

A Dissertation
Submitted in Partial Fulfillment of the
Requirements for the Degree of
Doctor of Philosophy
At the

University of Connecticut

2017

2017

Approval Page

Doctor of Philosophy Dissertation

Sequence Specific DNA Damage on P53 Gene Fragments for Determination of Tissue Specific Cancers Using LC-MS/MS

&

Biosensors for Multiple Prostate Cancer Biomarker Detection

Presented by

Spundana Malla

Major advisor _____

James F. Rusling

Associate advisor _____

Ashis K. Basu

Associate advisor _____

John B. Schenkman

University of Connecticut

2017

Dedicated to

My Parents & Sister

Padma Malla, Ramakrishna Rao Malla
& Manasa Malla

Acknowledgement

As the famous saying goes,*" Life isn't about finding yourself. Life is about Creating yourself."*- George Bernard Shaw, my PhD career in chemistry contributed a lot in making, me the person I am today both professionally and personally. It made humble, understanding and extremely adaptable to different situations both good and bad ones. My PhD advisor Dr. James F. Rusling (Jim) played a vital role during this process over the past $5^{1/2}$ years. Jim is a perfect blend of both science and fun. In Jim's lab we were given an opportunity to think independently and extreme freedom for growth of intellect was provided. This helped me to grow and learn to become an independent, strong and self-sustained person that I am today. I would like to take this opportunity to express my utmost gratitude and appreciation to Jim for guiding me towards the right path and advising me on what not do when I am lost. It was a pleasure and honor to work under Jim's guidance which I will cherish for the years to come.

I am blessed to have the opportunity with Dr. John B. Schenkman is an epitome of knowledge and a completely down to earth person. I have never met a person so kind and virtuous like Dr. Schenkman. It would especially like to thank Dr. Schenkman for his timely advice, extreme support and encouraging words. I am fortunate to have great person like Dr. Dharamainder Choudhary in my committee who contributed immensely to my PhD career with his timely advice and guidance with the biological part of my thesis. He is the most approachable person and extremely friendly. I would like to leave a special note of gratitude to Dr. Choudhary for all his help throughout the years. Dr. Ingela Jansson helped me during the very beginning of my PhD career. She was very kind and erudite person. I would like to take this opportunity to thank her for her contribution towards my PhD career.

Dr. Ashis K. Basu is a perfect associate advisor one can ask for. He always had his doors open for me either it might be just for a simple signature or a long discussion about science, he was always willing to help. I would like to thank him for all the help and support he provided me with my thesis and his suggestions when I was stuck with a challenging situations. I would like to thank Dr. Jing Zhao and Dr. Alfredo Angeles Boza for their guidance with course work and guidance throughout the years. I would like to thank Dr. Xudong Yao and Dr. You-Jun Fu for their help with LC-MS troubleshooting and guidance. I would also like to thank Dr. Fatma Selampinar, who was the lecturer for the general chemistry course that I had to teach in the first two year of my graduate career, for her valuable suggestions. Dr. Selampinar guided me to be better at teaching.

I also want to thank my mentor's Dhanuka, Dana and Vigneshwaran and all Dr. Rusling group members: Brunah, Colleen, Yun, Abby Jones, Mohammed, Boya, Bhaskara, Greg, Gayatri and Jennifer for their everlasting discussion on both life and science and being extremely supportive and valuable suggestions. I had a wonderful time collaborating with Karteek, Di Jiang, Islam Mosa and Minh. I would also like to thank my friends Lavanya, Vasu, Santosh, Divya, Sravan, Spandana, Sourav, Kankana, Amit, Chandra, Kiran, Snehasis, Itti, Priyanka, Soumya and Sandeep.

Finally I would like to thank my family, mom, dad, sister, brother-in-law, husband, mother-in-law and father-in-law for their immense support and incessant love to pursue my passion.

Table of Contents

LIST OF SCHEMES

LIST OF FIGURES

LIST OF TABLES

Chapter 1

Introduction

1-1. Goal & Significance - Part I

Cancer is characterized by abnormal and uncontrolled growth of cells. Cancer is the second leading cause of death in United States of America.[1] The number of projected new cancer cases in 2016 are 1,685,210 and 59560 cancer deaths.[2] Cancer can be caused by external factors like tobacco, infections, radiation, alcohol consumption, exposure to environmental pollutants etc., It can also be due to internal factors like hormones, inherited gene mutations and immune conditions.

Toxicity screening plays a major role in drug development. Damage to genetic material by chemical agents is referred as genotoxicity. Toxicity screening assays are used to assess the safety of chemicals/environmental pollutants. Most common tests used commercially include Ames test, comet assay and chromosomal aberration/micronucleus assay. These assays are not high throughput and do not take into consideration of metabolic pathways that might lead to mutagenicity.[3,4,5] More over these assays do not give mechanism of DNA damage and no molecular level information. Current research focuses on development of high throughput toxicity screening assay using liquid chromatography-tandem mass spectrometry to determine the possible mutagenicity of chemicals/metabolites. Current method helps in understanding the mechanism of covalent interaction between chemical/environmental pollutants and their

metabolites to that of DNA. This LC-MS/MS method will also help us to predict the tissue specific cancer caused by chemicals/environmental pollutants.

1.2 Cancer etiology

Cancer can be caused due to both endogenous and exogenous factors.[6,7] Endogenous factors responsible for cancer include hormonal, estrogen and progesterone in case of breast cancer, testosterone in case of prostate cancer[8], bacterial infections, genetic inheritance etc., Exogenous factors include exposure to environmental pollutants like tobacco smoke, asbestos, dietary components, alcohol, radiation, immunosuppression, obesity etc.,[9] Cancer is not one disease and there are nearly 100 different types of cancer.[10] Symptoms and treatment of cancer depends on type of cancer and the stage of cancer. Some of the treatments include surgery, radiation chemotherapy, hormone therapy, biological therapy and stem cell treatment.[11]

1.3 Genotoxicity & Types of DNA damage

Genotoxicity is the property of chemicals to disrupt or damage genetic material which when not repaired might lead to cancer. Some of the common events involved in genotoxicity include DNA hydrolysis, covalent adduct formation, oxidative DNA damage, abasic site formation, DNA strand breaks etc.[12]

Thermodynamically DNA hydrolysis is favorable but is extremely slow indicated by the very high in half life, Scheme 1.1. This states that DNA is extremely stable in biological conditions.[13] Spontaneous hydrolysis of DNA accelerated by the presence of enzymes like phosphodiesterases, lanthanide ions and metal ions. Deamination of cytosine residues in another

mechanism of DNA damage which is enhanced 3-5 times faster upon alkylation on the 5th position of the cytosine.[14,15]

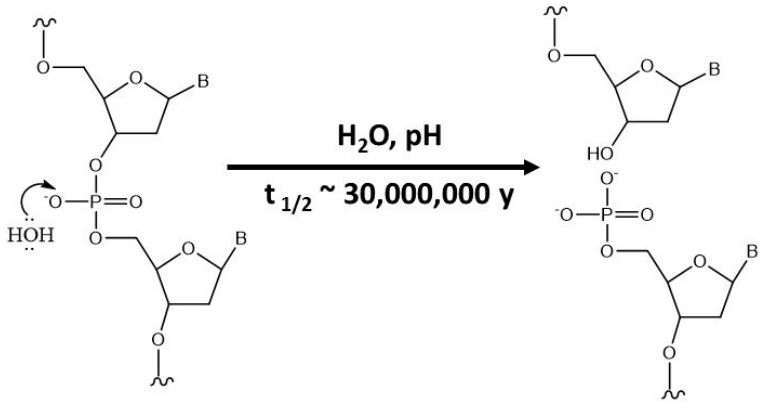

Scheme 1.1. Mechanism of DNA hydrolysis at neutral pH. B is used to represent presence of nucelobases (A, T, G or C).[16]

Hydrolysis of glycosidic bond is often termed as depurination as it more feasible at purine bases, guanine and adenine rather than cytosine or thymine. Acid catalyzed hydrolysis of glycosidic bond of DNA is as shown in Scheme 1.2. Abasic site formed during depurination are cytotoxic and mutagenic.[17]

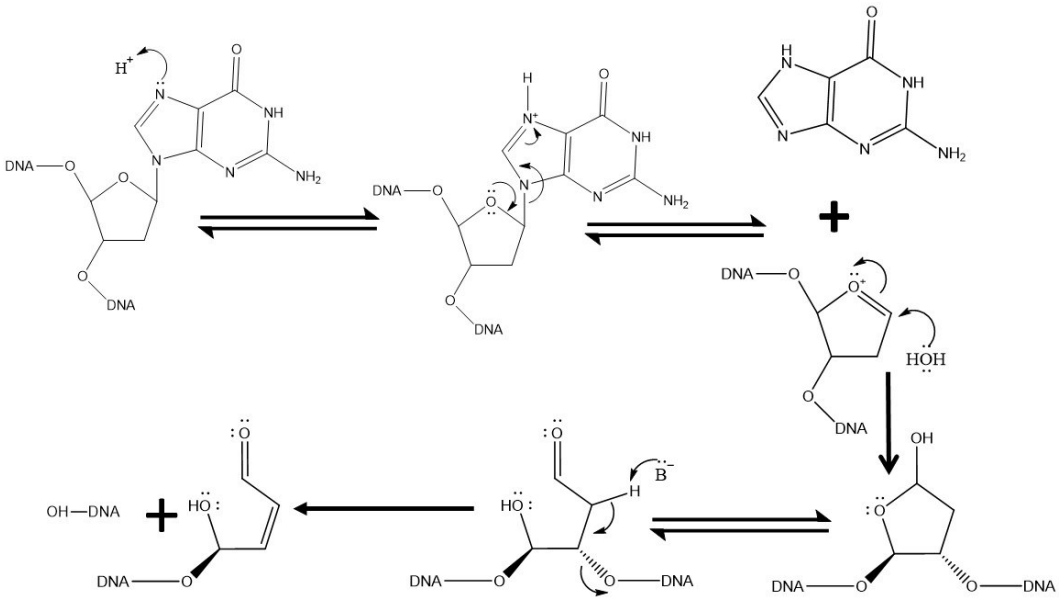

Scheme 1.2. Acid catalyzed hydrolysis of glycosidic bond of DNA.

DNA alkylation. Heteroatoms within DNA are preferential targets for DNA alkylation N7 position of guanine is the most nucleophilic site in DNA and preferential site of reaction for small diffusible alkylating agents. Some bulky chemicals/drugs cannot bind to N7 position of guanine due to steric effects and hence bind to exocyclic amine of guanine.[18] Some of the preferential sites of alkylation in DNA bases are as shown in Scheme 1.3.

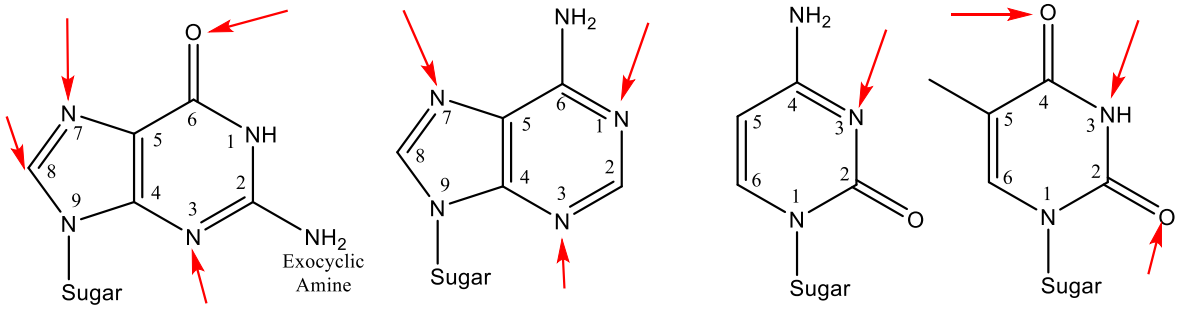

Deoxyguanosine **Deoxyadenosine** **Deoxycytosine** **Thymidine**

Scheme 1.3. Structure of DNA nucleobases along with the preferential site of reactivity highlighted with an arrow.

DNA Oxidation. DNA oxidative damage can be either due to cellular metabolic or exposure to some toxic environmental chemicals that might result in reactive oxygen species.[19] Some of the ROS species include oxygen free radicals such as superoxide radical anion (O_2^-), hydroxyl radical (OH•), hydrogen peroxide (H_2O_2), nitrous oxide (NO) etc., Guanine is the most easily oxidized nucleobase due its low oxidative potential.[20]

1.4 Xenobiotics and Reactive Metabolites

Xenobiotics are foreign substances that may be chemicals[21], drugs, environmental pollutants, food additives, hydrocarbons, carcinogens, pesticides found in the organisms but not naturally present or anticipated be present.[22] Drugs like antibiotics present in human body at higher concentrations are also considered to be xenobiotics as they are not produced inside

characteristically.[23] Xenobiotics are often widely used in context of environmental toxins or pollutants as they enter the biological system of humans or animals and undergo changes leading to adversative effects.[24,25] Xenobiotics are often lipophilic, once they enter the body they are transported to other parts of body via blood stream. Due to lipophilic nature, they usually accumulated in fat tissues and slowly drain into circulation causes prolonged effects. Once they enter the circulation, most of the time they are eliminated form body via detoxification pathways. Usually detoxification occurs by metabolism in liver.[26] Hepatocytes containing xenobiotic metabolizing enzymes (XMEs) convert the fat-soluble chemicals to water soluble products thus facilitating their elimination.[27]

Xenobiotics or chemicals after entering the human body can be processed by numerous pathways that cause the chemicals to interact with specific receptors to have a positive or negative effect eventually leading to detrimental effect.[28] Under metabolic pathways via metabolic enzymes the lipophilic chemicals can be converted to its corresponding products that are majorly water soluble.[29] These products can either excreted out via kidneys or bile referred as detoxification, whereas some of the products are reactive electrophiles that actively bind to variety of biomolecules like proteins, lipids and DNA that can potentially lead to toxic effects.[30]

Polycyclic Aromatic Hydrocarbons (PAHs) are some of most commonly occurring xenobiotics in the environment that cause cancer and other health effects.[31] PAHs are also referred as polynuclear aromatic hydrocarbons (PNAs) that have only carbons and hydrogens and composed of multiple aromatic rings fused together.[32] They are usually formed during thermal combustion of organic molecules and further recombination. The natural sources of PAHs are forest fires, oils seeps, volcanic eruptions etc., whereas anthropogenic sources include burning fossil fuel, coal tar, wood, garbage etc. PAHs include 100s of chemicals that are neutral,

non-polar with very poor solubility in water and cannot degrade easily under natural condition.[33,34] Some of the common examples of PAHs are Naphthalene, Anthracene, Benzo[a]anthracene, Pyrene, Benzo[a]pyrene (B[a]P) etc.[35] Toxicity of all the PAHs are not available but US Environmental Protection Agency (EPA) assessed the risks of mixture of PAHs and showed all PAHs are almost as potent as B[a]P which is one of the most potent PAH.[36] Benzo[a]pyrene is one of the most commonly studied carcinogen due its significant presence in tobacco smoke, coal tar, grilled meats and its high risk of causing lung cancer.[37,38]

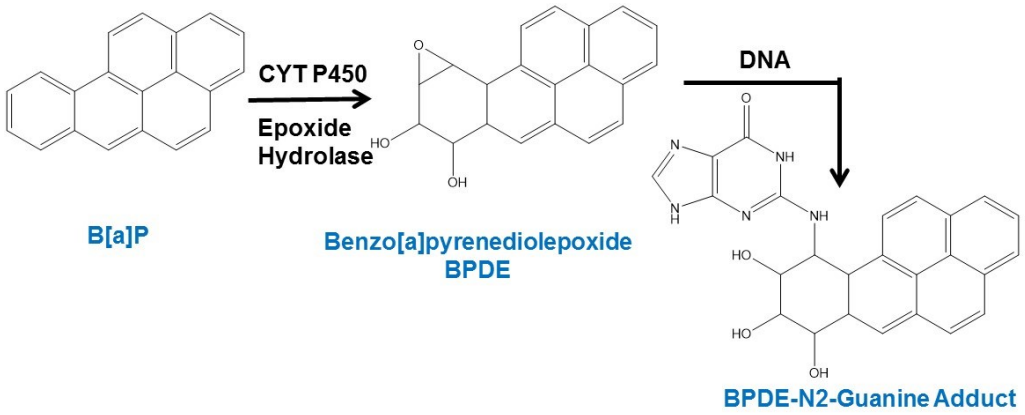

Scheme 1.4. CYT P450 mediated conversion of Benzo[a]pyrene (B[a]P) in the presence of epoxide hydrolase to benzo[a]pyrenediolepoxide and subsequent covalent binding to exocyclic amine of guanine in DNA.

Benzo[a]pyrene requires metabolic activation prior to reaction with macromolecules like DNA and proteins to show their adverse biological effects.[39] Oxidation of B[a]P is catalyzed by cytochrome P450 (Cyt p450) enzymes and microsomal epoxide hydrolases leading to reactive metabolite of B[a]P, which is Benzo[a]pyrene-7,8-dihydrodiol-9,10-epoxide (BPDE), Scheme 1.4.[40] This metabolite of B[a]P is highly carcinogenic and it is classified as class group 1 carcinogen by International agency for research on cancer (IARC).[41] BPDE is highly reactive to DNA, forming DNA adducts specifically at guanine residues, Scheme 1.4. It is known that the

most abundant DNA adduct is 10-(deoxyguanosin-N^2-yl)-7,8,9-trihydroxy-7,8,9,10-tetrahydro-BaP (dG-N^2-BPDE).[42,43]

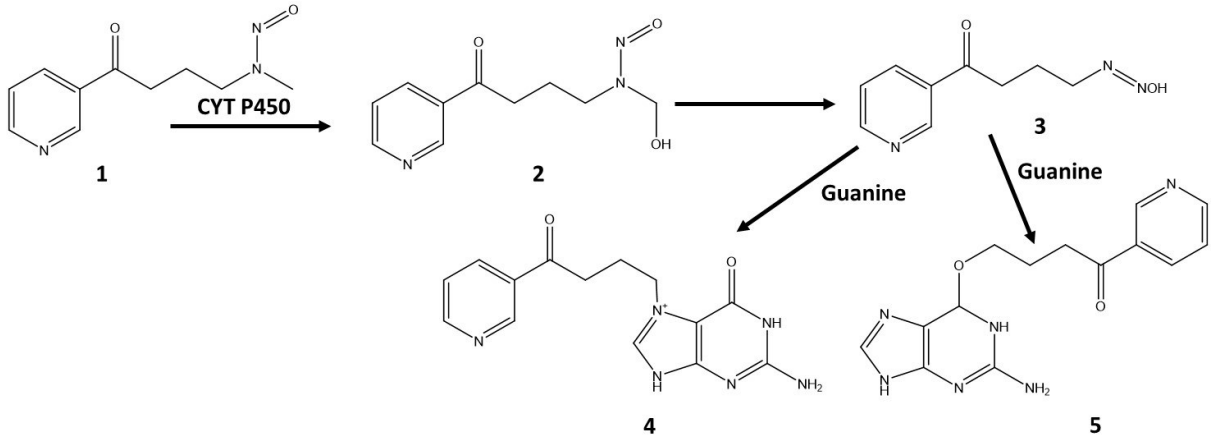

Scheme 1.5. CYT P450 catalyzed conversion of NNK (1) to α-hydroxyl metabolite of NNK (2) which forms 4-oxo-4-(3-pyridyl)-1-butane-daizohydroxide upon losing a formaldehyde (3), (3) reacts with guanine in DNA to form 7-[4-oxo-4-(3-pyridyl)but-1-yl]Gua (**4**) or O^6-[4-oxo-4-(3-pyridyl)but-1-yl]Guaadducts (**5**)

Nicotine derived nitrosamine ketone (NNK) is a tobacco specific carcinogen which is known to cause lung cancer.[44] NNK is also known as 4-(methylnitrosamino)-1-(3-pyridyl)-1-butanone which is naturally synthesized in tobacco leaves and enters human body via tobacco smoke and nicotine burning.[45] NNK also requires metabolic activation to form adducts with DNA via Cyt P450 enzymes leading to reactive metabolites. P450 activated metabolite process for NNK referred as α-hydroxylation. The hydroxylation reactions at methylene and methyl carbons adjacent to N-nitroso groups results in reactive metabolite formation that can potentially cause guanine adducts with DNA.[46] P450 mediated carbonyl reduction of NNK catalyzed by β-hydroxy steroid dehydrogenase or carbonyl reductases, produces 4-(methylnitrosamino)-1-(3-pyridyl)-1-butanol (NNAL) a major metabolite of NNK in smokers.[47] Mediation of p450

metabolic pathway is the most pivotal part of DNA adduct formation and hence no tumor formation. As in the absence of NNK α-hydroxylation reactive electrophiles are not generated leading to no adduct formation.[48]

Aflatoxins are potential cancer causing chemicals that mainly cause hepatocellular carcinoma. Aflatoxins are normally produced from molds *Aspergillus flavus and Aspergillus parasiticus* that grows on food, decaying vegetation,dairy, soil etc.[49] Aflatoxin B1 (AFB1) is considered to be most toxic and causes acute hepatotoxicity and hepatic necrosis that eventually leads to cancer.[50] AFB1 is usually consumed from contaminated food products, dairy and dairy products with aflatoxins from livestock consuming contaminated feed.[51] AFB1 requires metabolic activation to wield its carcinogenic effect. Metabolic activation of AFB1 to AFB1 exo-8,9-epoxide via Cyt P450 metabolic pathway almost readily reacts with DNA exclusively at N7 position of guanine forming AFB1-N7-Gua adducts, Scheme 1.6.[52,53]

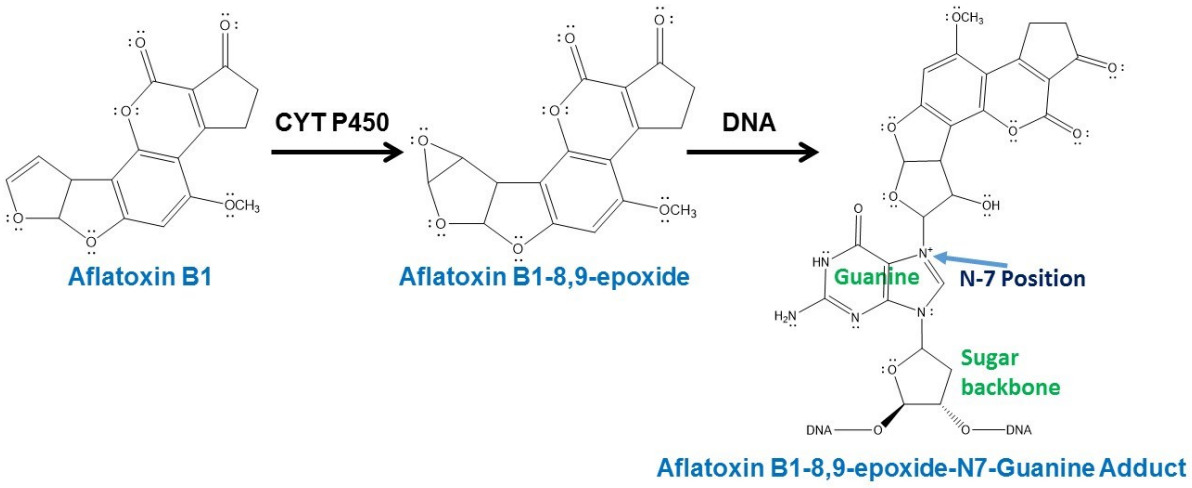

Scheme 1.6. CYT P450 catalyzed conversion of Aflatoxin B1 to Aflatoxin B1-8,9-epoxide. Aflatoxin B1-8,9-epoxide reacts with N7 position of guanine to form covalent adduct.

1.5 Cytochrome P450 enzymes

Cytochrome P450 (CYP P450) enzymes are cysteinato-heme enzymes which play a major role in oxidative transformation of xenobiotic compounds. The prosthetic group consists of iron (III) protoporphyrin IX covalently linked to the protein by sulfur atom of a proximal cysteine ligand.[54,55] Common reaction catalyzed by CYP P450 enzymes is as shown in equation 1. Catalytic cycle of CYP P450 enzymes is as shown in scheme 1.7. Briefly environmental pollutant/chemical/drug forms complex with Fe^{3+} of CYP P450. This complex is reduced by CYP reductase at the same time flavoprotein is oxidized using NADPH. An oxygen molecule now binds to the reduced complex, oxidizing the drug/substrate and CYP P450 complex. This oxidized complex releases the oxidized drug regenerating the CYP P450.

$$RH + O_2 + NADPH + H^+ \rightarrow ROH + H_2O + NADP^+ \qquad \textbf{Equation (1)}$$

Scheme 1.7. Schematic representation of catalytic cycle of cytochrome P450 enzymes.

1.6 P53 Gene and Organ specific cancer

P53 gene is tumor suppressor gene located on the short arm of chromosome 17. Tumor suppressor genes provide protection against cancer. P53 gene codes for P53 protein that is associated with cell cycle regulation and cell death. Mutations within the tumor suppressor gene

can lead to faulty P53 protein which in might lead to cancer.[56,57] Mutations within the P53 gene are often sequence specific in co-relation with organ specific cancer. P53 gene is frequently mutated in human cancers (>50%) [58,59,60] there are demonstrated links between human exposure to various carcinogens and specific mutations in the p53 gene leading to the development of specific cancers.[61] P53 gene has 11 exons and most mutations in the p53 gene occur in the DNA binding domain, exons 5 - 8 (Scheme 1.8).[62]

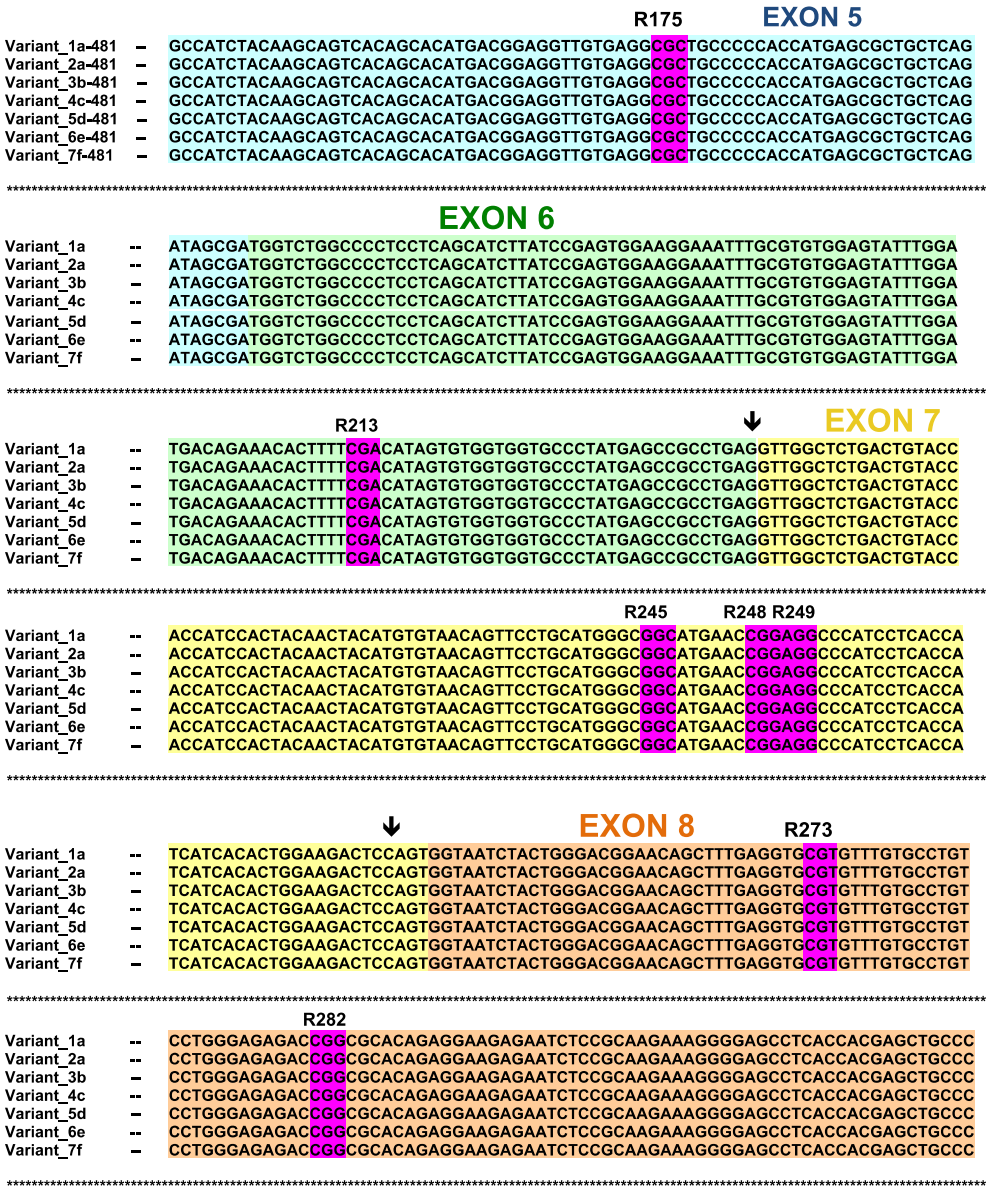

Scheme 1.8. Exons 5 to 8 of the p53 gene (hotspots are in purple)

1.7 Liquid Chromatography Tandem Mass Spectrometry

Mass spectrometry is a valuable tool in the prediction and characterization of xenobiotics and metabolites of xenobiotics. Usually mass spectrometry is coupled with liquid chromatography to aid in separation of complex samples and also to increase the sensitivity. Liquid chromatography in conjunction with mass spectrometry is used in this thesis to characterize and quantitate the amount of DNA damage by various chemicals.

MS Instruments used in this study include AbSciex QTrap 4000 and ABSciex QSTAR. AbSciex QTrap 4000 is a triple quadrupole mass spectrometer mainly used for quantitation and AbSciex QSTAR is quadruple time of flight mass spectrometer used for characterization of both small molecules and biomolecules. Different modes of mass spectrometer used include product ion scan for characterization and multiple reaction monitoring for quantitation.

Product ion scan is a tandem or MS^2 mass spectrometry technique in which a precursor ion is selected in the first quadruple, energy applied in the second quadruple and all the product ions formed in the third quadruple were scanned and detected in the third quadruple, resulting in a MS/MS spectrum as shown in Scheme 1.9.

Single reaction monitoring is a tandem or MS^2 mass spectrometry technique in which a precursor ion is selected in the first quadruple, energy applied in the second quadruple to fragment the precursor ion and only one fragment selected in the third quadruple. Resulting in an chromatogram corresponding to the transition selected. When multiple reaction are monitored simultaneously it is called as multiple reaction monitoring.

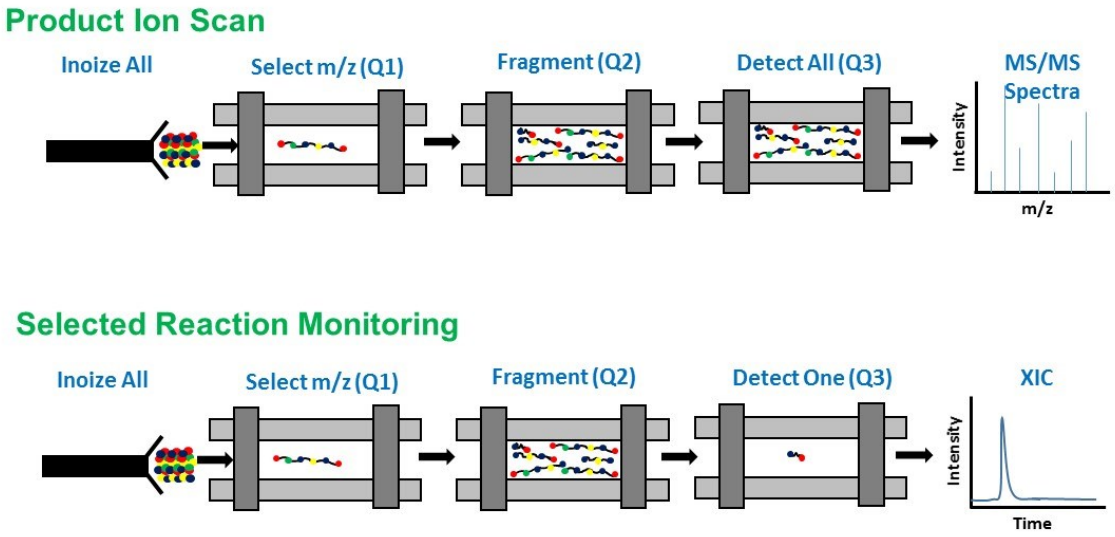

Scheme 1.9. Different modes of tandem mass spectrometry modes used for characterization and quantitation.

Typically reverse phase chromatography with binary solvent system consisting of 10 mM Ammonium acetate as aqueous buffer and methanol/acetonitrile as organic buffer is used for separation and MS analysis of small molecules (metabolites of xenobiotics and nucleobase adducts) and ion pair reverse phase chromatography with binary solvent system containing 25 mM triethyl ammonium biocarbonate as aqueous buffer and methanol as organic buffer was used for separation and MS analysis of oligonucleotides.

1.8 Summary I

This thesis focuses on developing high throughput LC-MS/MS methodology for screening chemicals for their genotoxic potential and co-relating with the sequence specific cancer. Methodology involves reacting chemicals with P53 gene fragments and co-relating the sequence specific DNA damage with organ specific cancer. Chapter 2 focuses on determining

the chemoselectivity of benzo[a]pyrenediolepoxide on exon 7 of P53 gene fragments and differentiating the selectivity and site specificity difference between small ss-oligonucleotides with large ds-oligonucleotides.

1.9 References

1. Heron, M.; Anderson, R. N. Changes in the Leading Cause of Death: Recent Patterns in Heart Disease and Cancer Mortality. *NCHS Data Brief* **2016**, *254*, 1-8.
2. Siegel, R. L.; Miller, K. D.; Jemal, A. Cancer statistics, 2016. *CA: a cancer journal for clinicians* **2016**, *66*, 7-30.
3. Irving, R. M.; Elfarra, A. A. Role of reactive metabolites in the circulation in extrahepatic toxicity. *Expert opinion on drug metabolism & toxicology* **2012**, *8*, 1157-1172.
4. Russell, C.; Rahman, A.; Mohammed, A. R. Application of genomics, proteomics and metabolomics in Drug discovery, development and clinic. *therapeutic delivery* **2013**, *4*, 395-413.
5. Kang, S. H.; Kwon, J. Y.; Lee, J. K.; Seo, Y. R. Recent advances in in vivo genotoxicity testing: prediction of carcinogenic potential using comet and micronucleus assay in animal models. *Journal of cancer prevention* **2013**, *18*, 277-288.
6. Feigelson, H. S.; Ross, R. K.; Yu, M. C.; Coetzee, G. A.; Reichardt, J. K.; Henderson, B. E. Genetic susceptibility to cancer from exogenous and endogenous exposures. *J. Cell. Biochem.* **1996**, *63*, 15-22.
7. Doll, R.; Peto, R. The causes of cancer: quantitative estimates of avoidable risks of cancer in the United States today. *J. Natl. Cancer Inst.* **1981**, *66*, 1192-1308.
8. Henderson, B. E.; Ross, R. K.; Pike, M. C.; Casagrande, J. T. Endogenous hormones as a major factor in human cancer. *Cancer Res.* **1982**, *42*, 3232-3239.
9. https://www.cancer.gov/about-cancer/causes-prevention/risk
10. Henderson, B. E.; Ross, R. K.; Pike, M. C.; Casagrande, J. T. Endogenous hormones as a major factor in human cancer. *Cancer Res.* **1982**, *42*, 3232-3239.

11. https://medlineplus.gov/cancer.html

12. Sancar, A.; Lindsey-Boltz, L. A.; Ünsal-Kaçmaz, K.; Linn, S. Molecular mechanisms of mammalian DNA repair and the DNA damage checkpoints. *Annu. Rev. Biochem.* **2004**, *73*, 39-85.

13. Gates, K. S. An overview of chemical processes that damage cellular DNA: spontaneous hydrolysis, alkylation, and reactions with radicals. *Chem. Res. Toxicol.* **2009**, *22*, 1747-1760.

14. Shen, J. C.; Rideout, W. M.,3rd; Jones, P. A. The rate of hydrolytic deamination of 5-methylcytosine in double-stranded DNA. *Nucleic Acids Res.* **1994**, *22*, 972-976.

15. Lutsenko, E.; Bhagwat, A. S. Principal causes of hot spots for cytosine to thymine mutations at sites of cytosine methylation in growing cells: a model, its experimental support and implications. *Mutation Research/Reviews in Mutation Research.* **1999**, *437*, 11-20.

16. Schroeder, G. K.; Lad, C.; Wyman, P.; Williams, N. H.; Wolfenden, R. The time required for water attack at the phosphorus atom of simple phosphodiesters and of DNA. *Proc. Natl. Acad. Sci. U. S. A.* **2006**, *103*, 4052-4055.

17. Boiteux, S.; Guillet, M. Abasic sites in DNA: repair and biological consequences in Saccharomyces cerevisiae. *DNA repair* **2004**, *3*, 1-12.

18. Dipple, A. DNA adducts of chemical carcinogens. *Carcinogenesis* **1995**, *16*, 437-441.

19. Cooke, M. S.; Evans, M. D.; Dizdaroglu, M.; Lunec, J. Oxidative DNA damage: mechanisms, mutation, and disease. *FASEB J.* **2003**, *17*, 1195-1214.

20. Kawanishi, S.; Hiraku, Y.; Oikawa, S. Mechanism of guanine-specific DNA damage by oxidative stress and its role in carcinogenesis and aging. *Mutation Research/Reviews in Mutation Research* **2001**, *488*, 65-76.

21. Coleman, J.; Blake-Kalff, M.; Davies, E. Detoxification of xenobiotics by plants: chemical modification and vacuolar compartmentation. *Trends Plant Sci.* **1997***, 2*, 144-151.

22. Soucek, P. In *Xenobiotics;* Schwab, M., Ed.; Encyclopedia of Cancer; Springer Berlin Heidelberg: Berlin, Heidelberg, 2012; pp 3964-3967.

23. Fatta-Kassinos, D.; Kalavrouziotis, I.; Koukoulakis, P.; Vasquez, M. The risks associated with wastewater reuse and xenobiotics in the agroecological environment. *Sci. Total Environ.* **2011***, 409*, 3555-3563.

24. Soto, A. M.; Sonnenschein, C.; Chung, K. L.; Fernandez, M. F.; Olea, N.; Serrano, F. O. The E-SCREEN assay as a tool to identify estrogens: an update on estrogenic environmental pollutants. *Environ. Health Perspect.* **1995***, 103 Suppl 7*, 113-122.

25. Valavanidis, A.; Vlahogianni, T.; Dassenakis, M.; Scoullos, M. Molecular biomarkers of oxidative stress in aquatic organisms in relation to toxic environmental pollutants. *Ecotoxicol. Environ. Saf.* **2006***, 64*, 178-189.

26. Shimada, T. Xenobiotic-metabolizing enzymes involved in activation and detoxification of carcinogenic polycyclic aromatic hydrocarbons. *Drug metabolism and pharmacokinetics* **2006***, 21*, 257-276.

27. Mansuy, D. Metabolism of xenobiotics: beneficial and adverse effects. *Biol. Aujourdhui* **2013***, 207*, 33-37.

28. Liebler, D. C.; Guengerich, F. P. Elucidating mechanisms of drug-induced toxicity. *Nature reviews Drug discovery* **2005***, 4*, 410-420.

29. Anzenbacher, P.; Anzenbacherova, E. Cytochromes P450 and metabolism of xenobiotics. *Cellular and Molecular Life Sciences CMLS* **2001***, 58*, 737-747.

30. Guengerich, F. P.; MacDonald, J. S. Applying mechanisms of chemical toxicity to predict drug safety. *Chem. Res. Toxicol.* **2007***, 20*, 344-369.

31. Harvey, R. G. *Polycyclic aromatic hydrocarbons: chemistry and carcinogenicity;* CUP Archive: 1991;

32. Wilson, S. C.; Jones, K. C. Bioremediation of soil contaminated with polynuclear aromatic hydrocarbons (PAHs): a review. *Environmental pollution* **1993***, 81*, 229-249.

33. Haritash, A.; Kaushik, C. Biodegradation aspects of polycyclic aromatic hydrocarbons (PAHs): a review. *J. Hazard. Mater.* **2009***, 169*, 1-15.

34. Feng, X.; Pisula, W.; Müllen, K. Large polycyclic aromatic hydrocarbons: synthesis and discotic organization. *Pure and Applied Chemistry* **2009***, 81*, 2203-2224.

35. Fetzer, J. C. The chemistry and analysis of large PAHs. *Polycyclic Aromatic Compounds* **2007***, 27*, 143-162.

36. Nisbet, I. C.; LaGoy, P. K. Toxic equivalency factors (TEFs) for polycyclic aromatic hydrocarbons (PAHs). *Regulatory toxicology and pharmacology* **1992***, 16*, 290-300.

37. Denissenko, M. F.; Pao, A.; Tang, M.; Pfeifer, G. P. Preferential formation of benzo (a) pyrene adducts at lung cancer mutational hotspots in p53. *Science* **1996***, 274*, 430.

38. Sims, P.; Grover, P.; Swaisland, A.; Pal, K.; Hewer, A. Metabolic activation of benzo (a) pyrene proceeds by a diol-epoxide. *Nature* **1974***, 252*, 326-328.

39. Luch, A.; Baird, W. M.; Luch, A. Metabolic activation and detoxification of polycyclic aromatic hydrocarbons. *The Carcinogenic Effects of Polycyclic Aromatic Hydrocarbons*, 19-96.

40. Lemieux, C. L.; Douglas, G. R.; Gingerich, J.; Phonethepswath, S.; Torous, D. K.; Dertinger, S. D.; Phillips, D. H.; Arlt, V. M.; White, P. A. Simultaneous measurement of benzo [a]

pyrene-induced Pig-a and lacZ mutations, micronuclei and dna adducts in mutaTMmouse. *Environ. Mol. Mutagen.* **2011***, 52*, 756-765.

41. Mastrangelo, G.; Fadda, E.; Marzia, V. Polycyclic aromatic hydrocarbons and cancer in man. *Environ. Health Perspect.* **1996***, 104*, 1166-1170.
42. Arlt, V. M.; Poirier, M. C.; Sykes, S. E.; John, K.; Moserova, M.; Stiborova, M.; Wolf, C. R.; Henderson, C. J.; Phillips, D. H. Exposure to benzo [a] pyrene of Hepatic Cytochrome P450 Reductase Null (HRN) and P450 Reductase Conditional Null (RCN) mice: Detection of benzo [a] pyrene diol epoxide-DNA adducts by immunohistochemistry and 32 P-postlabelling. *Toxicol. Lett.* **2012***, 213*, 160-166.
43. Luch, A. *The carcinogenic effects of polycyclic aromatic hydrocarbons;* World Scientific: 2005; .
44. Akopyan, G.; Bonavida, B. Understanding tobacco smoke carcinogen NNK and lung tumorigenesis (Review). *Int. J. Oncol.* **2006***, 29*, 745-752.
45. Adams, J. D.; Lee, S. J.; Vinchkoski, N.; Castonguay, A.; Hoffmann, D. On the formation of the tobacco-specific carcinogen 4-(methylnitrosamino)-1-(3-pyridyl)-1-butanone during smoking. *Cancer Lett.* **1983***, 17*, 339-346.
46. Krishnan, S.; Hvastkovs, E. G.; Bajrami, B.; Schenkman, J. B.; Rusling, J. F. Human cyt P450 mediated metabolic toxicity of 4-(methylnitrosamino)-1-(3-pyridyl)-1-butanone (NNK) evaluated using electrochemiluminescent arrays. *Molecular BioSystems* **2009***, 5*, 163-169.
47. Jalas, J. R.; Hecht, S. S.; Murphy, S. E. Cytochrome P450 enzymes as catalysts of metabolism of 4-(methylnitrosamino)-1-(3-pyridyl)-1-butanone, a tobacco specific carcinogen. *Chem. Res. Toxicol.* **2005***, 18*, 95-110.

48. Hecht, S. S. Biochemistry, biology, and carcinogenicity of tobacco-specific N-nitrosamines. *Chem. Res. Toxicol.* **1998**, *11*, 559-603.

49. Davis, N. D.; Diener, U. L.; Eldridge, D. W. Production of aflatoxins B1 and G1 by Aspergillus flavus in a semisynthetic medium. *Appl. Microbiol.* **1966**, *14*, 378-380.

50. Clifford, J. I.; Rees, K. R. The action of aflatoxin B1 on the rat liver. *Biochem. J.* **1967**, *102*, 65-75.

51. Henry, S. H.; Bosch, F. X.; Troxell, T. C.; Bolger, P. M. Policy forum: public health. Reducing liver cancer--global control of aflatoxin. *Science* **1999**, *286*, 2453-2454.

52. Kobertz, W. R.; Wang, D.; Wogan, G. N.; Essigmann, J. M. An intercalation inhibitor altering the target selectivity of DNA damaging agents: synthesis of site-specific aflatoxin B1 adducts in a p53 mutational hotspot. *Proc. Natl. Acad. Sci. U. S. A.* **1997**, *94*, 9579-9584.

53. Johnson, W. W.; Guengerich, F. P. Reaction of aflatoxin B1 exo-8,9-epoxide with DNA: kinetic analysis of covalent binding and DNA-induced hydrolysis. *Proc. Natl. Acad. Sci. U. S. A.* **1997**, *94*, 6121-6125.

54. Meunier, B.; De Visser, S. P.; Shaik, S. Mechanism of oxidation reactions catalyzed by cytochrome P450 enzymes. *Chem. Rev.* **2004**, *104*, 3947-3980.

55. Guengerich, F. P. Cytochrome P450 enzymes. *Am. Sci.* **1993**, *81*, 440-447.

56. Livingstone, L. R.; White, A.; Sprouse, J.; Livanos, E.; Jacks, T.; Tlsty, T. D. Altered cell cycle arrest and gene amplification potential accompany loss of wild-type p53. *Cell* **1992**, *70*, 923-935.

57. Nakamura, Y.; White, R.; Vogelstein, B. Chromosome 17 Deletions and p53 Gene Mutations. *J. Immunol.* **1982**, *128*, 1566.

58. Soussi, T.; Wiman, K. G. Shaping genetic alterations in human cancer: the p53 mutation paradigm. *Cancer Cell* **2007***, 12*, 303-312.

59. Cheok, C. F.; Verma, C. S.; Baselga, J.; Lane, D. P. Translating p53 into the clinic. *Nat. Rev. Clin. Oncol.* **2011***, 8*, 25-37.

60. Ozaki, T.; Nakagawara, A. p53: the attractive tumor suppressor in the cancer research field. *J. Biomed. Biotechnol.* **2011**, 603925, 13 pp.

61. Pfeifer, G. P.; Besaratinia, A. Mutational spectra of human cancer. *Hum. Genet.* **2009***, 125*, 493-506.

62. Soussi, T. TP53 mutations in human cancer: database reassessment and prospects for the next decade. *Adv. Cancer Res.* **2011***, 110*, 107-139.

CHAPTER 2

Chemical Selectivity of Nucleobase Adduction Relative To In Vivo Mutation Sites On Exon 7 Fragment of P53 Tumor Suppressor Gene

2-1 ABSTRACT

Damage to p53 tumor suppressor gene is found in half of all human cancers. Databases integrating studies of large numbers of tumors and cancer cell cultures show that mutation sites of specific p53 codons are correlated with specific types of cancers. If the most frequently damaged p53 codons in vivo correlate with the most frequent chemical damage sites in vitro, predictions of organ-specific cancer risks might result. Herein, we describe LC-MS/MS methodology to reveal metabolite-adducted nucleobases within codons by LC-MS/MS for oligonucleotides that are longer than 20 base pairs. Specifically, we used a known carcinogen, benzo[a]pyrene-7,8-dihydrodiol-9,10-epoxide (BPDE) to determine the most frequently adducted nucleobases within codons. We used a known sequence of 32 base pairs (bp) representing part of p53 exon 7 with 5 possible reactive *hot spots*. This is the first nucleobase reactivity study of a double stranded DNA p53 fragment featuring more than 20 base pairs with multiple reactive sites. We reacted the 32 bp fragment with benzo[a]pyrene metabolite BPDE that undergoes nucleophilic substitution by DNA bases. Liquid chromatography-mass spectrometry (LC-MS/MS) was used for sequencing of oligonucleotide products from the

reacted 32 bp fragment after fragmentation by a restriction endonuclease. Analysis of the adducted p53 fragment compared with unreacted fragment revealed guanines of codons 248 and 244 as most frequently targeted, which are also mutated with high frequency in human tumors. Codon 248 is mutated in non-small cell and small cell lung, head and neck, colorectal and skin cancer, while codon 244 is mutated in small cell lung cancer, all of which involve possible BDPE exposure. Results suggest the utility of this approach for screening of adducted p53 gene by drugs and environmental chemicals to predict risks for organ specific cancers.

2-2. Introduction

Cancer is the second most common cause of death worldwide.[1] Tumor suppressor genes in humans provide cancer protection pathways by coding for proteins that control cellular stress by inducing cell-cycle arrest, apoptosis and senescence.[2] *TP53* (or p53) was confirmed as a tumor suppressor gene in the 1980s,[3] and other tumor suppressor genes such as retinoblastoma (RB), Wilms Tumor 1 (WT1), Adenomatosis Polyposis Coli (APC), and p16 have also been discovered. The *p53* gene encodes p53 protein, which is involved in cell cycle regulation leading to cancer protection.[4-7]

Tumor suppressor genes can be damaged by xenobiotic chemicals, by their metabolites and by radiation. Mutations in the *p53* gene have been found in 50% of human cancers.[8-12] Moreover, there are well-documented links between human exposure to various carcinogens and specific mutated codons in the *p53* gene leading to the development of specific cancers.[11-13] Most mutations in the *p53* gene occur in exons 5 to 8.[14,15]

Thus, mutational spectra on the *p53* gene are correlated with the incidence of tissue specific cancers. For example, data in the p53 database handbook[13] show that highly mutated reactive *hot spots* include codons 157, 158, 248, 249 in lung cancer, codon 273 in brain and prostate cancer, codons 175, 248 and 273 in breast cancer and codons 175, 282 and 248 in liver cancer.[13,16] Codon *hot spots* for reactions of metabolites on the *p53* gene have been linked to human exposure to particular carcinogens. Specifically, components of tobacco smoke are related to lung cancer, tobacco smoke and alcohol to head and neck cancers, aromatic amines to bladder cancer, aflatoxine-B1 and hepatitis B virus to liver cancer and ultraviolet light to skin cancer. Thus, exposure to specific carcinogens that lead to damage to the *p53* gene can be correlated with organ-specific cancers.

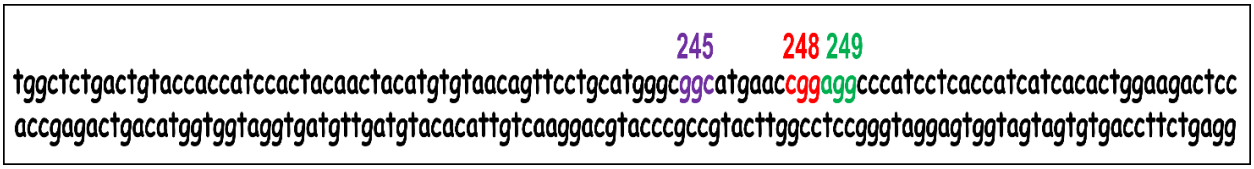

Scheme 2.1. Exon 7 of the p53 gene. Known highly reactive hotspots 245, 248 and 249 are in purple, red and green respectively. Codons 244 and 247 are additional hot spots.[13]

These relationships between the mutational spectra of p53 to organ-specific cancers are clearly indicated in large databases integrating extensive p53 research.[13,17] These data include genomic studies of patient tumors and cell lines, and show that **the** *p53* gene has 7 reactive hot spots between bases 361 and 920 of the reading frame, one in exon 5, one in exon 6, five in exon 7 (Scheme 2.1), and two in exon 8. Screening of a wide range of carcinogens by assessing reactive hot spots on p53 in vitro could identify reactive nucleobases within codons that, if correlated with mutational spectra, could be used to predict tissue specific cancers. This sort of information is not available for large libraries of potentially reactive compounds or metabolites on p53, and is almost non-existent for other tumor suppressor genes.[18] New methods for screening reactive metabolites for sequence specific tumor suppressor gene damage would be valuable tools to assess the potential of new drugs and environmental chemicals for organ-specific carcinogenicity.

Mass spectrometry (MS) is a valuable tool for structural analysis of DNA, and LC-MS/MS methodologies have been developed over the past decade for sizing and sequencing oligonucleotides of up to 20 base pairs (bp).[19-23] Harsch, reacted a 10 base pair oligonucleotide derived from hypoxanthine-guanine phosphoribosyltransferase gene (HPRT gene) with benzo[c]phenanthrene and determined positional isomers in the product.[24] Chowdhury and

Guengerich reacted a 15 base pair oligonucleotide incorporating hot spot codon 157 on exon 5 of p53 gene with mutagenic molecules benzo[a]pyrene-7,8-dihydrodiol-9,10-epoxide (BPDE) and N-hydroxy-4-aminobiphenyl (N-OH-4ABP) and used MS/MS to determine site reactivity.[25] They also determined C-4 oxidized abasic sites on a 15-mer oligonucleotide.[21] Sharma et. al., reacted a 17-mer incorporating codon 135 of p53 with 2-acetylAminofluorene (AAF), and observed multiple adducts formed from reactions with guanosines.[26] Satterwhite et. al., reacted a 21-mer of p53 containing codon 273 with BPDE.[27] Xiong et. al., reacted a 14 mer ds DNA containing hot spot codons 157 and 158 with BPDE. Xiong et. al., reacted a 14 mer ds DNA containing hot spot codons 157 and 158 with BPDE.[19] Sharma et. al., studied a 15 base pair DNA containing codon 135 with 2-AAF and [28] and also investigated 14 mer ds DNA with codons 157 and 158 [29] in reactions with BPDE, AAF and N-OH-4ABP.

Previous studies have been restricted to ds-oligonucleotides smaller than 20 bp to enable direct LC-MS/MS sequencing. The short strands studies thus far contained only a single reaction site, and thus did not address relative reactivity between different sites or correlations with mutation frequencies in tumors. Further, short strands may exhibit altered structural specificity in nucleophilic addition compared to natural tumor suppressor genes that may show tertiary and quaternary structural influences on codon reactivity.[30-34]

In this paper, we report an LC-MS/MS study of ds fragment of 32 bp of p53 gene exon 7, from codon 242 to 253. This fragment exhibits up to 5 reactive hot spots,[13-17] and our work represents metabolite reactivity of a p53 strand (>20base pairs) with multiple mutation sites. The 32 bp fragment was chosen to be long enough to mimic higher order structure-reactivity of DNA.[32] This fragment was reacted with BPDE, the major DNA-reactive metabolite of

benzo[a]pyrene,[35-37] and then a restriction enzyme was used to cleave the fragment into smaller fragments to enable LC-MS/MS sequencing.

Benzo[a]pyrene is a Group I carcinogen,[38] and its reactive metabolite BDPE is implicated in lung, head and neck, colorectal and skin cancer. Mutational hot spots within this 32 bp fragment include 248, 245, and 249 associated with non-small cell lung cancer, 248, 249 and 244 for small cell lung cancer, 248 for head and neck cancer, 248 and 245 for colorectal cancer, 248 and 247 for skin cancer.[13,14,15,18] Using the approaches described herein, we found that the most frequently BPDE-adducted guanines were within codons 244 and 248, which correlate with frequently mutated p53 sites in several cancers.

2-3. Experimental Section

Caution. *Benzo[a]pyrene-r-7,t-8-dihydrodiol-t-9,10-epoxide (+/-) (anti) (anti BPDE) is a chemical carcinogen. Protective measures including wearing gloves and protective eyewear and doing experiments in a closed hood were taken.*

2-3.1. Chemicals and Reagents. Benzo[a]pyrene-r-7,t-8-dihydrodiol-t-9,10-epoxide (+/-) (anti) (anti BPDE) was from National Cancer Institute Chemical Carcinogen Reference Standard Repository. Triethylammonium bicarbonate (TEAB, 1.0 M, pH 8.4-8.6) and 4-nitrobenzyl alcohol were from Sigma-Aldrich. Custom made single stranded DNA oligomers and the 32-base pair oligonucleotide were from Sigma-Aldrich. HPLC grade solvents, methanol, tetrahydrofuran and water were from Fischer Scientific. Restriction enzyme, NIaIII was from New England Biolabs.

2-3.2. Reactions of Oligonucleotides with BPDE. Reactions with BPDE were done with 4 single stranded (ss) oligonucleotides and the double stranded (ds) 32 bp portion of P53 gene representing codons 242 to 253. 0.1 nmol of each of the 4 ss oligonucleotides were treated with 100 nmol BPDE in a reaction volume of 150 µL at 37°C for 48 hours in dark, 10 mM Tris buffer, pH 7.4. 2.5 µmol of ds 32 bp fragment was reacted with 0.1 µmole of BPDE in volume of 150 µL at 37°C for 48 hours in dark, 10 mM Tris buffer, pH 7.4. A minimum of three replicates of DNA and BPDE reactions were done.

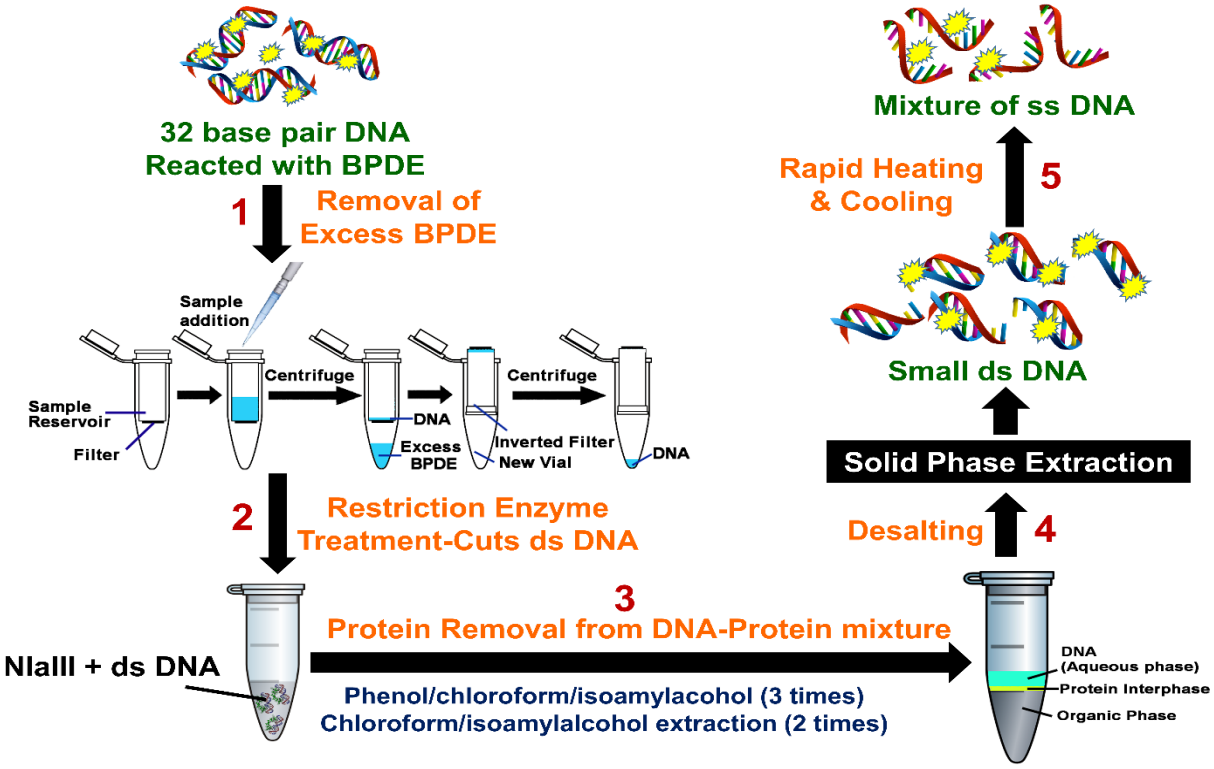

Scheme 2.2 Protocol for sample preparation of 32-base pair p53 fragment reacted with BPDE involving steps: (1) removal of excess BPDE from DNA reaction mixture; (2) restriction enzyme treatment to cut DNA into smaller fragments; (3) protein removal; (4) desalting and (5) rapid heating and cooling to give ss DNA.

2-3.3. Removal of excess BPDE. ss DNA fragments were extracted from the BPDE-ss DNA mixture by extracting with 150 μL of ethylacetate for three times. DNA was recovered from the aqueous phase. Samples were then dried and reconstituted in 100 μL of pure water to make a final concentration of 1 μM ss DNA.

For the ds-DNA-BPDE mixtures, Millipore 3000 Dalton mass cutoff filter vials were used to remove unreacted BPDE (Scheme 2.2). Reaction mixture from above was put into a 3000 Da mass cutoff filter, (catalog # UFC500396) and centrifuged at 13000 rpm for 30 min. ds-DNA was retained on the filter, while the smaller BPDE molecules pass through. The filter was then removed, inverted and placed into a new centrifuge vial, and centrifuged for another 30 min. Approximately 50 μL of the DNA solution was recovered. Recovered solutions of ds oligonucleotides were subjected to restriction enzyme treatment (Scheme 2.2).

2-3.4 Restriction enzyme treatment on ds DNA. Approximately 50 μg (2.5 μmol) of DNA was recovered from above step. 50 units (5 μL) of restriction enzyme, NIaIII was added to 50 μg of the ds 32 bp oligonucleotides to which 20 μL of 10X NE buffer supplied by New England Biolabs, was added and the reaction volume made up to 200 □L with pure water. This reaction mixture was incubated at 37 °C for 8 hours. The resulting solution is mixture of DNA fragments, protein and salt from the NE reaction buffer given by the manufacturer**.**

2-3.5 Removal of Proteins from DNA-Protein-Salt mixture. Proteins were removed from the DNA samples by extraction using 200 μL of water-saturated phenol/chloroform/isoamylalcohol, 25/24/1. Each extraction step involves vortexing on a rotor for 10 min followed by centrifugation for 10 min prior to aqueous phase collection. DNA in the aqueous phase was collected and the extraction procedure was repeated twice more. Further extraction of DNA contained in the aqueous phase was done twice with 200

µL of water-saturated chloroform/isoamylalcohol, 24/1. Finally the aqueous phases were combined and organic phase was discarded. The resulting sample containing DNA and salt was approximately 200 µL.

2-3.6 Desalting. Solid phase extraction (SPE) was performed to remove salt from DNA-salt mixtures to obtain samples suitable for LC-MS/MS analysis. Waters Oasis HLB cartridges were used for desalting. The method involves initial equilibration of the cartridge with methanol and water. Sample was loaded and then washed with 5% methanol in water to remove salts followed by elution with 100 % methanol. The resultant DNA sample was dried and reconstituted in 100 µL pure water. The ds DNA samples were heated and cooled rapidly to convert ds DNA to ss DNA and stored at -20 ºC until LC-MS/MS analysis.

2-3.7 LC-MS/MS analysis. A Waters Capillary LC-XE (Milliford, MA) chromatograph with a Gemini C-18 column (0.3 mm X 150 mm, 5µ for ds DNA fragments & 0.5 mm X 150 mm, 3µ for ds DNA fragments) and photodiode array detector were used. Separation featured a binary solvent consisting of A - 25 mM TEAB and B - methanol. Separation was achieved with a gradient of 0 % to 10% B for 10 min followed by increase from 10 to 50 % B for 100 min and 50 to 100 % B for the final 10 min at flow rate 10 µL/min. m-Nitrobenzylalcohol increases signal intensity and charge states of oligonucleotide fragments in negative mode, which enhances the fragmentation of oligonucleotides in tandem mass spectrometry.[39] Thus, 0.1 % m-nitrobenzyl alcohol was infused at a flow rate of 3 µL/min to mix with the LC flow post-column using a three way connector before entering the mass spectrometer to produce supercharged oligonucleotide fragments.

ss-DNA fragments were analyzed with an AB Sciex Qtrap 4000 mass spectrometer interfaced to the capillary LC. Enhanced multiple charge (EMC) mode for sizing (molecular weight measurement) and enhanced product ion mode (EPI) for sequencing of ss-DNA fragments in negative mode were employed. Potentials -4500 V (ion spray voltage), 130 V (declustering potential), -60 eV (collision energy), and 20eV (collision energy spread) were used while GS1, GS2, and temperature were kept at 35, 20, and 350°C, respectively.

For analysis of ds-DNA samples, an AB Sciex QSTAR mass spectrometer was interfaced with the capillary LC. Negative ion mode with a -4500 V ion spray voltage, -130 V declustering potential and 300°C temperature was used. DNA fragments were subjected to time of flight mass scan (TOF-MS) mode for sizing of unreacted and adducted DNA fragments and product ion scan mode was used at -45 eV collision energy for MS/MS sequencing. Only singly adducted fragments were discussed in this study.

2-4. Results

Initial studies centered on reacting single-strand fragments GGCGGCATG (ss-DNA Fragment 1), including hot spot codon 244 and 245, AACCGGAGGCCCATCCTCA (ss-DNA Fragment 2), including hot spot codon 248 and 249, TGAGGATGGGCCTCCGGTTCATG (ss-DNA Fragment 3, complementary to fragment 2) and CCGCCCATG (ss-DNA Fragment 4, complementary to fragment 1) with BPDE to optimize the LC-MS/MS methodology without using the restriction enzyme.

Our protocol for the 32 base pair exon 7 fragment involves reacting p53 oligonucleotide sequences with BPDE, then using restriction enzymes to cut the reacted fragment into smaller fragments suitable for LC-MS/MS (Scheme 2.3). Our 32 bp exon 7 fragment extends from codon

242 to 253 and includes possible reactive hot spots at codons 244, 245, 247, 248 and 249 related to the various cancers described above. All codons contain guanine except 247 (ACC), which contains a possible reactive adenine. Within this sequence, codon 248 is the most frequently mutated in all cancers.[13] Codons 245, 248 and 249 are adducted for most cancers related to BPDE, which adds to DNA bases by nucleophilic substitution. Our 32 base pair fragment is a combination of ss-DNA fragment 1 and ss-DNA fragment 2 with four additional bases CATG added before the ss-DNA fragment 1. This was done in order to eliminate the possibility of having terminal guanines with enhanced reactivity.

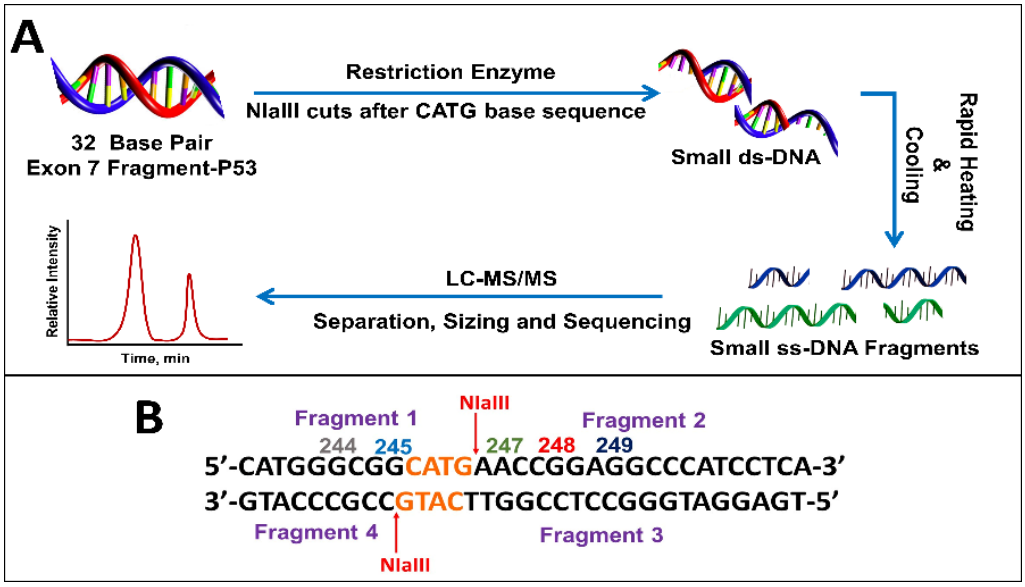

Scheme 2.3. (A) Sample preparation for LC-MS/MS sizing and sequencing of fragment. (B) 32 bp exon 7 fragment showing cut points for restriction enzyme NIaIII along with resulting fragments obtained.

In order to sequence products of 32 base pair oligonucleotide reactions with BPDE by LC-MS/MS, we used the restriction enzyme NlaIII, which cuts DNA after the sequence CATG (Scheme 2.3). For our 32 bp fragment, this results in two fragments of 13 and 19 bases that are

double stranded except for 4 bases at their ends (Scheme 2.3B). 13 mer was obtained instead of the expected 9 mer since the efficiency of restriction enzymes to cut the dsDNA decreases drastically when the recognition site in closer to the 5' end. A minimum of 3-4 extra bases flanking the recognition site on the 5' prime end was required for restriction enzyme to act on ds-DNA.[40] These two ds-fragments were rapidly heated and cooled to give in 4 ss-oligonucleotide fragments (Scheme 3A).

We used enhanced multiple charge scanning to size the ss-oligonucleotides, followed by collision-induced dissociation (CID) MS/MS for sequencing. CID of oligonucleotides shows a characteristic fragmentation pattern (**Scheme 2.4**) featuring a_n-b_n and w_n ions.[41-44] Adduction of BPDE to specific nucleobases within codons was monitored by comparing un-adducted oligonucleotides to those reacted with BPDE, and detecting the difference in m/z of the a_n-b_n and w_n ions.

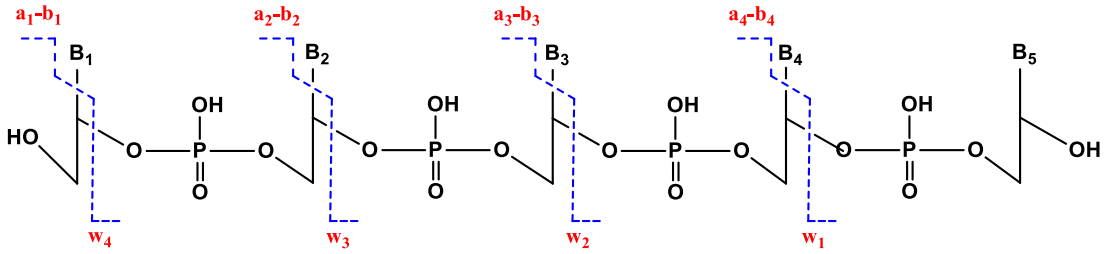

Scheme 2.4. Collision Induced Dissociation (MS/MS or tandem MS) of DNA fragments resulting in the generation of w_n and a_n-b_n ions.

Enhanced multiple charge scans (EMC) were used to determine the m/z of standard and BPDE-adducted DNA fragments that have an additional mass of 302.323. Expected multiple charged species possible were calculated using the online database Mongo oligomass calculator.[45]

We first present results for the ss-Fragments. Possible m/z for standard and singly adducted ss-DNA fragments are as shown in Table 1 for ss-Fragment 1. With the ionization conditions used,

we observed an m/z of 1388.9 for unreacted ss-Fragment 1 with a charge of -2 and m/z of 1540.5 for the reacted fragment indicating a singly adducted strand also with charge -2. Multiple peaks for a single fragment ion were observed due to isotopic distribution, (see Figure 2-1, fragment ion 1540.5).

Table 2-1: Calculated multiple charged species for standard and single adducted ss-Fragment 1.

ss-Fragment 1 : GGCGGCATG		
Charge	**m/z**	
	Standard	**Singly Adducted**
-1	2778.854	3081.177
-2	1388.923	1540.084
-3	925.612	1026.386
-4	693.957	769.538
-5	554.964	615.429
-6	462.302	512.689
-7	396.115	439.304
-8	346.474	384.264

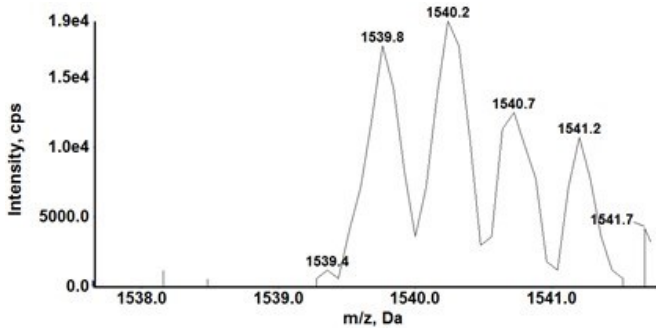

Figure 2-1. Isotopic distribution pattern for ss-DNA Fragment 1, m/z 1540.5 z=-2, measured on a Qtrap mass spectrometer

Extracted ion chromatogram of a selected ion as a function of retention time of singly adducted ss-DNA fragment **1** of m/z 1540.5 shows (Figure 2-2A) that there is a possibility of 2 positional isomers for the singly adducted ss-Fragment 1 at retention times 38.67 and 43.75 min. CID of fragment ion 1540.5 for Peak I is as shown in Figure 2-2B and for Peak II in Figure 2-2C.

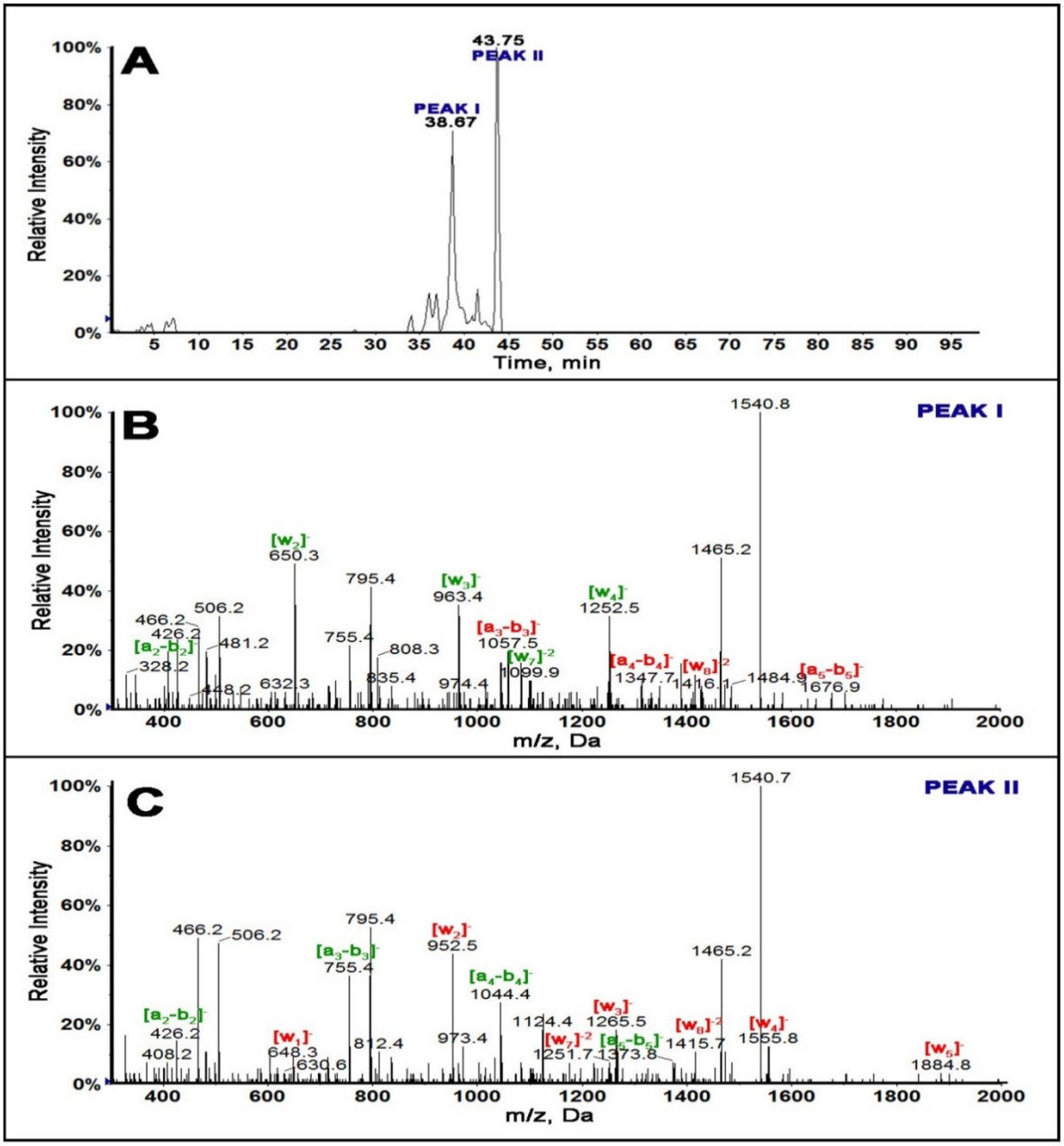

Figure 2-2. LC-MS of ss-DNA fragment **1** (A) Extracted ion chromatogram for fragment m/z 1540.5 representing z = -2 singly adducted fragment 1. (B) MS/MS spectrum of singly adducted BPDE ss- DNA fragment 1, m/z 1540.5 for peak I eluting at 38.67 min and (C) MS/MS of peak II eluting at 43.75 min. (1540.7 or 1540.8 m/z was observed instead of 1540.5 due to isotopic distribution)

Differences in m/z of a-b and w ions between the standard ss-DNA fragment **1** and the singly adducted DNA fragment help locate the exact reacted position on a given oligonucleotide.[46-48] Table 1 summarizes fragment ions obtained for standard ss-DNA fragment **1**, singly adducted ss-fragment **1** for peaks I and II. Red numbers indicate those ions increased in mass by 302.32 from adducting with BPDE compared to the unreacted fragment.

MS/MS spectrum for peak I of singly adducted ss-fragment **1** (Figure 2-2B) reveals increase in mass of all the ions from a_3-b_3 to a_6-b_6 and w_8 compared with that of unreacted ss DNA standard (Table 2-2). This indicates covalent binding of BPDE on the second G base, GG*CGGCATG. This is additionally confirmed by the presence of ion a_2-b_2 with an m/z of 426.2^- and all ions from w_1 to w_7 with m/z the same as that of the standard.

Table 2-2. Fragment ions for standard ss-DNA Fragment 1 of m/z 1388.9 and singly adducted BPDE Fragment 1 ion with m/z of 1540.5 from LC-MS/MS.

Fragment Ion	**m/z**		
	Standard	**Peak I**	**Peak II**
a_2-b_2	$[426.2]^-$	$[426.2]^-$	$[426.2]^-$
a_3-b_3	$[755.5]^-$	$[1057.5]^-$	$[755.4]^-$
a_4-b_4	$[1044.7]^-$	$[1347.7]^-$	$[1044.3]^-$
a_5-b_5	$[1373.5]^-$	$[1676.9]^-$	$[1373.8]^-$
w_1	$[346.2]^{-1}$	$[346.2]^-$	$[648.3]^-$
w_2	$[650.3]^-$	$[650.3]^-$	$[952.5]^-$
w_3	$[963.4]^-$	$[963.4]^-$	$[1265.5]^{-2}$
w_4	$[1252.8]^-$	$[1252.5]^-$	$[1555.8]^-$
w_5	$[1582.0]^-$	n/d	$[1884.7]^-$
w_6	n/d	n/d	n/d
w_7	$[1099.7]^{-2}$	$[1099.9]^{-2}$	$[1251.6]^{-2}$
w_8	$[1263.3]^{-2}$	$[1416.1]^{-2}$	$[1415.7]^{-2}$

MS/MS spectrum for peak II of singly adducted ss- fragment **1** (Figure 2-2C) reflects increases in m/z for all the w ions compared to unreacted standard (Table 2-2). This indicates

covalent binding of BPDE to the last G base, GGCGGCATG*, which was supported by all a-b ions having m/z similar to unreacted standard.

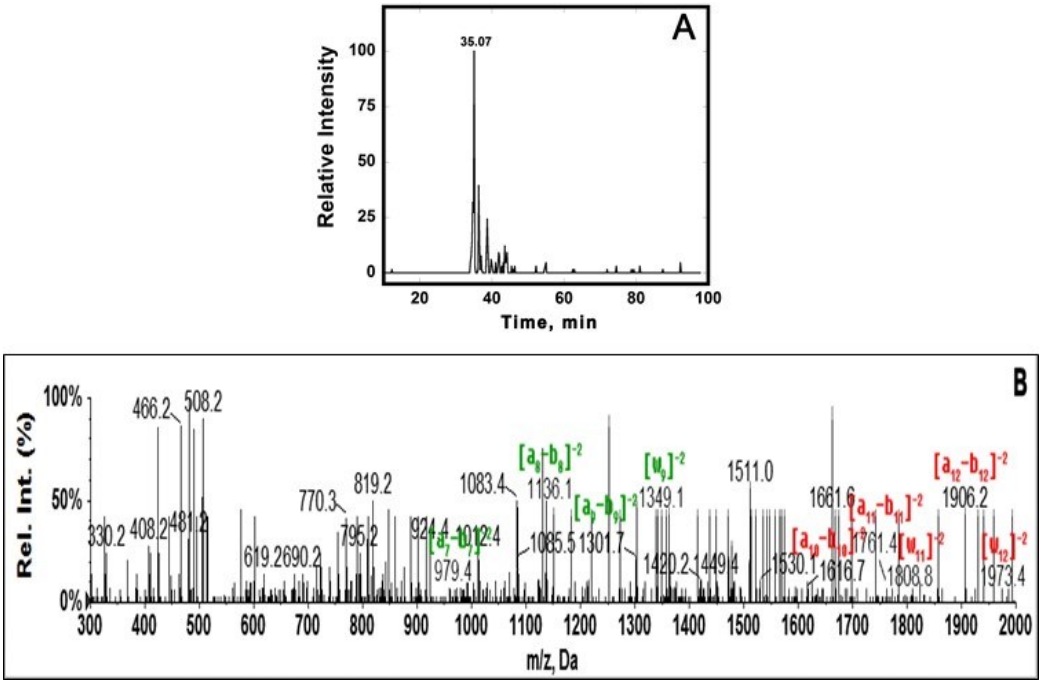

Figure 2-3. LC-MS/MS of ss-DNA fragment 2 (A) Extracted ion chromatogram of singly adducted ss-DNA Fragment 2 fragment, m/z 1511.0. (B) MSMS spectra of fragment ion 1511.0 showing the obtained a_n-b_n and w_n ions. Ions with m/z similar to standard are shown in green and ions with increased m/z shown in red.

Singly adducted fragment of ss-DNA Fragment 2 has an m/z of 1511.0 with a charge of -4. Extracted ion chromatogram of 1511.0 is as shown in Figure 2-3A. XIC of 1511.0 show one major peak indicating that there is one major adduct on ss-DNA Fragment 2. MSMS spectra for singly adducted ss-DNA Fragment 2, m/z 1511.0 is as shown in Figure 2-3B. All a_n-b_n ions up to a_9-b_9 have m/z similar to that of standard. Increase in m/z was observed for a_{10}-b_{10}. This indicates that the possible modification is on base 9, (AACCGGAGG*CCCATCCTCA). This was further confirmed

with w_n ions. Increase in m/z for w_{11}, w_{12}, and w_{13} ions and ions below w_{10} have m/z similar to that of standard. Table 2-3 shows the m/z for standard and adducted ss-DNA Fragment 2.

Table 2-3. Calculated m/z for standard and singly adducted DNA fragments of ss-DNA Fragment 2. (m/z highlighted in red were the ions with increased m/z compared to that of standard corresponding to BPDE adducted)

Fragment Ion	m/z	
	Standard	Singly adducted
a_7-b_7	$[979.4]^{-2}$	$[979.4]^{-2}$
a_8-b_8	$[1136.1]^{-2}$	$[1136.1]^{-2}$
a_9-b_9	$[1301.0]^{-2}$	$[1301.0]^{-2}$
a_{10}-b_{10}	$[1465.5]^{-2}$	$[1616.7]^{-2}$
a_{11}-b_{11}	$[1073.0]^{-3}$	$[1761.4]^{-2}$
a_{12}-b_{12}	$[1169.4]^{-3}$	$[1906.2]^{-2}$
w_8	$[1204.4]^{-2}$	$[1204.4]^{-2}$
w_9	$[1349.1]^{-2}$	$[1349.1]^{-2}$
w_{10}	$[1492.9]^{-2}$	$[1493.2]^{-2}$
w_{11}	$[1657.5]^{-2}$	$[1808.8]^{-2}$
w_{12}	$[1214.4]^{-3}$	$[1973.4]^{-2}$

Singly adducted ss-DNA Fragment 4 has m/z of 1480.2 with a charge of -2. Extracted ion chromatogram (XIC) of 1480.2 is as shown in Figure 2-4A. XIC of 1480.2 showed three major peaks indicating that there are three major adducts on ss-DNA Fragment 4, the complement of fragment 1.

MSMS spectra for singly adducted ss-DNA Fragment 4, m/z 1480.2 is as shown in Figure 2-4B for Peak 1. All a_n-b_n ions up to a_3-b_3 have m/z similar to that of standard. Increase in m/z was observed for a_4-b_4, a_5-b_5 and a_6-b_6. This indicates that the possible modification is on base 3, (CCG*CCCATG). This was further confirmed with w_n ions. Increase in m/z for w_7 and

w_8 ions and all ions below w_6 have m/z similar to that of standard. Table 2-4 shows the m/z for standard and adducted ss-DNA Fragment 4.

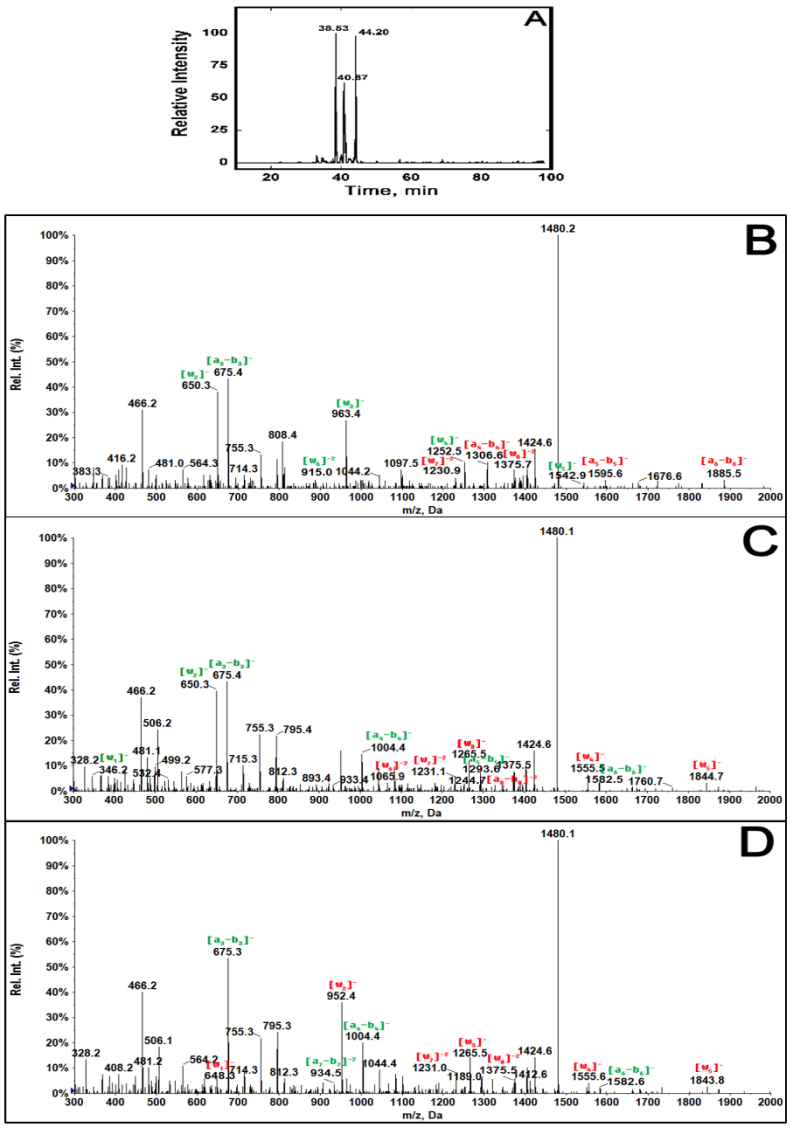

Figure 2-4. LC-MS/MS of ss Fragment 4 (A) Extracted ion chromatogram of singly adducted ss Fragment 4 fragment with m/z 1480.2. (B) MSMS spectra of Peak 1 (C) MSMS spectra of Peak 2 (D) MSMS spectra of Peak 3 showing the obtained a_n-b_n and w_n ions. Ions with m/z similar to standard are shown in green and ions with increased m/z shown in red.

MSMS spectra for singly adducted ss-DNA Fragment 4, m/z 1480.2 is as shown in Figure 2-4C for Peak 2. All a_n-b_n ions up to a_7-b_7 have m/z similar to that of standard. Increase in m/z was observed for a_8-b_8. This indicates that the possible modification is on base 7, (CCGCCCA*TG). This was further confirmed with w_n ions. Increase in m/z for w_3, w_4, w_5, w_6, w_7 and w_8 ions and ions w_1 and w_2 have m/z similar to that of standard. Table 2-4 shows the m/z for standard and adducted ss-DNA Fragment 4.

Table 2-4: Calculated m/z for standard and singly adducted DNA fragments of ss-DNA Fragment 4. (m/z highlighted in red were the ions with increased m/z compared to that of standard corresponding to BPDE adducted)

Fragment	m/z			
	Standard	**Peak1**	**Peak 2**	**Peak 3**
a_2-b_2	$[386.2]^-$	$[426.2]^-$	$[386.2]^-$	$[386.2]^-$
a_3-b_3	$[675.4]^-$	$[675.4]^-$	$[675.4]^-$	$[675.4]^-$
a_4-b_4	$[1004.4]^-$	$[1306.6]^-$	$[1004.4]^-$	$[1004.4]^-$
a_5-b_5	$[1293.8]^-$	$[1595.6]^-$	$[1293.8]^-$	$[1293.8]^-$
a_6-b_6	$[1583.0]^-$	$[1885.5]^-$	$[1582.5]^-$	$[1582.6]^-$
a_7-b_7	$[1872.2]^{-2}$	n/d	n/d	$[934.5]^{-2}$
a_8-b_8	$[1092.2]^{-2}$	n/d	$[1244.7]^{-2}$	n/d
w_1	$[346.2]^{-2}$	$[346.2]^{-2}$	$[346.2]^{-2}$	$[648.23]^-$
w_2	$[650.4]^-$	$[650.3]^-$	$[650.3]^-$	$[952.4]^-$
w_3	$[963.6]^-$	$[963.4]^-$	$[1265.5]^-$	$[1265.6]^{-2}$
w_4	$[1252.8]^-$	$[1252.5]^-$	$[1555.5]^-$	[1554.6]-
w_5	$[1541.9]^-$	$[1542.9]^-$	$[1844.7]^-$	[1843.8]-
w_6	$[1831.2]^-$	$[915.0]^{-2}$	$[1066.6]^{-2}$	$[1066.6]^{-2}$
w_7	$[1079.7]^{-2}$	$[1230.9]^{-2}$	$[1231.1]^{-2}$	$[1231.0]^{-2}$
w_8	$[1224.3]^{-2}$	$[1375.7]^{-2}$	$[1375.6]^{-2}$	$[1375.5]^{-2}$

MSMS spectra for singly adducted ss-DNA Fragment 4, m/z 1480.2 is as shown in Figure 2-4D for Peak 3. All a_n-b_n ions have m/z similar to that of standard. This indicates that the possible modification is on base 9, (CCGCCCATG*). This was further confirmed with w_n

ions showing increase in m/z for all w_n ions. Table 4 shows the m/z for standard and adducted fragment 4.

Singly adducted ss-DNA Fragment 3 has m/z of 1935.5 with a charge of -4. Extracted ion chromatogram of 1935.5 is as shown in figure 2-5A. XIC of 1935.5 show one major peak indicating that there is one major adduct on ss-DNA Fragment 4. MSMS spectra for singly adducted ss-DNA Fragment 3, m/z 1935.5 is as shown in Figure 2-5B. Increase in m/z for w_n ions w_{20}, w_{21}, w_{22} and w_{23} indicate that the modification is on 5th base (GTGAG*GATGGGCCTCCGGTTCATG).

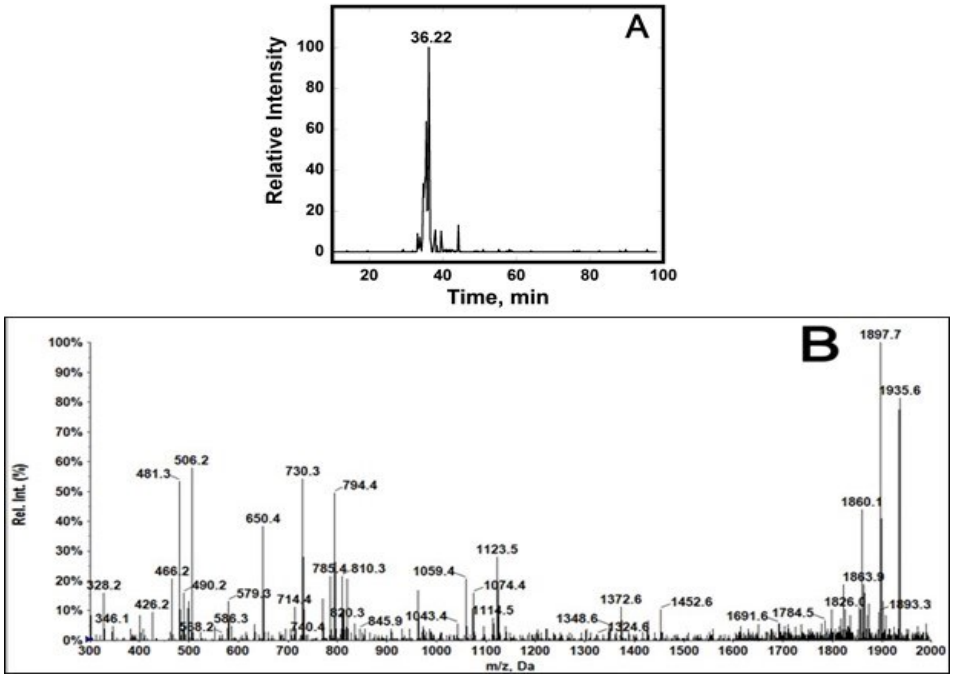

Figure 2-5. LC-MS/MS of ss-DNA Fragment 3 (A) Extracted ion chromatogram of singly adducted ss-DNA Fragment 3, m/z 1935.5. (B) MSMS spectra of fragment ion of m/z, 1935.5 charge -4 showing the obtained a_n-b_n and w_n ions. Ions with m/z similar to standard are shown in green and ions with increased m/z shown in red

Table 2-5. Standard single stranded DNA fragments with their corresponding base adducted in comparison with the hot spot database.[13]

Standard ss-DNA	Sequence	LC-MS/MS DATA		Common Hot Spots from Database[13-15,18]
		Base adducted	Codon	
Fragment 1	GGCGGCATG	GG*CGGCATG	244[b]	244[b], 245[a,d]
		GGCGGCATG*	246	244[b], 245[a,d]
Fragment 2	AACCGGAGGC CCATCCTCA	AACCGGAGG*C CCATCCTCA	249[a,b]	248[a,b,c,d,e], 249[a,b,]
Complementary Strands				
Fragment 3	GTGAGGATGGGCCTCCGGTTC ATG	GTGAG*GATGGGCCTCCGGTTC ATG		
Fragment 4	CCGCCCATG	CCG*CCCATG		
		CCGCCCA*TG		
		CCGCCCATG*		

Note: Possible cancers due to BPDE a. Non Small Cell lung cancer, b. Small Cell lung cancer, c. Head and Neck cancer d. Colorectal cancer, e. Skin Cancer

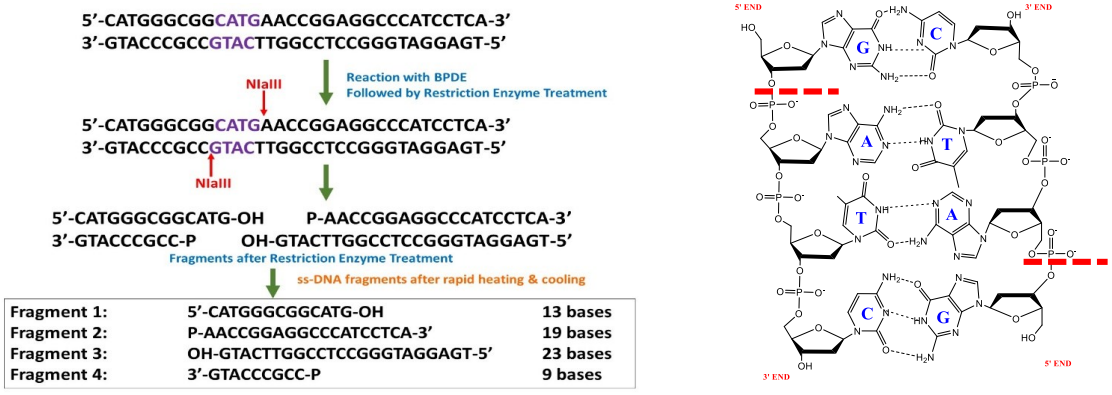

Scheme 2.5. A) Protocol for reaction of 32 base pairs DNA fragment with BPDE followed by restriction enzyme treatment and possible fragments. B) Example of bond breaking between O and P if restriction enzyme acts between G and A.

After establishing and optimizing reproducible methodology on the standard single stranded DNA fragments, the 32 bp ds-p53 exon 7 fragment, which is a combination of fragments **1** and **2** along with the complementary strand, was reacted with BPDE. Four bases, CATG were added to the front of fragment 1 to avoid terminal guanines. The sequence added is consistent with the exon 7 sequence. Excess BPDE was removed using mass cutoff filters, then the aqueous extract was treated with restriction enzyme NIaIII to cut the fragment into smaller fragments suitable for LC-MS (Schemes 2.3 and Scheme 2.5). Subsequently, heating and rapid cooling gave the four single stranded fragments. The m/z values possible for the standard four single stranded fragments and the single adducted fragments are shown in Table 2-6.

Table 2-6. Calculated m/z for standard and singly adducted DNA fragments obtained after restriction enzyme treatment of 32 base pair DNA (A) Fragment 1 (B) Fragment 2 (C) Fragment 3 (D) Fragment 4. m/z highlighted in red were the ions detected in MS spectrum.

(A) Fragment 1 5'-CATGGGCGGCATG-OH		
Charge	Standard	Single adducted
-1	4014.656	4316.979
-2	2006.824	2157.986
-3	1337.546	1438.320
-4	1002.908	1078.489
-5	802.124	862.589
Charges up to -12 are possible only few shown here		

(B) Fragment 2 P-AACCGGAGGCCCATCCTCA-OH		
Charge	Standard	Single adducted
-1	5821.771	6124.094
-2	2910.381	3061.543
-3	1939.918	2040.692
-4	1454.686	1530.267
-5	1163.547	1224.012
Charges up to -18 are possible only few shown here		

(C) Fragment 3 OH-GTACTTGGCCTCCGGGTAGGAGT-OH		
Charge	Standard	Single adducted
-1	7110.654	7412.977
-2	3554.823	3705.985
-3	2369.546	2470.320
-4	1776.907	1852.488
-5	1421.324	1481.789
-6	1184.269	1234.656

(D) Fragment 4 OH-GTACCCGCC-P		
Charge	Standard	Single adducted
-1	2738.759	3041.082
-2	1368.875	1520.037
-3	912.247	1013.021
-4	683.933	759.514
Charges up to -8 are possible only few shown here		

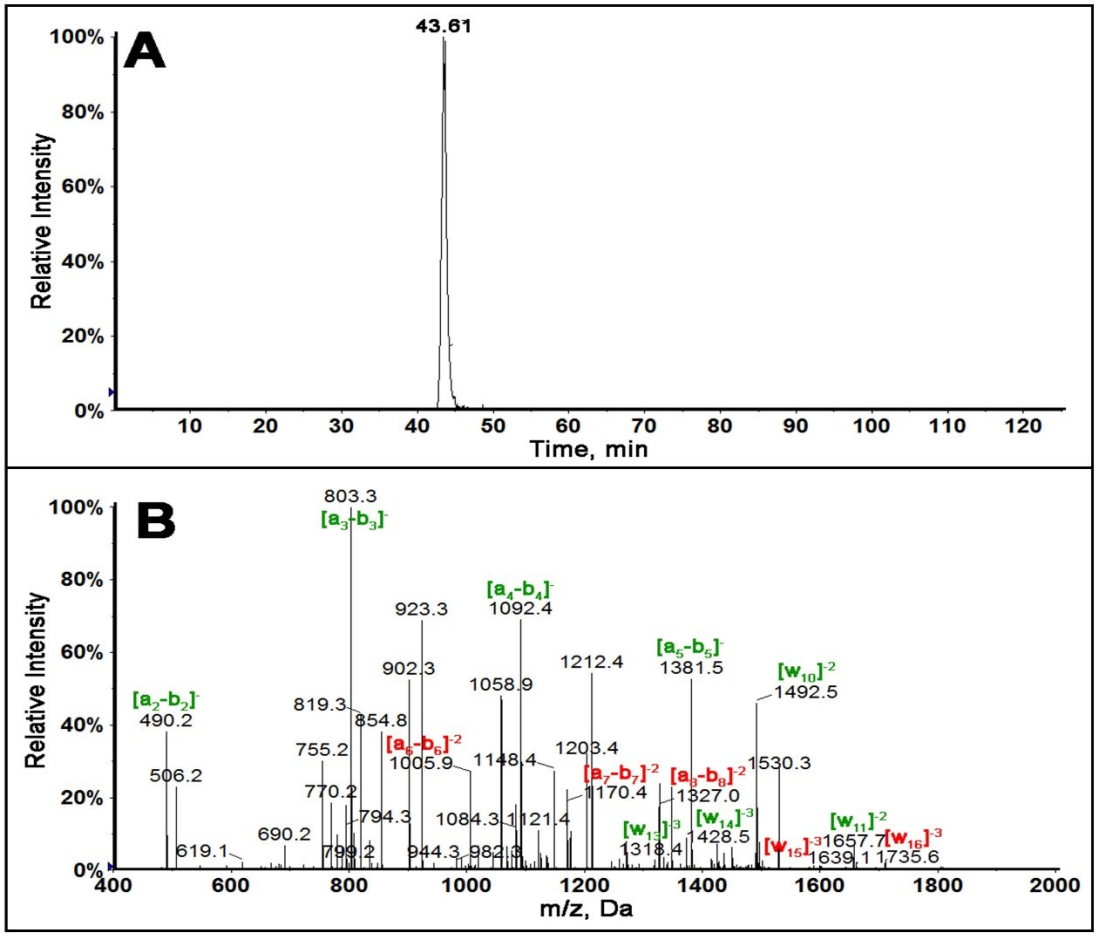

Figure 2-6. LC-MS of ds-32 bp exon 7 fragment: (A) Extracted ion chromatogram of singly adducted fragment **2**, m/z 1530.3, z = -4. (B) MS/MS spectrum of 1530.3 showing a_n-b_n and w_n ions. Ions with m/z similar to standard labeled in green and ions with increased m/z in red.

In order to determine sequence specificity on the entire 32 bp fragment, collision induced dissociation (CID or MS/MS) was performed on all possible single adducted oligonucleotide fragments. Singly adducted fragment **2** is described here as the fragment containing hot spot 248 and 249 active for a number of cancers.[13-15,18] Singly adducted fragment 2 upon MS ionization produced a ion of m/z 1530.3 with z = -4. The extracted ion chromatogram (XIC) of m/z 1530.3

(Figure 2-6A) gave only one major peak indicating that there is one major adduct on the singly adducted fragment **2** of the reacted 32 bp fragment.

MS/MS spectra for singly adducted fragment **2**, m/z 1530.3, (Figure 2-6B) shows all a_n-b_n ions up to a_5-b_5 have m/z similar to that of unreacted standard. An increase in m/z of 302.323 (z = -1) was observed for a_6-b_6, a_7-b_7, a_8-b_8. This suggests that the possible modification is on base 5, (AACCG*GAGGCCCATCCTCA). This was confirmed by increases in m/z for w_{15} and w_{16} ions, while all w ions below w_{14} have m/z similar to that of unreacted standard (Table 2-7).

Table 2-7. Fragment ions for unadducted fragment **2** m/z 1454.6 and singly adducted fragment **2** m/z 1530.3 of the ds-32 bp exon 7 fragment from LC-MS/MS

Fragment ion	m/z	
	Unadducted	Singly Adducted
a_2-b_2	$[490.2]^-$	$[490.2]^-$
a_3-b_3	$[803.3]^-$	$[803.3]^-$
a_4-b_4	$[1092.4]^-$	$[1092.4]^-$
a_5-b_5	$[1381.5]^-$	$[1381.5]^-$
a_6-b_6	$[1710.6]^-$	$[1005.8]^{2-}$
a_7-b_7	$[1019.4]^{2-}$	$[1170.4]^{2-}$
a_8-b_8	$[1176.2]^{2-}$	$[1327.0]^{2-}$
w_9	$[1348.0]^{2-}$	$[1348.0]^{2-}$
w_{10}	$[1492.7]^{2-}$	$[1492.5]^{2-}$
w_{11}	$[1657.7]^{2-}$	$[1657.7]^{2-}$
w_{12}	n/d	n/d
w_{13}	$[1318.4]^{3-}$	$[1318.4]^{3-}$
w_{14}	$[1428.3]^{3-}$	$[1428.3]^{3-}$
w_{15}	$[1538.0]^{3-}$	$[1639.2]^{3-}$
w_{16}	$[1634.5]^{3-}$	$[1735.8]^{3-}$

Similar experiments were done on the other singly adducted fragments obtained from the reacted ds-32 bp fragment, giving fragment **1** (m/z 1437.8, z = -3), Fragment 3 (m/z 1012.7, z = -3) and fragment **4** (m/z 1234.9, z = -6). MS/MS spectra are shown in supporting information file (Figure 2-7, 8 & 9 & Table 2-8, 9 & 10), and results summarized in Table 2-11. These results were identical

when the chemical reaction was done in the same buffer containing 10 mM NaCl, to see if reaction conditions would affect the specificity (Figure 2-10).

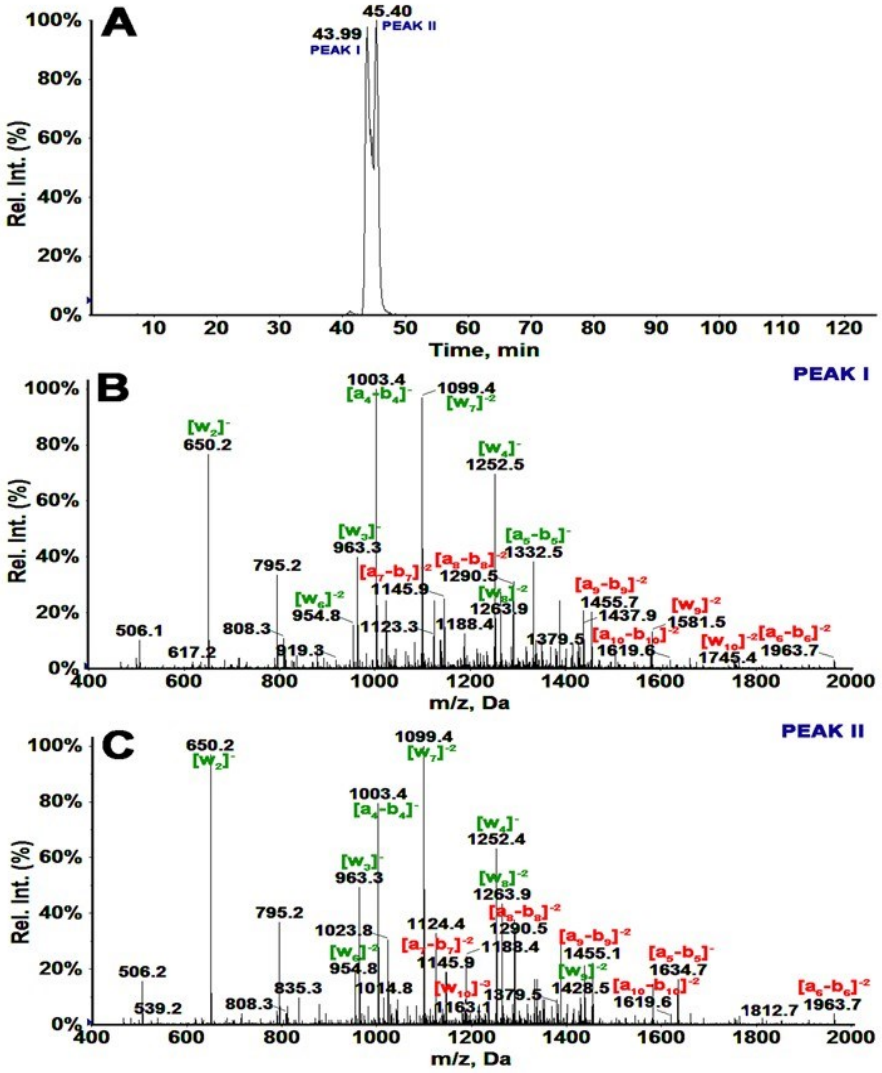

Figure 2-7. LC-MS of ds-32 bp exon 7 probe: (A) Extracted ion chromatogram of singly adducted fragment 1, m/z 1438.2. (B) MSMS spectra of Peak 1 (C) MSMS spectra of Peak 2 showing the obtained a_n-b_n and w_n ions. Ions with m/z similar to standard are shown in green and ions with increased m/z shown in red.

Table 2-8. Calculated m/z for standard and singly adducted DNA Fragment 1. (m/z highlighted in red were the ions with increased m/z compared to that of standard corresponding to BPDE adducted)

Fragment ion	m/z		
	Unadducted	Peak 1	Peak 2
a_4-b_4	$[1003.4]^-$	$[1003.4]^-$	$[1003.4]^-$
a_5-b_5	$[1332.5]^-$	$[1332.5]^-$	$[1634.7]^-$
a_6-b_6	$[1661.6]^-$	$[1963.7]^-$	$[1963.7]^-$
a_7-b_7	$[995.2]^{-2}$	$[1145.9]^{-2}$	$[1145.9]^{-2}$
a_8-b_8	$[1139.5]^{-2}$	$[1290.5]^{-2}$	$[1290.5]^{-2}$
a_9-b_9	$[1304.1]^{-2}$	$[1455.7]^{-2}$	$[1455.1]^{-2}$
a_{10}-b_{10}	$[1468.5]^{-2}$	$[1619.6]^{-2}$	$[1619.6]^{-2}$
w_2	$[650.2]^-$	$[650.2]^-$	$[650.2]^-$
w_3	$[963.3]^-$	$[963.3]^-$	$[963.3]^-$
w_4	$[1252.5]^-$	$[1252.5]^-$	$[1252.5]^-$
w_5	n/d	n/d	n/d
w_6	$[954.8]^{-2}$	$[954.8]^{-2}$	$[954.8]^{-2}$
w_7	$[1099.4]^{-2}$	$[1099.4]^{-2}$	$[1099.4]^{-2}$
w_8	$[1263.9]^{-2}$	$[1263.9]^{-2}$	$[1263.9]^{-2}$
w_9	$[1428.7]^{-2}$	$[1581.5]^{-2}$	$[1428.5]^{-2}$
w_{10}	$[1593.3]^{-2}$	$[1745.4]^{-2}$	$[1163.1]^{-3}$

Singly adducted fragment 1 has an m/z of 1438.2 with a charge of -3. Extracted ion chromatogram of 1438.2 is shown in Figure 2-7A. XIC of 1223.8 show two major peaks indicating that there are two major adduct on Fragment 1.

MSMS spectra for singly adducted Fragment 1, m/z 1438.2 is as shown in Figure 2-7B for Peak 1. All a_n-b_n ions up to a_5-b_5 have m/z similar to that of standard. Increase in m/z was observed for a_6-b_6, a_7-b_7, a_8-b_8. This indicates that the possible modification is on base 5, (CATGG*GCGGCATG). This was further confirmed with w_n ions. Increase in m/z for w_9 and w_{10} ions and all ions below w_8 have m/z similar to that of standard. Table showing the m/z for standard and adducted Fragment 1 is as shown in Table 2-8.

MSMS spectra for singly adducted Fragment 1, m/z 1438.2 is as shown in Figure 2-7C for Peak 2. All a_n-b_n ions up to a_5-b_5 have m/z similar to that of standard. Increase in m/z was observed for a_5-b_5, a_6-b_6, a_7-b_7 and a_8-b_8. This indicates that the possible modification is on base 4, (CATG*GGCGGCATG). This was further confirmed with w_n ions. Increase in m/z for w_{10} ion and all ions below w_9 have m/z similar to that of standard. Table showing the m/z for standard and adducted Fragment 1 is as shown in Table 2-8.

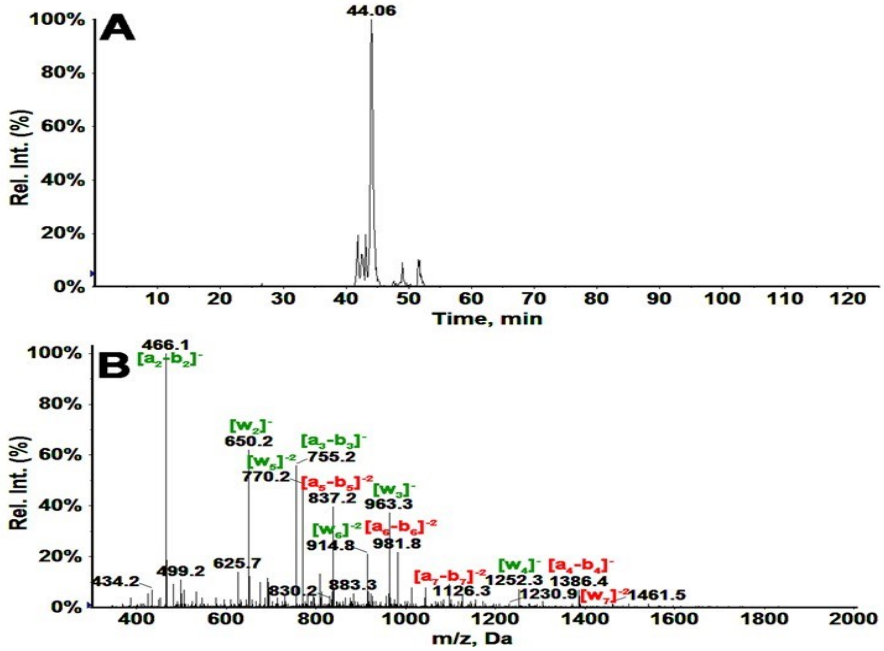

Figure 2-8. LC-MS of ds-32 bp exon 7 probe: (A) Extracted ion chromatogram of singly adducted Fragment 4, m/z 1012.6. (B) MSMS spectra of m/z 1012.6 showing the obtained a_n-b_n and w_n ions. Ions with m/z similar to standard are shown in green and ions with increased m/z shown in red.

Singly adducted Fragment 4 has an m/z of 1012.6 with a charge of -3. Extracted ion chromatogram of 1012.6 is as shown in Figure 2-8A. XIC of 1012.6 show one major peak indicating that there is one major adduct on Fragment 4. MSMS spectra for singly adducted Fragment 4, m/z 1012.6 is as shown in Figure 2-8B. All a_n-b_n ions up to a_3-b_3 have m/z similar to that of standard. Increase in m/z was observed for a_4-b_4, a_5-b_5, a_6-b_6, a_7-b_7 and a_8-b_8. This

indicates that the possible modification is on base 3, (CCG*CCCATG). This was further confirmed with w_n ions. Increase in m/z for w_7 ion and all ions below w_6 have m/z similar to that of standard. Table showing the m/z for standard and adducted Fragment 4 is as shown in Table 2-9.

Table 2-9. Calculated m/z for standard and singly adducted Fragment 4. (m/z highlighted in red were the ions with increased m/z compared to that of standard corresponding to BPDE adducted)

Fragment ion	m/z	
	Unadducted	Singly Adducted
a_2-b_2	$[466.1]^-$	$[466.1]^-$
a_3-b_3	$[755.2]^-$	$[755.2]^-$
a_4-b_4	$[1084.8]^-$	$[1386.4]^-$
a_5-b_5	$[1373.8]^-$	$[837.2]^{-2}$
a_6-b_6	$[1663.0]^-$	$[981.8]^{-2}$
a_7-b_7	$[975.6]^{-2}$	$[1126.3]^{-2}$
a_8-b_8	$[1132.2]^{-2}$	n/d
w_2	$[650.2]^-$	$[650.2]^-$
w_3	$[963.3]^-$	$[963.3]^-$
w_4	$[1252.5]^-$	$[1252.3]^-$
w_5	$[1541.7]^-$	$[770.2]^{-2}$
w_6	$[915.1]^{-2}$	$[914.8]^{-2}$
w_7	$[1079.4]^{-2}$	$[1230.9]^{-2}$

Singly adducted Fragment 3 has an m/z of 1234.4 with a charge of -6. Extracted ion chromatogram of 1234.4 is as shown in Figure 2-9A. XIC of 1012.6 show one major peak indicating that there is one major adduct on Fragment 3. MSMS spectra for singly adducted Fragment 3, m/z 1234.4 is as shown in Figure 2-9B. All a_n-b_n ions up to a_5-b_5 have m/z similar to that of standard. Increase in m/z was observed for a_6-b_6, a_7-b_7 and a_8-b_8 and w_{19}. This indicates that the possible modification is on base 5, (TGAGG*ATGGGCCTCCGGTTCATG). Table showing the m/z for standard and adducted Fragment 4 is as shown in Table 2-10.

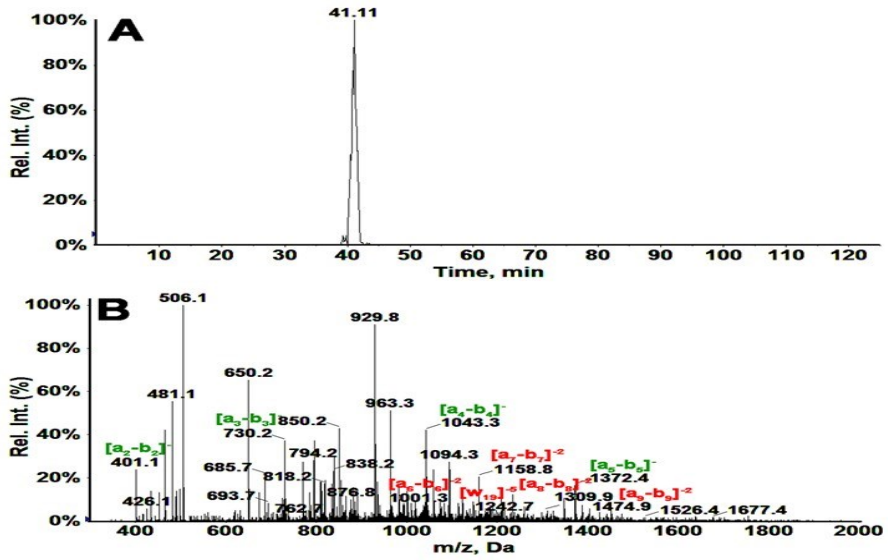

Figure 2-9. LC-MS of ds-32 bp exon 7 probe: (A) Extracted ion chromatogram of singly adducted Fragment 3, m/z 1234.4 (B) MSMS spectra of fragment ion m/z, 1234.4 showing the obtained a_n-b_n and w_n ions. Ions with m/z similar to standard are shown in green and ions with increased m/z shown in red

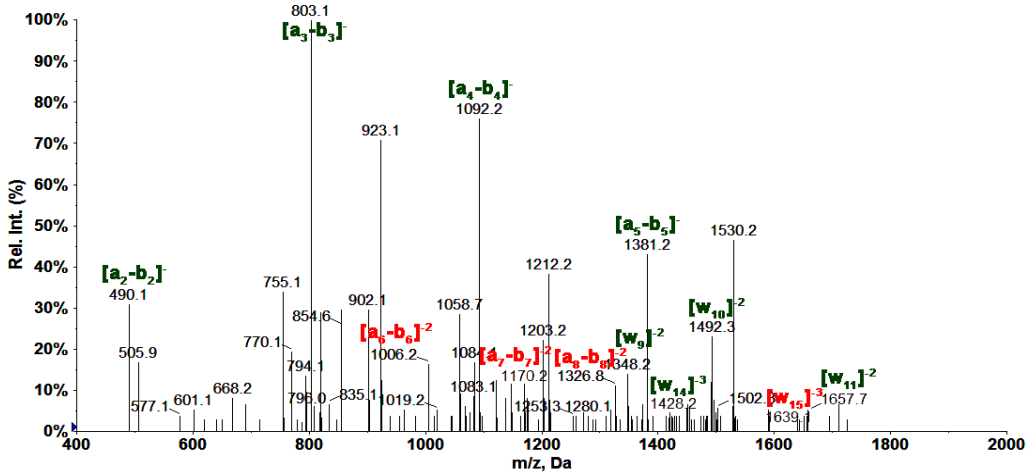

Figure 2-10. . LC-MS of ds-32 bp exon 7 probe: MS/MS spectrum of 1530.3 showing a_n-b_n and w_n ions. Ions with m/z similar to standard labeled in green and ions with increased m/z in red in 10mM Tris buffer, pH 7.4 and 0.1M NaCl

Table 2-10. Calculated m/z for standard and singly adducted DNA fragments of fragment 3. (m/z highlighted in red were the ions with increased m/z compared to that of standard corresponding to BPDE adducted)

Fragment ion	m/z	
	Unadducted	Singly Adducted Fragment
a_2-b_2	$[401.1]^-$	$[401.1]^-$
a_3-b_3	$[730.2]^-$	$[730.2]^-$
a_4-b_4	$[1043.3]^-$	$[1043.3]^-$
a_5-b_5	$[1372.4]^-$	$[1372.4]^-$
a_6-b_6	$[1702.0]^-$	$[1001.3]^{-2}$
a_7-b_7	$[1007.2]^{-2}$	$[1158.8]^{-2}$
a_8-b_8	n/d	$[1309.9]^{-2}$
a_9-b_9	$[1323.8]^{-2}$	$[1474.9]^{-2}$
w_{17}	$[1755.6]^{-3}$	n/d
w_{18}	$[1395.6]^{-3}$	n/d
w_{19}	$[1477.9]^{-4}$	$[1242.7]^{-5}$
w_{20}	$[1541.7]^-$	n/d
w_{21}	$[915.1]^{-2}$	n/d

Since the modification is relatively small in the adducted DNA fragments, we assume the adducted and unadducted fragments have only minor changes in electrospray ionization behavior and MS response. Relative abundance of specific adducted nucleobases within codons were estimated by comparing areas of the extracted ion chromatograms of adducted fragments to that of unadducted fragments, and these ratios were further compared with other adducted fragments ratios. Ratios of relative amounts of adduction in the 32 bp fragment for codons 248/244 was 1.5 and codons 248/243 was 1.3 with a relative standard deviation less than 6.5% (n=3). According to p53 handbook database,[13] the mutation frequency ratio of codons 248/243 is 24, 248/244 is 7, 248/249 is 2.7 and 248/245 is 2.1. Increased reactivity of codon 243 compared to p53 mutation frequency ratio may be related to guanine in codon 243 being the first guanine in our 32 bp fragment which may be more available for reaction due to its position near the end of the strand.

Table 2-11. Fragments of ds-32 bp exon 7 fragment with corresponding base adducted in comparison with the p53 database.[13]

Fragment Name	Sequence	LC-MS/MS DATA		Common Hot Spot Database[13-15,18]
		Base Adducted	Codon	
Fragment 1	**CATGGGCGGC ATG**	**CATG*GGCGGCATG**	**243**	**244[b], 245[a,d]**
		CATGG*GCGGCATG	**244[b]**	**244[b],245[a,d]**
Fragment 2	**AACCGGAGGC CCATCCTCA**	**AACCG*GAGGCCCA TCCTCA**	**248**	**248[a,b,c,d,e], 249[a,b]**
Complementary Strands				
Fragment 3	**TGAGGATGGGCCTCCGGTTCATG**		**TGAGG*ATGGGCCTCCG GTTCATG**	
Fragment 4	**CCGCCCATG**		**CCG*CCCATG**	

Note: Possible cancers due to BPDE a. Non Small Cell lung cancer, b. Small Cell lung cancer, c. Head and Neck cancer d. Colorectal cancer, e. Skin Cancer

2-5. DISCUSSION

The 32 bp p53 exon 7 fragment reacted with BPDE had all reactive bases as Gs, and the most frequently reacted guanine was in codon 248. Guanines within codons 243 and 244 were adducted to a lesser extent. Codon 248 is the major mutation hot spot for most tissue specific cancers such as lung, and head and neck. Thus, there is qualitative correlation of the high reactive frequency of codon 248 in our fragment with its high rate of mutation in many cancers, as well as the observed reactivity of codons 244 and 243. However, the relative mutation frequencies of codons 244 and 243 are lower that the relative reactivities we find in the 32 bp p53 fragment.

Differences in reactivity vs. mutation frequency in tumors at codons 244 and 245 is undoubtedly related to the complexity of living tumors and cell cultures as compared to our *in vitro* reaction system. In addition to complications from organ-based metabolism, which is

absent in our present reactions, differences may be due to DNA being bound to histones and other proteins *in vivo* as well as to in vivo DNA repair. Also, sequences in both 244 and 245 codons are GGC. Codon 243 is close to the end of the fragment, adjacent to an AT sequence, and may be partially unwound exposing the guanine adjacent to it due to fewer hydrogen bonds.[49] Codon 243 may thus be more reactive in the fragment than in the full *p53 gene.* Also, under *in vivo* conditions, a considerable fraction of cytosines are methylated which can mediate codon reactivity.[50,51] 5-Methyl cytosines increase the nucleophilicity of exocyclic amine of adjacent guanine as result of inductive electronic effects.[52] We are currently exploring this issue by additional experiments.

Covalent binding of BPDE preferentially targets guanines in DNA,[53,54] because guanine is the best nucleophile of all the DNA bases. The N7 position of guanine is the most nucleophilic site but the exocyclic amine group, also a good nucleophile, is the most favorable target for polyaromatic hydrocarbon diol epoxides like BPDE. This is because proximity of the N7 group to the hydrophilic sugar chain of the DNA makes it less susceptible to attack of hydrophobic pyrenyl moieties.[55-57]

All exocyclic amines of guanines in single stranded DNA are available for covalent reaction with BPDE. In double stranded DNA the exocyclic amines are involved in hydrogen bonding with the carbonyl oxygen atom of cytosine hence are not freely available for reactions with BPDE. Guanines specifically in the minor groove of duplex DNA can form covalent adducts with BPDE, thereby disrupting the hydrogen bonding between the GC base pair.[58-60]

As per p53 handbook, codon 247 is a hot spot for Melonoma and Skin Squamous Cell Carcinoma, admittedly with a small number of mutations. Although guanine is not in the codon,

the potential of BPDE to react with adenine exists. Since we did not find any adduction on any nucleobase within codon 247 in our study, selectivity of BPDE to guanines was further affirmed.

Our results are consistent with the fact that most damaged codons in tumors and cancer cell cultures involve guanines as the major site of attack by BPDE.[52,53,61] Guanines were also exclusive targets in the experiments with ss-oligonucleotides. Structural differences of ssDNA and dsDNA may play a role in sequence specific DNA damage. Short single stranded oligonucleotides used in our study have a more flexible structure unprotected with a complementary strand and featuring a free axis of rotation along the phosphodiester backbone.[62,63] Thus, while specificity would be expected to be much lower for ssDNA compared with that of dsDNA we still find that high mutation frequency codons 249 and 244 are highly reactive with BDPE in the short ss-fragments. These results suggest that the relative reactivity of the ds-DNA may be a combination of inherent chemistry of the codon sites and the ds- and higher structure of the DNA.

Double stranded DNAs are relatively inflexible due to GC and AT base pairing and double helical structure resulting in their complicated secondary and tertiary structures.[32] The double helical structure also features major and minor groves in duplex DNA. BPDE specifically attacks the electron donating exocyclic amine in the minor groove containing the nucleophilic GC base pair of DNA. Therefore reactivity of dsDNA will be different to that of ssDNA.[58,59] However in our experiments, we see that the ss-fragments and ds-32 bp fragment both have selective reactivity that includes codons with high frequency of mutation in p53. Thus, selectivity is different in the ss- and ds-fragments, but still exhibited by the single strands.

Very few studies thus far have focused on differential selectivity of specific base sequences.[64] Jernstroem, et. al suggest that guanines adjacent to or flanked by guanines are more

reactive[64-66] In contradiction, other studies predict that guanines flanked by pyrimidine bases are more reactive due to less steric effects as compared to guanines flanked by purine bases.[59,67-69] The reactive site of codon 248 in our 32 bp fragment is a guanine flanked by guanine, while codons 244 and 243 are guanines flanked by purine on one side and pyrimidine on the other side and show intermediate reactivity. Codon adduction sites in ss-DNA oligonucleotides are guanines sandwiched between one purine and one pyrimidine. Hence, our results are in qualitative agreement with the predictions quoted above. However, relating full guanine sequence specificity to adjacent bases is undoubtedly an oversimplification, and in addition to base sequence, specificity most likely involves complex structural and environmental factors *in vivo* including bound histones and proteins.

2-6. SUMMARY

In summary, we have described methodology to screen chemicals, drugs and metabolites for reactions with oligonucleotides to determine the most frequently adducted nucleobase within codons. Results show that LC-MS/MS and restriction enzymes can be used to prepare carcinogen modified oligonucleotides so as to identify the site of adduction on oligonucleotide fragments longer than 20 base pairs. Our 32 bp fragment reactions represent the first study of a p53 gene fragment representing more than 20 base pairs with multiple mutation hot spots. The highest reaction frequency was at codon 248, consistent with the highest mutation frequency of the p53 gene in many cancers. Also, BPDE reactivity found at codons 243 and 244 is consistent with these codons being mutated in tissue cancers. Chapter 3 will focus on effect of cytosine methylation on rate of BPDE adduction on Exon 7 of P53 gene using LC-MS/MS and Molecular modelling.

2-7. REFERENCES

1. Siegel, R. L.; Miller, K. D.; Jemal, A. Cancer statistics, 2016. *CA: a cancer journal for clinicians* **2016***, 66*, 7-30.

2. Haber, D.; Harlow, E. Tumor-suppressor genes: evolving definitions in the genomic age. *Nat. Genet.* **1997***, 16*, 320-322.

3. May, P.; May, E. Twenty years of p53 research: structural and functional aspects of the p53 protein. *Oncogene* **1999***, 18*, 7621-7636.

4. Isobe, M.; Emanuel, B. S.; Givol, D.; Oren, M.; Croce, C. M. Localization of gene for human p53 tumour antigen to band 17p13. *Nature* **1986***, 320*, 84-85.

5. Kern, S. E.; Kinzler, K. W.; Bruskin, A.; Jarosz, D.; Friedman, P.; Prives, C.; Vogelstein, B. Identification of p53 as a sequence-specific DNA-binding protein. *Science* **1991***, 252*, 1708-1711.

6. Matlashewski, G.; Lamb, P.; Pim, D.; Peacock, J.; Crawford, L.; Benchimol, S. Isolation and characterization of a human p53 cDNA clone: expression of the human p53 gene. *EMBO J.* **1984***, 3*, 3257-3262.

7. Maiuri, M. C.; Tasdemir, E.; Criollo, A.; Morselli, E.; Vicencio, J. M.; Carnuccio, R.; Kroemer, G. Control of autophagy by oncogenes and tumor suppressor genes. *Cell Death Differ.* **2009***, 16*, 87-93.

8. Soussi, T.; Wiman, K. G. Shaping genetic alterations in human cancer: the p53 mutation paradigm. *Cancer Cell* **2007***, 12*, 303-312.

9. Soussi, T. p53 alterations in human cancer: more questions than answers. *Oncogene* **2007***, 26*, 2145-2156.

10. Cheok, C. F.; Verma, C. S.; Baselga, J.; Lane, D. P. Translating p53 into the clinic. *Nat. Rev. Clin. Oncol.* **2011***, 8*, 25-37.

11. Pfeifer, G. P.; Besaratinia, A. Mutational spectra of human cancer. *Hum. Genet.* **2009***, 125*, 493-506.

12. Ozaki, T.; Nakagawara, A. p53: the attractive tumor suppressor in the cancer research field. *J. Biomed. Biotechnol.* **2011**, 603925, 1-13.

13. http://p53.free.fr/Database/p53_cancer_db.html (last accessed December 6, 2016).

14. Soussi, T. TP53 mutations in human cancer: database reassessment and prospects for the next decade. *Adv. Cancer Res.* **2011***, 110*, 107-139.

15. Leroy, B.; Anderson, M.; Soussi, T. TP53 Mutations in Human Cancer: Database Reassessment and Prospects for the Next Decade. *Hum. Mutat.* **2014***, 35*, 672-688.

16. Olivier, M.; Hussain, S. P.; Caron, d.,Fromentel Claude; Hainaut, P.; Harris, C. C. TP53 mutation spectra and load: a tool for generating hypotheses on the etiology of cancer. *IARC Sci. Publ.* **2004**, 247-270.

17. http://www.binfo.ncku.edu.tw/TAG/GeneFinder.php (Last accessed December 6, 2016)

18. States, J. C.; Ouyang, M.; Helm, C. W. Systems approach to identify environmental exposures contributing to organ-specific carcinogenesis. *Cancer Epidemiol* **2014***, 38*, 321-327.

19. Xiong, W.; Glick, J.; Lin, Y.; Vouros, P. Separation and Sequencing of Isomeric Oligonucleotide Adducts Using Monolithic Columns by Ion-Pair Reversed-Phase Nano-HPLC Coupled to Ion Trap Mass Spectrometry. *Anal. Chem. (Washington, DC, U. S.)* **2007***, 79*, 5312-5321.

20. Liao, Q.; Shen, C.; Vouros, P. GenoMass - a computer software for automated identification of oligonucleotide DNA adducts from LC-MS analysis of DNA digests. *J. Mass Spectrom.* **2009**, *44*, 549-560.

21. Chowdhury, G.; Guengerich, F. P. Tandem Mass Spectrometry-Based Detection of C4'-Oxidized Abasic Sites at Specific Positions in DNA Fragments. *Chem. Res. Toxicol.* **2009**, *22*, 1310-1319.

22. Chowdhury, G.; Guengerich, F. P. Liquid chromatography-mass spectrometry analysis of DNA polymerase reaction products. *Curr Protoc Nucleic Acid Chem* **2011**, *Chapter 7*, Unit 7.16.1-11.

23. Tretyakova, N.; Villalta, P. W.; Kotapati, S. Mass Spectrometry of Structurally Modified DNA. *Chem. Rev.* **2013**, *113*, 2395-2436.

24. Harsch, A.; Sayer, J. M.; Jerina, D. M.; Vouros, P. HPLC-MS/MS Identification of Positionally Isomeric Benzoc]phenanthrene Diol Epoxide Adducts in Duplex DNA. *Chem. Res. Toxicol.* **2000**, *13*, 1342-1348.

25. Chowdhury, G.; Guengerich, F. P. Direct detection and mapping of sites of base modification in DNA fragments by tandem mass spectrometry. *Angew. Chem. , Int. Ed.* **2008**, *47*, 381-384.

26. Sharma, V. K.; Glick, J.; Liao, Q.; Shen, C.; Vouros, P. GenoMass software: a tool based on electrospray ionization tandem mass spectrometry for characterization and sequencing of oligonucleotide adducts. *J. Mass Spectrom.* **2012**, *47*, 490-501.

27. Satterwhite, J. E.; Pugh, A. M.; Danell, A. S.; Hvastkovs, E. G. Electrochemical Detection of anti-Benzoa]pyrene Diol Epoxide DNA Damage on TP53 Codon 273 Oligomers. *Anal. Chem.* **2011**, *83*, 3327-3335.

28. Sharma, V. K.; Glick, J.; Liao, Q.; Shen, C.; Vouros, P. GenoMass software: a tool based on electrospray ionization tandem mass spectrometry for characterization and sequencing of oligonucleotide adducts. *J. Mass Spectrom.* **2012***, 47*, 490-501.

29. Sharma, V. K.; Xiong, W.; Glick, J.; Vouros, P. Determination of site selectivity of different carcinogens for preferential mutational hot spots in oligonucleotide fragments by ion-pair reversed-phase nano liquid chromatography tandem mass spectrometry. *Eur. J. Mass Spectrom.* **2014***, 20*, 63-72.

30. Bergonzo, C.; Galindo-Murillo, R.; Cheatham, T. E. Molecular modeling of nucleic Acid structure: electrostatics and solvation. *Curr Protoc Nucleic Acid Chem* **2014***, 55*, 7.9.1-7.9.27.

31. Kornyshev, A. A. Physics of DNA: unravelling hidden abilities encoded in the structure of 'the most important molecule'. *Phys. Chem. Chem. Phys.* **2010***, 12*, 12352-12378.

32. Cantor, C. R.; Schimmel, P. R. *Biophysical Chemistry - Part 1 The Conformation of Biological Macromolecules;* Freeman: 1980; pp. 155-201.

33. Chen, Z.; Zhang, G.; Chen, X.; Chen, J.; Liu, J. A label-free method for studying DNA sequence recognition of mitoxantrone based on resonance light-scattering technique. *J. Antibiot.* **2012***, 65*, 517-522.

34. Loechler, E. L. The role of adduct site-specific mutagenesis is understanding how carcinogen - DNA adducts cause mutations: perspective, prospects and problems. *Carcinogenesis* **1996***, 17*, 895-902.

35. Neilson, A. N.; Editor. *The Handbook of Environmental Chemistry, Volume 3: Anthropogenic Compounds, Part I: PAHs and Related Compounds: Chemistry;* Springer: 1997; pp. 41-45.

36. Gelboin, H. V. Benzoa]pyrene metabolism, activation, and carcinogenesis: role and regulation of mixed-function oxidases and related enzymes. *Physiol. Rev.* **1980**, *60*, 1107-1166.

37. Harvey, G. R. Metabolic activation, DNA binding, and mechanisms of carcinogenesis. *Polycyclic Aromatic Hydrocarbons: Chemistry and Carcinogenicity*, Cambridge University Press: New York, 1991, pp. 50-78.

38. http://monographs.iarc.fr/ENG/Classification/ (last accessed December 6, 2016).

39. Brahim, B.; Alves, S.; Cole, R. B.; Tabet, J. Charge enhancement of single-stranded dna in negative electrospray ionization using the supercharging reagent meta-nitrobenzyl alcohol. *J. Am. Soc. Mass Spectrom.* **2013**, *24*, 1988-1996.

40. Jung, V.; Pestka, S. B.; Pestka, S. Efficient cloning of PCR generated DNA containing terminal restriction endonuclease recognition sites. *Nucleic Acids Res.* **1990**, *18*, 6156.

41. Murray, K. K. DNA sequencing by mass spectrometry. *Journal of mass spectrometry* **1996**, *31*, 1203-1215.

42. Little, D. P.; Chorush, R. A.; Speir, J. P.; Senko, M. W.; Kelleher, N. L.; McLafferty, F. W. Rapid sequencing of oligonucleotides by high-resolution mass spectrometry. *J. Am. Chem. Soc.* **1994**, *116*, 4893-4897.

43. Potier, N.; Van Dorsselaer, A.; Cordier, Y.; Roch, O.; Bischoff, R. Negative electrospray ionization mass spectrometry of synthetic and chemically modified oligonucleotides. *Nucleic Acids Res.* **1994**, *22*, 3895-3903.

44. J. B. Fenn, M. Mann, C. K. Meng, S. F. Wong and C. M. Whitehouse, *Science,* 1989, **246**, 64-71.

45. http://mods.rna.albany.edu/masspec/Mongo-Oligo (last accessed December 6, 2016).

46. McLuckey, S. A.; Van Berker, G. J.; Glish, G. L. Tandem mass spectrometry of small, multiply charged oligonucleotides. *J. Am. Soc. Mass Spectrom.* **1992**, *3*, 60-70.

47. McLuckey, S. A.; Habibi-Goudarzi, S. Ion trap tandem mass spectrometry applied to small multiply charged oligonucleotides with a modified base. *J. Am. Soc. Mass Spectrom.* **1994**, *5*, 740-747.

48. Rozenski, J.; McCloskey, J. A. SOS: a simple interactive program for ab initio oligonucleotide sequencing by mass spectrometry. *J. Am. Soc. Mass Spectrom.* **2002**, *13*, 200-203.

49. Calladine, C.; Drew, H.; Luisi, B.; Travers, A. Twisting and Curving. In" Understanding DNA: The molecule and how it works", 3rd ed.; Elsevier Ltd, 2004; pp. 70-72.

50. Denissenko, M. F.; Chen, J. X.; Tang, M. S.; Pfeifer, G. P. Cytosine methylation determines hot spots of DNA damage in the human P53 gene. *Proc. Natl. Acad. Sci. U. S. A.* **1997**, *94*, 3893-3898.

51. Varley, K. E.; Gertz, J.; Bowling, K. M.; Parker, S. L.; Reddy, T. E.; Pauli-Behn, F.; Cross, M. K.; Williams, B. A.; Stamatoyannopoulos, J. A.; Crawford, G. E.; Absher, D. M.; Wold, B. J.; Myers, R. M. Dynamic DNA methylation across diverse human cell lines and tissues. *Genome Res.* **2013**, *23*, 555-567.

52. Guza, R.; Kotandeniya, D.; Murphy, K.; Dissanayake, T.; Lin, C.; Giambasu, G. M.; Lad, R. R.; Wojciechowski, F.; Amin, S.; Sturla, S. J.; Hudson, R. H.; York, D. M.; Jankowiak, R.; Jones, R.; Tretyakova, N. Y. Influence of C-5 substituted cytosine and related nucleoside analogs on the formation of benzo[a]pyrene diol epoxide-dG adducts at CG base pairs of DNA. *Nucleic Acids Res.* **2011**, *39*, 3988-4006.

53. Hermanson, G. *Nucleic acid and oligonucleotide conjugation and modification. Bioconjugate Techniques; 3rd* ed.; Audet. J., Preap, M., Eds.; Academic Press, 2013, 959-987.

54. Gates, K. S. An overview of chemical processes that damage cellular DNA: spontaneous hydrolysis, alkylation, and reactions with radicals. *Chem. Res. Toxicol.* **2009***, 22*, 1747-1760.

55. Beland, A. F., Poirier, M. C. *Methods to Assess DNA Damage and Repair: lnterspecies Comparisons*; Tardiff, R. G., Lohman, P. H., Wogan, G. N., Eds.; SCOPE, John Wiley & Sons: New York, 1994; *pp.* 29-55.

56. Baird, W. M.; Hooven, L. A.; Mahadevan, B. Carcinogenic polycyclic aromatic hydrocarbon-DNA adducts and mechanism of action. *Environ. Mol. Mutagen.* **2005***, 45*, 106-114.

57. Lenglet, G.; David-Cordonnier, M. H. DNA-Destabilizing Agents as an Alternative Approach for Targeting DNA: Mechanisms of Action and Cellular Consequences. *J. Nucleic Acids* **2010***, 290935,* 1-17.

58. Geacintov, N. E.; Cosman, M.; Hingerty, B. E.; Amin, S.; Broyde, S.; Patel, D. J. NMR solution structures of stereoisomeric covalent polycyclic aromatic carcinogen-DNA adducts: principles, patterns, and diversity. *Chem. Res. Toxicol.* **1997***, 10*, 111-146.

59. Penning, M., Poly Aromatic Hydrocarbons: Multiple Metabolic Pathways and the DNA Lesions formed. *The Chemical Biology of DNA Damage;* Geacintov, N. E., Broyde, S., Eds.; Wiley-VCH Verlag GmbH & Co. KGaA, 2010; pp 131-155.

60. Deligkaris, C.; Rodriguez, J. H. Non-covalent interactions of the carcinogen ( )-anti-BPDE with exon 1 of the human K-ras proto-oncogene. *Physical Chemistry Chemical Physics* **2014***, 16*, 6199-6210.

61. Pan, S.; Li, D.; Zhao, L.; Schenkman, J. B.; Rusling, J. F. Genotoxicity-Related Chemistry of Human Metabolites of Benzo [ghi] perylene (B [ghi] P) Investigated using Electro-Optical Arrays and DNA/Microsome Biocolloid Reactors with LC-MS/MS. *Chem. Res. Toxicol.* **2013***, 26*, 1229-1239.

62. Levitt, M. In *In Folding of nucleic acids;* Assoc. Sci. Publ: 1972; pp 147-71.

63. Lodish, H., Berk, A., Matsudaira, P., Kaiser, A. C., Krieger, M. Structure of Nucleic Acids. *Molecular Cell Biology*; 5th ed.; W. H. Freeman: New York, 2003; pp 102-107.

64. Jernström, B.; Gräslund, A. Covalent binding of benzo [a] pyrene 7, 8-dihydrodiol 9, 10-epoxides to DNA: molecular structures, induced mutations and biological consequences. *Biophys. Chem.* **1994***, 49*, 185-199.

65. Said, B.; Shank, R. C. Nearest neighbor effects on carcinogen binding to guanine runs in DNA. *Nucleic Acids Res.* **1991***, 19*, 1311-1316.

66. Rodriguez, F. A.; Cai, Y.; Lin, C.; Tang, Y.; Kolbanovskiy, A.; Amin, S.; Patel, D. J.; Broyde, S.; Geacintov, N. E. Exocyclic amino groups of flanking guanines govern sequence-dependent adduct conformations and local structural distortions for minor groove-aligned benzo[a]pyrenyl-guanine lesions in a GG mutation hotspot context. *Nucleic Acids Res.* **2007***, 35*, 1555-1568.

67. Musafija-Jeknic, T.; Luch, A.; Seidel, A.; Johns, C.; Pereira, C.; Baird, W. M. EFFECT OF NUCLEOTIDE SEQUENCE ON THE BINDING OF (–)–ANTI–DIBENZO–[a, l] PYRENE–11, 12–DIOL 13, 14–EPOXIDE TO SHORT OLIGODEOXYRIBONUCLEOTIDES. *Polycyclic Aromatic Compounds* **2005***, 25*, 103-111.

68. Schwartz, J. J.; Lau, H. H.; Baird, W. M. Base sequence selectivity in the binding of 7 (R), 8 (S)-dihydroxy-9 (S), 10 (R)-epoxy-7, 8, 9, 10-tetrahydrobenzo [a] pyrene to oligodeoxyribonucleotide duplexes. *Chem. Res. Toxicol.* **1994***, 7*, 29-40.

69. Margulis, L. A.; Ibanez, V.; Geacintov, N. E. Base-sequence dependence of covalent binding of benzo [a] pyrenediol epoxide to guanine in oligodeoxyribonucleotides. *Chem. Res. Toxicol.* **1993***, 6*, 59-63.

CHAPTER 3

Methyl-Cytosine-Driven Structural Changes Enhance Adduction Kinetics of an Exon 7 fragment of the p53 Gene

3-1. Abstract

Methylation of cytosine (C) at C-phosphate-guanine (CpG) sites enhances reactivity of DNA towards electrophiles. Mutations at CpG sites on the p53 tumor suppressor gene that can result from these adductions are in turn correlated with specific cancers. Here we describe the first restriction-enzyme-assisted LC-MS/MS sequencing study of the influence of methyl cytosines (MeC) on kinetics of p53 gene adduction by model metabolite benzo[a]pyrene-7,8-dihydrodiol-9,10-epoxide (BPDE), using methodology applicable to correlate gene damage sites for drug and pollutant metabolites with mutation sites. This method allows direct kinetic measurements by LC-MS/MS sequencing for oligonucleotides longer than 20 base pairs (bp). We used MeC and non-MeC (C) versions of a 32 bp exon 7 fragment of the p53 gene. Methylation of all 19 cytosines increased the rate constant 3-fold for adduction on G at the major reactive CpG in codon 248 vs. the non-MeC fragment. Rate constants for non-CpG codons 244 and 243 were not influenced significantly by MeC. Conformational and hydrophobicity changes in the MeC-p53 exon 7 fragment revealed by CD spectra and molecular modeling increase the BPDE binding constant to G in codon 248 consistent with a pathway in which preceding reactant binding greatly facilitates the rate of covalent S_N2 coupling.

3-2. Introduction

The p53 (or TP53) tumor suppressor gene codes for p53 protein that regulates cell division, cell death, genomic stability and suppresses cancer. P53 gene mutations occur in over 50% of human cancers,[1] and are located selectively in exons 5-8, and alter the p53 protein so as to minimize cancer protection. Furthermore, mutation sites are clearly correlated with specific cancers,[2,3] so that prediction of the most reactive p53 codons toward new chemicals and their metabolites could be a valuable tool to aid in toxicity and cancer prediction. Within the p53 gene, 42 CpG sites are methylcytosines (MeC),[4,5] and are the most frequently mutated codons or *hot spots.*[6,7] Non-CpG MeC related to GC>AT transitions are known in lung, head and neck cancer.[2,8]

Reactants such as benzo[a]pyrene-7,8-dihydrodiol-9,10-epoxide (BPDE), 7,12-dimethylbenz(a)anthracene diol epoxide, acrolein, and mitocin C, are more reactive towards MeCpG sites on the genes.[4,5] Limited repair of these reacted sites contributes to their role as mutational hot spots. Polyaromatic hydrocarbon (PAHs) metabolites preferentially react with MeCpG sites.[9] E.g., benzo[a]pyrene is metabolized to BPDE by a sequential pathway involving cytochrome P450s and epoxide hydrolase,[10,11] and reacts with DNA in S_N2 reactions to form nucleobase adducts that lead to mutations.[12] Previous studies of alkylated CpGs on DNA exon 5 analogs using [$^{15}N_3$, $^{13}C_1$]-labeled guanines and oligonucleotide hydrolysis revealed 2-3 fold increases in yields of BPDE adduction for MeCs.[13] MeCpG's also enhanced DNA-acrolein adduction 2-fold.[14,15] A 21-base pair (bp) oligonucleotide with a CpG site gave MeC-dependent voltammetry suggesting enhanced BPDE reactivity.[16] A 14 bp oligonucleotide with four MeCpG sites gave 3-4 fold increased adduction yields compared to unmethylated CpG.[17] In the 1990s, Geacintov measured strong non-covalent binding between BPDE and ds-poly(dG-dC).(dG-dC)

oligonucleotides and proposed enhanced subsequent coupling with MeCs related to stronger binding in a preceding step.[18,19] This model was supported by the studies of alkyl-C exon 5 analogs.[13]

We recently reported a restriction-enzyme-assisted LC-MS/MS DNA sequencing method that extends reactive codon measurements to ds-DNA lengths longer than 20-bp.[20] For a 32 bp exon 7 p53 duplex fragment, we found adduct yields for reaction with BPDE in the order of codons 248>243>244. In the present paper, we adapt this method for the first time to elucidate relationships between codon-specific reaction kinetics with metabolites, and evaluate the influence of subtle but important MeC-related p53 gene structure changes on reaction kinetics. This approach enabling studies of longer nucleotides that have been previously possible are amenable to uncover the influence of important structural changes relevant to the reactivity of the entire gene.

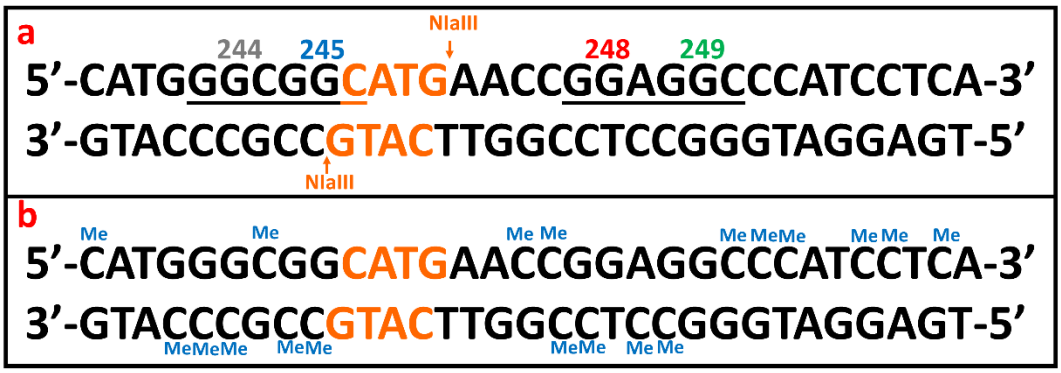

Scheme 3-1. Exon 7 32 bp fragment of p53 gene with major hot spots 244, 245, 248 and 249 labeled grey, blue, red and green. Restriction enzyme cleavage site CATG in orange a) all-C version b) MeC version, all Me except C in restriction enzyme cleavage site.

We compared a MeC form (19 MeCs) with a non-MeC form (Scheme 3-1) of the 32-bp exon 7 p53 fragment. G in codon 248 CpG had the largest rate constant, which was 3-fold for the MeC

version compared to all-C. Rate constants for reactive G's in non-CpG codons were 5-8 fold smaller than codon 248 MeCpG. Conformational and hydrophobicity changes in the MeC-p53 fragment revealed by circular dichroism (CD) and molecular modeling combine to increase the binding constant of BPDE at the codon 248 site to greatly facilitates the rate of the S_N2 coupling reaction in line with the preceding non-covalent binding pathway.

3-3. Experimental Section

3-3.1 Chemicals and Reagents. Benzo[a]pyrene-r-7,t-8-dihydrodiol-t-9,10-epoxide (±) (anti) (anti-BPDE) was from National Cancer Institute Chemical Carcinogen Reference Standard Repository. Triethylammonium bicarbonate (1.0 M, pH 8.6), HPLC-grade methanol, acetonitrile and water were obtained from Sigma Aldrich. Custom made 32 base oligonucleotide fragments exon 7 p53 that were methylation on all C's (MeC) or had no MeCs were from Sigma Aldrich. All oligonucleotides were HPLC purified and the mass of non-MeC forward fragment is 9820, reverse fragment is 9833 and for the MeC version, forward strand has a mass of 9961 indicating the presence of 10 MeC and for reverse strand 9960 indicating the presence of 9 MeC. Restriction enzyme NlaIII was from New England Biolabs.

Caution. Benzo[a]pyrene-r-7,t-8-dihydrodiol-t-9,10-epoxide (±) (anti) (anti BPDE) is a known chemical carcinogen. Protective measure like wearing gloves and protective eyewear were taken while doing experiment. All experiments were performed in a closed hood.

3-3.2 Reaction of Exon 7 Fragments with BPDE. 100 μg (~5 nmol) of ds-32 base pair exon 7 fragment is reacted with 50 nmol of BPDE in a total reaction volume of 150 μL, 10mM Tris

buffer pH 7.4 and 50 mM sodium chloride in the dark controlled at 25 ± 0.5 °C. This reaction was performed at various time intervals 2, 4, 6, 8, 12 and 24 hours for both unmethylated C and fully MeC versions of the ds-32 base pair exon 7 fragment. Reactions were stopped by adding cold acetonitrile and excess BPDE was removed using 3000 da molecular weight cut off filters (from EMD Millipore, UFC500396), which allows BPDE to pass through and DNA was collected from the filter as described previously.[20] These ds-32 base pair P53 gene fragments were subjected to restriction enzyme treatment and purification steps before subjected to LC-MS/MS analysis. All LC-MS/MS samples were run in triplicates.

3-3.3 Circular Dichroism. Circular dichroism experiments on the C and MeC ds-32 base pair exon 7 oligonucleotides were performed on Jasco spectrophotometer (J-710), in 10mM Tris buffer pH 7.4 and 50 mM sodium chloride. Parameter used within the spectrophotometer include sensitivity of 100mdeg, wavelength range 195nm to 230nm with a bandwidth of 5.0 nm.

3-3.4 Restriction enzyme treatment on ds-32 base pair DNA. Approximately 100 µg of ds-32 base pair was recovered from the reaction mixture and treated with 10 µL (100 units) of NlaIII enzyme, 20 µL of 10X NE buffer (from New England Biolabs) and the volume was made up to 200 µL with water. The reaction mixture was incubated at 37°C for 8 hours. DNA fragments were extracted from restriction enzyme reaction mixture using a previously described protocol using phenol/chloroform/isoamylalcohol, 25/24/1 and chloroform/isoamylalcohol, 24/1 to remove proteins. Briefly mixture of DNA and RE enzymes was vortexed with equal volume of phenol/chloroform/isoamyl alcohol for 15 min followed by centrifugation for 10 min, organic phase discarded and aqueous phase was collected (for 3 times), and then repeated the same

process with chloroform /isoamylalcohol (2 times). Finally the obtained DNA fragments from aqueous phase were subjected to desalting using Water's Oasis HLB cartridges (WAT094226) by solid phase extraction. Briefly cartridges were washed with methanol and water for equilibration followed by sample addition and washing the salts with 5% methanol and elution with 100 % methanol. Obtained samples were evaporated in a rotovap, re-dissolved in water and heated and cooled to obtain ss fragments. Stored at -20°C until use.

3-3.5 LC-MS/MS Analysis. Thermo Scientific Ultimate 3000 UPLC with Gemini C-18 column (0.5 mm ID and 3µ particle size and 150mm length) was used. A binary solvent system with 25 mM triethyl ammonium bicarbonate as buffer A and 100 % methanol as solvent B was used. Separation protocol was 0-3 % B (Methanol) for 3 min, then increased gradient from 3 to 27 % B (Methanol) for 24 min, then back to 3 % for 3 min. Between each run a wash is performed with gradient from 3% B isocratic for 2 min followed by 3-80 % B for 24 min followed by equilibrating back to 3 % for 4 min at 10 µL/min. m-Nitrobenzylalcohol was used via syringe pump post column through three way connector to increase the intensity and charge states of oligonucleotide fragments. Absciex Q-Tof and QTRAP 4000 instruments were used in negative mode. Product ion scanning was used for qualitative evaluation of site selective of BPDE-DNA adduction and multiple reaction monitoring (MRM) was used for the kinetic studies at a particular reactive site. For the AB Sciex QSTAR, -4500 ion spray voltage, -130 declustering potential and 300°C temperature was used with collision energy from -42 to -50 eV for MS/MS analysis. MRM on the QTRAP 4000 was done with ion spray voltage of -4500, curtain gas at 45 units, -115 V declustering potential and collision energy varying from -60 to -80 eV was used. All samples were run in triplicate.

The protocol for analyzing the 32 base pair p53 exon 7 fragments was described previously. Briefly, restriction enzyme NlaIII is used to cut the 32 bp DNA 4 smaller fragments for LC-MS/MS analysis. Product ion scan or collision induced dissociation (CID) was used to sequence the oligonucleotides. CID of oligonucleotides gives characteristic a_n-b_n and w_n ions. Comparing the MS/MS spectrum of un-adducted oligonucleotides with that of adducted oligonucleotides determines the exact site of adduction. Fragments obtained after restriction enzyme treatment for methylated 32 base pair DNA fragment are shown in Scheme 3-2.

Scheme 3-2. The four smaller fragments produced after restriction enzyme and heat treatment for 32 base pair MeC-exon 7 fragment.

3-3.6 Molecular modeling. A and B form's of 32-base pair P53 DNA was modeled using make-na software[21] and modified with cytosines methylated using Maestro software and minimized.[22] Solvated models of these modified oligonucleotides were created using CHIMERA software.[23,24] Amber solvation model was used for solvation with a box size of 1Å to accommodate water molecules. Autodock 4.2.6 was used for docking studies. Prepared biomolecule (Solvated MeC and C 32 base pair exon 7 fragment) were imported into the software. Lamarckian genetic algorithm (LGA) was used in Autodock 4.2.6 to find binding energy between the gene fragments and BPDE. Grid or volume for docking studies were kept constant for all the confirmations and set to be at maximum. Binding energies, binding constants and the distance between the

exocyclic amine of the reactive guanine and epoxide carbon of BPDE were calculated.[33] Steps for molecular modeling are given below.

STEPS

A and B form's of 32-base pair P53 DNA was modelled using make-na software and modified with cytosines methylated using Maestro software and minimized. Solvated models of these modified olignucloetides were created using CHIMERA software. Amber solvation model was used for solvation with a box size of 1Å to accommodate water molecules.

Autodock 4.2.6 was used for docking studies. Prepared biomolecule (Solvated MeC and C 32 base pair exon 7 fragment) were imported into the software. Lamarckian genetic algorithm (LGA) was used in Autodock 4.2.6 to find binding energy between the gene fragments and BPDE. Grid or volume for docking studies were kept constant for all the confirmations and set to be at maximum (126X x 126Y x 126Z dimensions). Binding energies, binding constants and the distance between the exocyclic amine of the reactive guanine and epoxide carbon of BPDE were calculated.[25]

Procedure for Docking

1. Import the biomolecule
2. Add Hydrogens to the biomolecule
3. Compute gasteiger charges
4. Now input the Ligand
5. Save the output format of the ligand to be in PDBQT (autodock suitable format)
6. Preparation for grid
    a. Choose Macromolcule (32 bp DNA)
    b. Save as PDBQT

c. Choose ligand (from set map types)

d. Set grid size (maximum grid size used for our study 126 X 126 X 126).

e. Save out put file as .gpf (grid format for autodock).

f. Run autogrid from run option.

7. Docking

a. Select macromolecule and ligand similar to above from docking menu.

b. Search Paparmeters given as # of GA runs to be 100, population size 150, maximum evaluations 250000, maximumber of generations 27000 and other factors kept default. Accept the parameters.

c. Docking parameter kept default.

d. Output saved as default.

e. Run autodock from run menu.

3-4. Results and Discussion

BPDE was reacted with an exon 7 fragment in solution, the BPDE-adducted oligonucleotide is cut by restriction enzyme NlAIII, then denatured by heat to obtain 4 single strand (ss) fragments (Scheme 3-1) that were analyzed by LC-MS/MS sequencing. MS/MS spectra of undamaged fragments were compare to that of singly adducted fragments to identify BPDE-adducted strands (Table 3-1). The extracted ion chromatogram (XIC) for singly adducted methylated ss-Fragment 2, m/z 1038.5 z = -6 (Figure 3-1a) shows a single peak, indicating only one singly-adducted fragment 2 for the MeC exon 7 fragment. The MS/MS spectrum (Figure 3-1b) shows a_n-b_n values similar to the undamaged MeC exon 7 up to a_5-b_5 and an increase in m/z from a_6-b_6 and above indicating adduction on the 5^{th} base.

(AA^{Me}C^{Me}CG*GAGG^{Me}C^{Me}C^{Me}CAT^{Me}C^{Me}CT^{Me}CA, * = adduction site). This is confirmed by w ions similar to unreacted MeC fragment up to w_{14} with an increase in w_{15} (Table 3-2). Similar MS/MS spectra were analyzed for Fragment 1. (see Figure 3-2 & Table 3-3. MS/MS spectra indicated two positional isomers for singly adducted fragment 1: (^{Me}CATGG*G^{Me}CGGCATG) and (^{Me}CATG*GG^{Me}CGGCATG).

Table 3-1. Calculated m/z for fragment 1, fragment 2, fragment 3 and fragment 4 for unadducted and singly adducted (increase in mass of 302.323, BPDE) of methylated, unmethylated versions of 32 base pair exon 7 fragment. Unmodified cytosine in methylated version shown in red. m/z obtained for each fragment is highlighted in bold.

CATGGGCGGCATG Fragment 1				
z	**C**	**C Add**	**MeC**	**MeC Add**
1	4014.6	4316.9	4042.6	4344.9
2	2006.8	2158.0	2020.8	2171.9
3	1337.5	1438.3	1346.9	1447.6
4	**1002.9**	**1078.5**	**1009.9**	**1085.5**
5	802.1	862.6	807.7	868.2
6	668.3	718.6	672.9	723.3
7	572.7	615.8	576.7	619.8

AACCGGAGGCCCATCCTCA, Fragment 2				
z	**C**	**C Add**	**MeC**	**MeC Add**
1	5821.8	6124.1	5933.8	6236.1
2	2910.4	3061.5	2966.4	3117.5
3	1939.9	2040.7	1977.2	2078.0
4	1454.7	1530.3	1482.7	1558.3
5	1163.547	1224.012	1185.9	1246.4
6	**969.4**	**1019.8**	**988.1**	**1038.5**
7	830.8	874.006	846.8	890.

CCGCCCATG, Fragment 3				
Z	**C**	**C Add**	**MeC**	**MeC Add**
1	2738.8	3041.0	2808.7	3111.0
2	1368.9	1520.0	1403.8	1555.0
3	**912.3**	**1013.0**	**935.6**	**1036.3**
4	683.9	759.5	701.4	777.0
5	546.9	607.4	560.9	621.4
6	455.6	506.0	467.3	517.7
7	390.4	433.6	400.4	443.6
8	341.5	379.2	350.2	388.0

TGAGGATGGGCCTCCGGTTCATG, Fragment 4				
Z	**C**	**C Add**	**MeC**	**MeC Add**
1	7110.6	7413.0	7166.7	7469.0
2	3554.8	3706.0	3582.8	3734.0
3	2369.5	2470.3	2388.2	2489.0
4	1776.9	1852.5	1790.9	1866.5
5	1421.3	1481.8	1432.5	1493.0
6	**1184.3**	**1234.6**	**1193.6**	**1243.9**
7	1014.9	1058.1	1022.9	1066.1
8	887.9	925.7	894.9	932.7

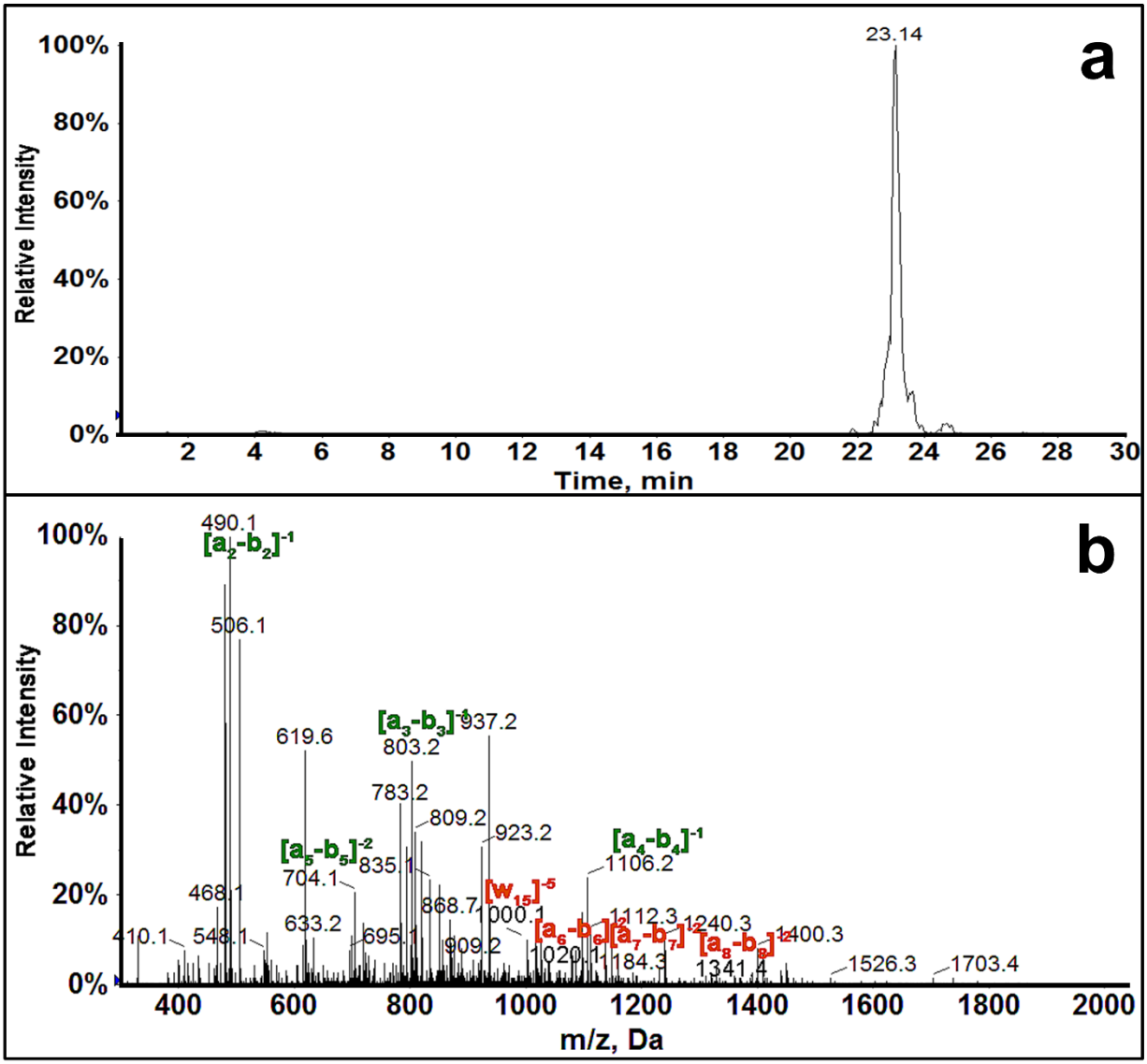

Figure 3-1. LC-MS/MS of sub-Fragment 2 of methylated version of 32 base pair exon 7 fragment. a) Extracted ion chromatogram of sub-Fragment 2, m/z 1038.5 with z = -6. b) MS/MS spectra of 1038.5 m/z ion eluting at 23.14 min.

Table 3-2: MS/MS fragment ions (a_n-b_n and w_n ions) for fragment 2 obtained. Increase in m/z for a_n-b_n and w_n ions indicating BPDE adduction shown in red.

Ion	NonMeC Fragment 2	MeC Fragment 2
a_2-b_2	$[490.1]^{-1}$	$[490.1]^{-1}$
a_3-b_3	$[803.2]^{-1}$	$[803.2]^{-1}$
a_4-b_4	$[1106.2]^{-1}$	$[1106.2]^{-1}$
a_5-b_5	$[704.2]^{-2}$	$[704.2]^{-2}$
a_6-b_6	$[869.0]^{-2}$	$[1020.2]^{-2}$
a_7-b_7	$[1033.6]^{-2}$	$[1184.7]^{-2}$
a_8-b_8	$[1190.2]^{-2}$	$[1341.4]^{-2}$
w_{13}	$[1009.8]^{-4}$	$[1009.8]^{-4}$
w_{14}	$[1092.2]^{-4}$	$[1092.2]^{-4}$
w_{15}	$[939.4]^{-4}$	$[1000.1]^{-5}$
w_{16}	n/d	$[1060.4]^{-5}$
w_{17}	n/d	$[1404.6]^{-4}$

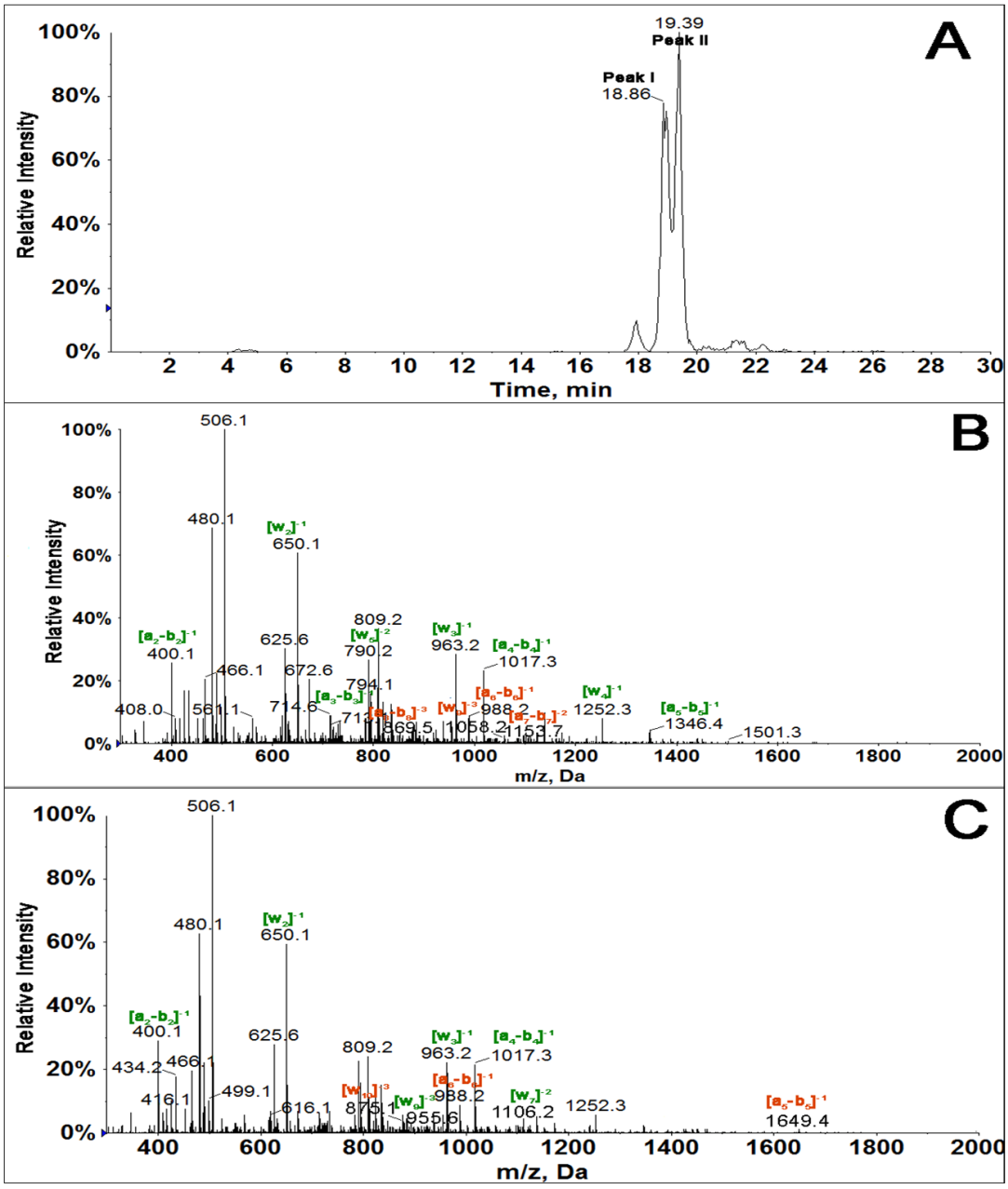

Figure 3-2. LC-MS/MS of Fragment 1 of MeC 32 base pair exon 7 fragment. A) Extracted ion chromatogram of Fragment 1, m/Z 1085.4 with a charge of -4 B) MS/MS spectra of 1085.4 m/z fragment ion eluting at 18.86 min (Peak I) C) B) MS/MS spectra of 1085.4 m/z fragment ion eluting at 19.39 min (Peak II)

Table 3-3: MS/MS fragment ions (a_n-b_n and w_n ions) for fragment 1 obtained. Increase in m/z for a_n-b_n and w_n ions indicating BPDE adduction shown in red.

Ion	NonMeC Fragment 1	MeC-Frag1 Peak 1	MeC-Frag1 Peak II
a_2-b_2	$[400.1]^{-1}$	$[400.1]^{-1}$	$[400.1]^{-1}$
a_3-b_3	$[713.5]^{-1}$	$[713.5]^{-1}$	$[713.5]^{-1}$
a_4-b_4	$[1017.3]^{-1}$	$[1017.3]^{-1}$	$[1017.3]^{-1}$
a_5-b_5	$[1346.4]^{-1}$	$[1346.4]^{-1}$	$[1649.4]^{-1}$
a_6-b_6	$[837.2]^{-2}$	$[988.2]^{-2}$	$[988.2]^{-2}$
a_7-b_7	$[1002.1]^{-2}$	$[1153.7]^{-2}$	$[1153.7]^{-2}$
a_8-b_8	$[768.8]^{-3}$	$[869.5]^{-3}$	$[869.5]^{-3}$
w_2	$[346.1]^{-1}$	$[346.1]^{-1}$	$[346.1]^{-1}$
w_2	$[650.1]^{-1}$	$[650.1]^{-1}$	$[650.1]^{-1}$
w_3	$[963.2]^{-1}$	$[963.2]^{-1}$	$[963.2]^{-1}$
w_4	$[1252.3]^{-1}$	$[1252.3]^{-1}$	$[1252.3]^{-1}$
w_5	$[790.2]^{-2}$	$[790.2]^{-2}$	$[790.2]^{-2}$
w_6	$[954.7]^{-2}$	$[954.7]^{-2}$	$[954.7]^{-2}$
w_7	$[1106.3]^{-2}$	$[1106.3]^{-2}$	$[1106.3]^{-2}$
w_8	$[847.2]^{-3}$	$[847.2]^{-3}$	$[847.2]^{-3}$
w_9	$[955.6]^{-3}$	$[1058.2]^{-3}$	$[955.6]^{-3}$
w_{10}	$[1066.6]^{-3}$	n/d	$[875.1]^{-4}$
w_{11}	$[1168.1]^{-3}$	[951.6]	n/d

Kinetics. Multiple reaction monitoring (MRM) was then used to quantify BPDE adduction at each reactive codon vs. reaction time. Transitions were selected specific to the ss-fragment monitored (Table 3-4). For example, transition 1085.4→650.0 for singly adducted MeC fragment 1, and 1009.9→650.0 for unadducted fragment 1. Here 1085.4 and 1009.9 are m/z of precursor ions of single adducted fragment 1 and unadducted fragment 1, respectively, with charge -4. M/z 650.0 represents the product ion of precursor 1085.4 (Figure 3-2 b&c) which is also the major transition for the unadducted precursor ion, m/z 1009.9.

Table 3-4: MRM Transition selected for quantitation of methylated, unmethylated and single adducted version of 32 base pair exon 7 fragment of 53 gene.

Un Methylated	**Methylated**
1048->383 = Internal Standard	1048->383 = Internal Standard
1078.5->650 = Adducted Fragment 1	1085->650 = Adducted Fragment 1
1003->650 = Fragment 1	1009.9->650 = Fragment 1
1224>923 = Adducted Fragment 2	890->803 = Adducted Fragment 2
1163.5->923 = Fragment 2	846.8->803 = Fragment 2
1184.3->730 = Adducted Fragment 3	1066->650 = Adducted Fragment 3
1234.6->730 = Fragment 3	1022.9->650 = Fragment 3
1013->755 = Adducted Fragment 4	1036->650 = Adducted Fragment 4
912->755 = Fragment 4	935->650 = Fragment 4

The relative amount of BPDE adduction was measured as ratio of peak area for XIC of adducted fragment to total peak area of the corresponding adducted+unadducted fragment. Relative amounts of BPDE adduction were plotted vs. time for G's in codons 248, 244 and 243 (Figure 3-3a).

Expressions in eq (1) define k_1 as the pseudo-first order rate constant, and k_2 as the second order rate constant, where C_o is initial amount of unreacted exon 7 fragment and C the amount unreacted at time t. Linear plots that fit eq 1 were obtained (Figure 3-3b), as shown for codon 248 for MeC and all C exon 7 fragments. We obtained k_1 from the slopes, and k_2 from k_1 (eq 1).

$$ln\ C = ln\ C_o - k_1 t\ ; \quad k_2 = k_1/[BPDE] \quad (1)$$

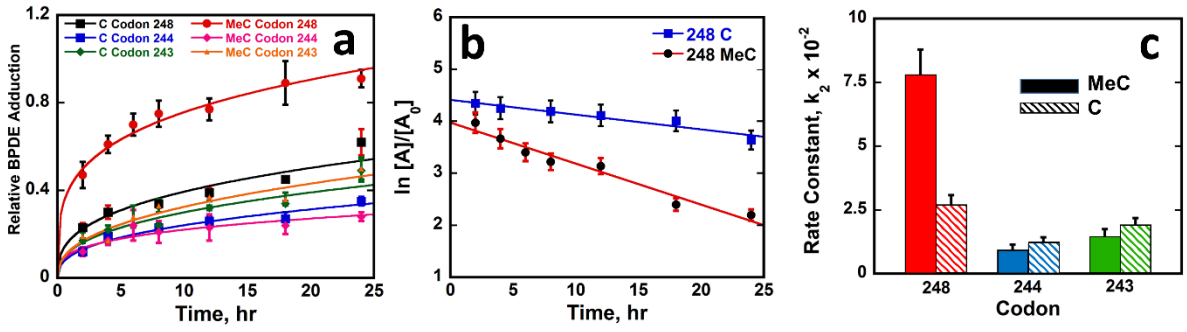

Figure 3-3. Kinetic study of BPDE adduction on MeC and all-C 32 bp p53 exon 7 gene fragments: a) Relative amount of BPDE adducted to guanine within codons 248, 244 and 243. b) Rate plots showing natural log of relative amount of undamaged oligo fragments (*ln [A]/[A₀]*) vs time. c) Bar graph showing comparative rate constants k_2 ($s^{-1}M^{-1}$) calculated from the slope of rate plots for BPDE adduction. Error bars represent SD for n=3.

Kinetic results show that k_2 for BPDE adduction on codon 248 CpG is nearly 3-fold larger for the MeC fragment vs. C-only (Figure 3c, Table 3-5). Rate constants for non-CpG adduct at codons 244 and 243, are ~20% smaller for MeC vs C-only, but differences are not statistically significant. The k_2 ratio of the MeC oligonucleotide for codons 248/244 is ~9, close to ratio of mutational frequencies in the p53 gene.[2] For MeC exon 7 (Table 3-5)., codon 248/243 k_2 ratio is 5.3 while the mutation ratio is a bit larger at 24. These results demonstrate the influence of MeC on CpG sites like codon 248 in the p53 gene to greatly increase reaction rates of MeCpG sites. Results show negligible influence of MeC on reactive non-CpG guanines.

Table 3-5. Rate constants k_1 and k_2 and ratios for different reactive sites.

Rate Constant	MeC Codon			C Codon		
	248	**244**	**243**	**248**	**244**	**243**
k_1, s^{-1} ($x10^6$)	26±3	3.0±0.7	4.8±1.0	9.0±1.3	4.0±0.7	6.3±0.9
k_2, $s^{-1}M^{-1}$ ($x10^2$)	7.8±1.0	0.9±0.2	1.4±0.3	2.7±0.4	1.2±0.2	1.9±0.3
Rate Constant Ratios						
Me-C/C	**Ratio**	**Me-C/Me-C Codon**		**C-C Codon**		
248	2.9	**248/244** 8.7		**248/244** 2.2		
244	0.8	**248/243** 5.4		**248/243** 1.4		
243	0.8					

Note. Rate constants k_1, for codon 244 and 243 in the methylated fragments are not significantly different according to t-test at 95% confidence interval.

Structural Analysis. Additional studies were aimed at molecular interpretation of the kinetics. Circular dichroism (CD) spectra of full MeC and C-only versions of the exon 7 fragments (Figure 3-4), suggest different conformations. The MeC exon 7 has an intense negative CD peak at 210 nm and an intense positive peak near 270 nm similar to a pure A-DNA structure,[26] but also a minimum near 245 nm characteristic of B-DNA. For the non-MeC exon 7, the first minimum is shifted to longer wavelength and is weaker, and a maximum at 265 nm is broad, with a shoulder at ~285 nm more characteristic of B DNA[26] (Figure 3-4). We interpret both CD spectra in terms of mixed A-B DNA structures, with MeC's driving structure toward the A.

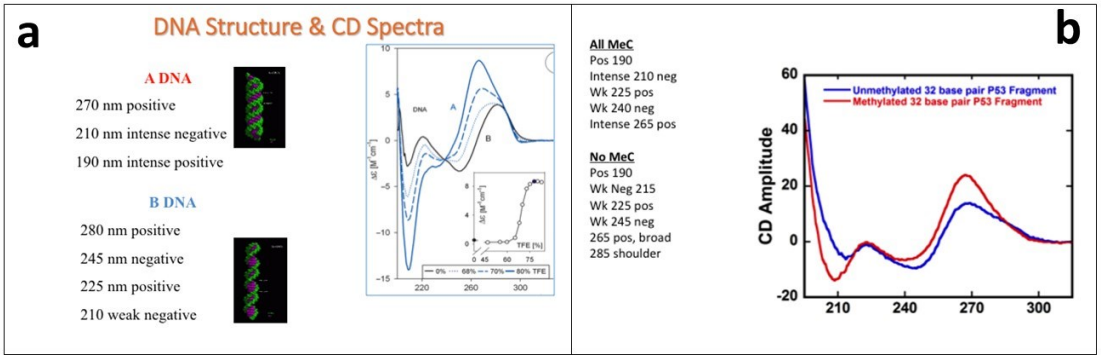

Figure 3-4. a) Circular dichroism showing transition from A to B form of DNA. Reproduced from J. Kypr et. al., *Nucleic Acid Research,* 2009, *37,* 1713-1725. B) Interpretation of CD spectra of the P53 exon fragment in terms of A and B-DNA. Results suggest transition from mixed A- and B-DNA towards more A-DNA content upon methylation of C's.

Molecular Modeling. A and B forms of Me-C and C versions of exon 7 were constructed and molecular modeling was done using Autodock software. Structures were solvated with water and docked with the most reactive isomer (+)anti-BPDE. BPDE conformations at optimal docking sites were in the minor groove close to codon 248 for conformations with the most negative binding free energy. Conformations with distances between reactive exocyclic amine of G in codon 248 and the epoxide carbon of BPDE less 4.5 Å were considered, due to probability of subsequently forming covalent bonds. Optimal binding of BPDE to guanine in codon 248 (Figure 3-5) gave binding free energies (ΔG_b) for B and A conformations (Table 3-6) which were used to calculate binding constants (K_b) from $K_b = -\Delta G_b/RT$, where R is the ideal gas constant and T in Kelvin. Larger K_b's were found for MeC versions in both A and B form of DNA compared to all-C counterparts. For conformations approximating experimental ones, MeC A-form had 5-fold higher K_b than all-C A-form. Smaller interatomic distances of reactive atoms were found in A-form of DNA (Figure 3-5, Table 3-6) indicating better accessibility for BPDE,

with the smallest distance for the MeC A-form. Docking studies were also done with (-) anti BPDE, which gave qualitatively similar results but less dramatic K_b differences. As a control, we modeled BPDE binding to ds-poly(dG-dC).(dG-dC) oligonucleotides with all MeCs and all C, and found 5-fold larger K_b for MeC version similar to experimental measurements.[18] Thus, modeling of MeC exon 7 fragment as an A DNA structure and all-C version closer to B DNA agreed well with a pathway featuring preceding non-covalent binding of BPDE in the minor groove near codon 248 that "sets up" subsequent fast S_N2 covalent coupling.

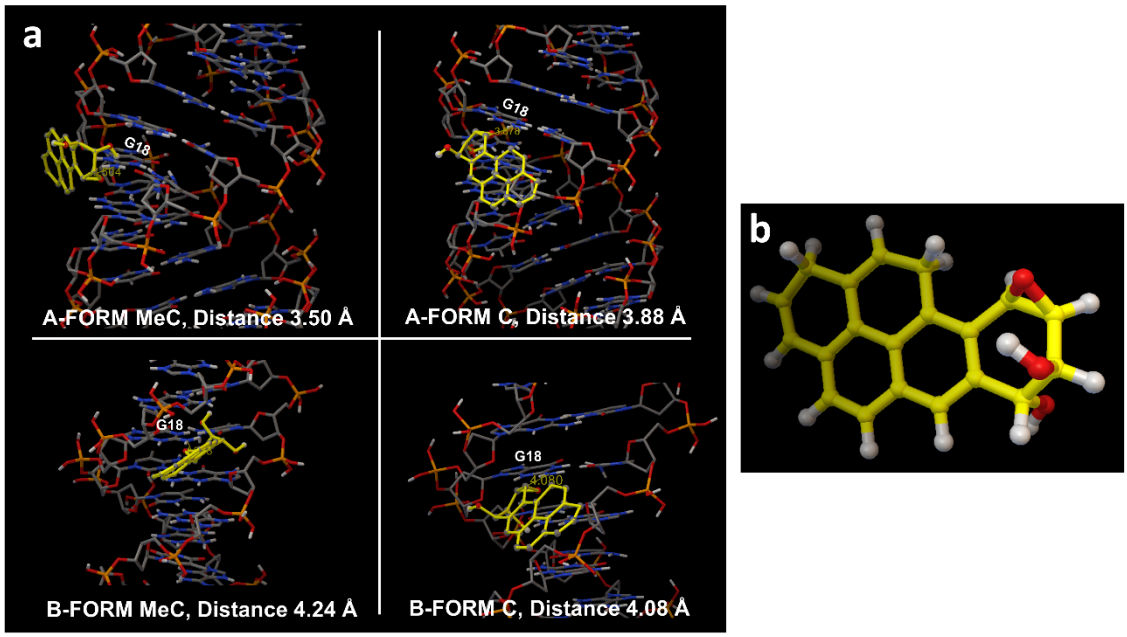

Figure 3-5. a) Models of BPDE docked close to reactive guanine in codon 248 in A and B forms of the 32 bp exon 7 p53 fragment in MeC and C versions. Distance is between exocyclic amine of reactive G and epoxide carbon in Å. (Water is removed for clarity; solvated models with water in SI.) b) Model of Benzo[a]pyrene-r-7,t-8-dihydrodiol-t-9,10-epoxide (+) (anti)

Table 3-6. Computed binding free energies, binding constant and distance between exocyclic amine of reactive G in codon 248 and epoxide carbon of BPDE.

DNA	Binding Energy kcal.mol^{-1}, ΔG	Binding Constant, K_b, M^{-1},	Distance, Å
B Form-C	-3.47	3.48×10^2	4.08
B Form-MeC	-4.10	1.00×10^3	4.24
A Form-C	-3.84	6.58×10^2	3.88
A Form-MeC	-4.80	3.32×10^3	3.50

It's very likely that stronger binding to the A DNA-like structure of the MeC exon 7 is also influenced considerably by hydrophobic interactions that increase for A DNA-like MeC oligonucleotides. An indirect indication of this effect was found in preliminary modeling studies without water, in which similar trends were found in K_b for systems in Figure 3-5, but K_b differences between A MeC and B all-C forms were much smaller. We thus attribute a part of the increases in K_b (Table 3-6) for both the A and B forms of the MeC p53 fragments to the hydrophobic influence on water structure that tends to increase affinity of BPDE for the codon 248 minor groove.

Our findings of B-like to A-like structural changes for conversion from the C→MeC exon 7 duplexes are consistent with earlier literature.[27,28] Crystalized oligonucleotides are predominantly B DNA, but can transition to dehydrated A-forms upon methylation when rich in CG regions, and intermediate structures between A and B have been crystallized.[29,30] The A form

has a wider minor groove that provides better accessibility for BPDE.[26] This enables a shorter distance for the reactive exocyclic amine of G to the epoxide carbon of BPDE in A-form than in B form (Table 3-6). Earlier computations showed that epigenetic modifications alter the structure of the DNA making sites of adduction more accessible.[31-34]

Methods utilized above provide a straightforward approach to directly study kinetics of gene damage reactions. Results suggest that methylcytosines, which predominate in tumor suppressor genes,[4] and influence the kinetics of S_N2 reactions with BPDE mainly at CpG sites of tumor suppressor genes. In the p53 exon 7 fragment studied, codons 248, 244 and 243 were the reactive sites for MeC and all-C versions. Codon 248, the featuring CpG, gave the fastest reaction with the MeC fragment reacting 3-fold faster than the non-MeC version (Table 3-5). CD spectra and computation modeling uncovered a change in conformation from a mixed A-B to a more A-like duplex structure that drives free-energy for noncovalent binding of BPDE in the codon 248 region more negative for the MeC version, due to better access to the minor groove site and increased hydrophobicity. The resulting larger k_b most likely lowers activation free energy to contribute significantly to the faster kinetics of S_N2 coupling of BPDE to MeCpG in codon 248. The structural change does not significantly influence non-CpG codons 244 and 243 that have similar kinetics for MeC and C versions. The hydrolysis-free methodology used here to measure direct kinetics of damage by metabolites to oligonucleotides longer than 20 bp is applicable to correlate gene damage sites for drug and pollutant metabolites with mutation sites. We speculate that these longer nucleotides are more amenable than shorter fragments to uncover the influence of important structural changes relevant to the reactivity of the entire gene.

3-5. Conclusion

Methodology described is directly adaptable to other chemicals and other tumor suppressor gene fragments to investigate kinetics of their DNA damage reactions. Molecular dynamics modeling can be used as an auxiliary tool to gain a more complete assessment of the chemistry of the associated reaction events. This quantitative methodology can be adapted to multiple chemicals and multiple exons across multiple tumor suppressor genes to expanding knowledge of genotoxicity chemistry pathways in relation to organ specificity of carcinogenesis. Next chapter focuses on development of Magnetic bio-colloid based technology coupled with LC-MS/MS for screening chemicals/prodrugs which require metabolic activation to cause DNA toxicity and co-relation with organ specific cancer.

3-6. References

1. Levine, A. J.; Oren, M. The first 30 years of p53: growing ever more complex. *Nature Reviews Cancer* **2009***, 9*, 749-758.

2. http://p53.free.fr/Database/p53_database.html, last accessed 12/06/2016.

3. http://p53.iarc.fr/TP53SomaticMutations.aspx, last accessed 12/06/2016.

4. Jabbari, K.; Bernardi, G. Cytosine methylation and CpG, TpG (CpA) and TpA frequencies. *Gene* **2004***, 333*, 143-149.

5. Bird, A. DNA methylation patterns and epigenetic memory. *Genes Dev.* **2002***, 16*, 6-21.

6. Tornaletti, S.; Pfeifer, G. P. Complete and tissue-independent methylation of CpG sites in the p53 gene: implications for mutations in human cancers. *Oncogene* **1995***, 10*, 1493-1499.

7. Denissenko, M. F.; Chen, J. X.; Tang, M. S.; Pfeifer, G. P. Cytosine methylation determines hot spots of DNA damage in the human P53 gene. *Proc. Natl. Acad. Sci. U. S. A.* **1997***, 94*, 3893-3898.

8. Kouidou, S.; Agidou, T.; Kyrkou, A.; Andreou, A.; Katopodi, T.; Georgiou, E.; Krikelis, D.; Dimitriadou, A.; Spanos, P.; Tsilikas, C. Non-CpG cytosine methylation of p53 exon 5 in non-small cell lung carcinoma. *Lung Cancer* **2005***, 50*, 299-307.

9. Patel, Y. M.; Park, S. L.; Carmella, S. G.; Paiano, V.; Olvera, N.; Stram, D. O.; Haiman, C. A.; Le Marchand, L.; Hecht, S. S. Metabolites of the Polycyclic Aromatic Hydrocarbon Phenanthrene in the Urine of Cigarette Smokers from Five Ethnic Groups with Differing Risks for Lung Cancer. *PloS one* **2016***, 11*, 1-15.

10. Nelson, D. R. Cytochrome P450: Structure, Mechanism, and Biochemistry, (ed. Paul R. O.) 183-245 (Kluwer Academic/Plenum Publishers, 2005).

11. Wasalathanthri, D. P.; Malla, S.; Bist, I.; Tang, C. K.; Faria, R. C.; Rusling, J. F. High-throughput metabolic genotoxicity screening with a fluidic microwell chip and electrochemiluminescence. *Lab on a Chip***2013***, 13*, 4554-4562.

12. Yang, S. K.; Deutsch, J.; Gelboin, H. V. Benzo (a) pyrene metabolism: activation and detoxification. *Polycyclic Hydrocarbons and Cancer* **2012***, 1*, 205-232.

13. Guza, R.; Kotandeniya, D.; Murphy, K.; Dissanayake, T.; Lin, C.; Giambasu, G. M.; Lad, R. R.; Wojciechowski, F.; Amin, S.; Sturla, S. J.; Hudson, R. H.; York, D. M.; Jankowiak, R.; Jones, R.; Tretyakova, N. Y. Influence of C-5 substituted cytosine and related nucleoside analogs on the formation of benzo[a]pyrene diol epoxide-dG adducts at CG base pairs of DNA. *Nucleic Acids Res.* **2011***, 39*, 3988-4006.

14. Wang, H.; Zhang, S.; Hu, Y.; Tang, M. Mutagenicity and sequence specificity of acrolein-DNA adducts. *Chem. Res. Toxicol.* **2009***, 22*, 511-517.

15. Wang, H. T.; Weng, M. W.; Chen, W. C.; Yobin, M.; Pan, J.; Chung, F. L.; Wu, X. R.; Rom, W.; Tang, M. S. Effect of CpG methylation at different sequence context on acrolein- and BPDE-DNA binding and mutagenesis. *Carcinogenesis* **2013***, 34*, 220-227.

16. Satterwhite, J. E.; Trumbo, C. M.; Danell, A. S.; Hvastkovs, E. G. Electrochemical Study on the Effects of Epigenetic Cytosine Methylation on Anti-Benzo [a] pyrene Diol Epoxide Damage at TP53 Oligomers. *Anal. Chem.* **2013***, 85*, 1183-1191.

17. Glick, J.; Xiong, W.; Lin, Y.; Noronha, A. M.; Wilds, C. J.; Vouros, P. The influence of cytosine methylation on the chemoselectivity of benzo [a] pyrene diol epoxide-oligonucleotide adducts determined using nanoLC/MS/MS. *Journal of mass spectrometry* **2009***, 44*, 1241-1248.

18. Geacintov, N. E.; Shahbaz, M.; Ibanez, V.; Moussaoui, K.; Harvey, R. G. Base-sequence dependence of noncovalent complex formation and reactivity of benzo [a] pyrenediol epoxide with polynucleotides. *Biochemistry (N. Y.)* **1988***, 27*, 8380-8387.

19. Deligkaris, C.; Rodriguez, J. H. Non-covalent interactions of the carcinogen ( )-anti-BPDE with exon 1 of the human K-ras proto-oncogene. *Physical Chemistry Chemical Physics* **2014***, 16*, 6199-6210.

20. Malla, S.; Kadimisetty, K.; Fu, Y.; Choudhary, D.; Jansson, I.; Schenkman, J. B.; Rusling, J. F. Chemical selectivity of nucleobase adduction relative to in vivo mutation sites on exon 7 fragment of p53 tumor suppressor gene. *Chemical Science* **2015***, 6*, 5554-5563.

21. http://structure.usc.edu/make-na/server.html last accessed 12/06/2016

22. Schrodinger, L., maestro, New York, NY, (2006).

23. http://www.rbvi.ucsf.edu/chimera/ last accessed 12/06/16

24. Pettersen, E. F.; Goddard, T. D.; Huang, C. C.; Couch, G. S.; Greenblatt, D. M.; Meng, E. C.; Ferrin, T. E. UCSF Chimera—a visualization system for exploratory research and analysis. *Journal of computational chemistry* **2004***, 25*, 1605-1612.

25. Morris, G. M. *et al*. AutoDock4 and AutoDockTools4: Automated docking with selective receptor flexibility. *Journal of computational chemistry* **30**, 2785-2791 (2009).

26. Kypr, J.; Kejnovska, I.; Renciuk, D.; Vorlickova, M. Circular dichroism and conformational polymorphism of DNA. *Nucleic Acids Res.* **2009***, 37*, 1713-1725.

27. Vargason, J. M.; Henderson, K.; Ho, P. S. A crystallographic map of the transition from B-DNA to A-DNA. *Proc. Natl. Acad. Sci. U. S. A.* **2001***, 98*, 7265-7270.

28. Banyay, M.; Gräslund, A. Structural effects of cytosine methylation on DNA sugar pucker studied by FTIR. *J. Mol. Biol.* **2002***, 324*, 667-676.

29. Hunter, C. A. Quantifying intermolecular interactions: guidelines for the molecular recognition toolbox. *Angewandte Chemie International Edition* **2004**, *43*, 5310-5324.

30. Ng, H. L.; Kopka, M. L.; Dickerson, R. E. The structure of a stable intermediate in the A B DNA helix transition. *Proc. Natl. Acad. Sci. U. S. A.* **2000**, *97*, 2035-2039.

31. Carvalho, A. T.; Gouveia, L.; Kanna, C. R.; Wärmländer, S. K.; Platts, J. A.; Kamerlin, S. C. L. Understanding the structural and dynamic consequences of DNA epigenetic modifications: Computational insights into cytosine methylation and hydroxymethylation. *Epigenetics* **2014**, *9*, 1604-1612.

32. Song, Q.; Qiu, Z.; Wang, H.; Xia, Y.; Shen, J.; Zhang, Y. The effect of methylation on the hydrogen-bonding and stacking interaction of nucleic acid bases. *Structural Chemistry* **2013**, *24*, 55-65.

33. Morris, G. M.; Huey, R.; Lindstrom, W.; Sanner, M. F.; Belew, R. K.; Goodsell, D. S.; Olson, A. J. AutoDock4 and AutoDockTools4: Automated docking with selective receptor flexibility. *Journal of computational chemistry* **2009**, *30*, 2785-2791.

34. Kumalo, H. M.; Bhakat, S.; Soliman, M. E. Theory and applications of covalent docking in drug discovery: merits and pitfalls. *Molecules* **2015**, *20*, 1984-2000.

CHAPTER 4

Assessing p53 Gene Damage from Metabolites at High Throughput using Magnetic Biocolloids and LC-MS/MS

4-1. Abstract

Codon specific mutations on p53 tumour suppressor gene are correlated with organ specific cancer. Chemical or drug metabolites cause specific codon damage on P53 and thus tissue specific cancer can be predicted from the available P53 databases. The majority of chemicals or drugs require metabolic activation to form reactive metabolite that cause genotoxic effects that can measured as DNA damage. Herein we report a high throughput 96 well plate magnetic bio-colloid reactor approach with restriction enzyme-assisted LC-MS/MS sequencing to screen chemicals for sequence specific gene damage. Metabolic enzymes on the magnetic beads bio-activate test chemical to form metabolites that, if reactive enough, react with DNA. Aflatoxin B1 was used as a model compound and 8 different cyt P450 enzymes from various organ tissues were used to quantitatively determine which enzymes play major roles in bioactivation of aflatoxin B1. Cyt P450s convert aflatoxin B1 aflatoxin B1-8,9-epoxide which reacts with DNA in an Sn2 reaction to form N7-guanine adducts. These adducts cause depurination and subsequent strand breaks. A 32 base pair exon 7 fragment of p53 gene was used to reveal abasic sites and a strand break at codon 249, correlated to possible liver cancer. Human liver microsomes and cyt P50 3A5

supersomes showed highest reactivity for of Aflatoxin B1, estimated by comparing the amount of N7-guanine adducts formed from various enzyme sources. Other compounds studied include NNK and styrene.

4-2. Introduction

Toxicity screening plays a major role in drug development. Approximate cost to bring a new drug into the market is $ 1.7 billion.[1,2] Toxicity screening contributes to nearly one third of the cost in drug development, but 20-40% of drug candidates fail at the phase III clinical test level due to toxicity issues not revealed by prior bioassay and animal toxicity tests.[3,4] New, rapid, reliable pathway-based screening assays that take in account metabolic activation[5] are important for improving safety and lowering cost of new drugs and environmental chemicals. [6-8]Genotoxicity refers to damage to genetic material by chemical agents and their metabolites. [8-10] we developed a restriction enzyme-assisted LC-MS/MS sequencing method to identify reactive codons and measure sequence specific reaction rates of codon damage using a p53 tumor suppressor gene fragment. to correlate with organ specific cancer and to determine the effect of cytosine methylation and kinetics of Benzo[a]pyrene-diolepoxide covalent adduction with DNA.[11,12,] Mutations of p53 have been identified in >50% of human cancers,[13] and mutation sites are correlated with specific cancers.[14,15] For example, mutations of codons 157, 158, 248, 249 occur in lung cancer, codon 273 in brain and prostate cancer, codons 175, 248 and 273 in breast cancer and codons 175, 282, 248, 249 in liver cancer.[16] These mutations are located in p53 exons 5-8, and alter the p53 protein coded by the gene to minimize or eliminate cancer protection. Thus, prediction of metabolite reaction sites on p53 codons is a valuable tool to aid in cancer prediction related to new chemicals and drugs.[17] We report here for the first time the combination of restriction enzyme-assisted LC-MS/MS sequencing with 96 well plate-magnetic-biocolloid enzyme reactors to determine the effect of reactive metabolite reactions on sequence specific DNA damage. The 96-well plate approach hs allows evaluating multiple metabolic enzymes simultaneously. Aflatoxin B1 Aflatoxin B1 is a mycotoxin produced by *Aspergillus*

flavus and *Aspergillus parasiticus,* was used as a model test chemical. Aflatoxin is a mycotoxin present in foods including rice, oil seeds, peanuts, and corn.[18] Aflatoxin B1 is metabolically converted by cyt P450 enzymes to the DNA-reactive aflatoxin B1-8,9-epoxide that covalently binds to the N7 position of guanines.[19,20] DNA damage due to aflatoxin B1 metabolites include covalent DNA adducts, abasic site formation, strand breaks and oxidative DNA damage. Aflatoxin B1 is associated with G-T transversion at codon 249 of P53 gene and is often associated with liver cancer.[21]

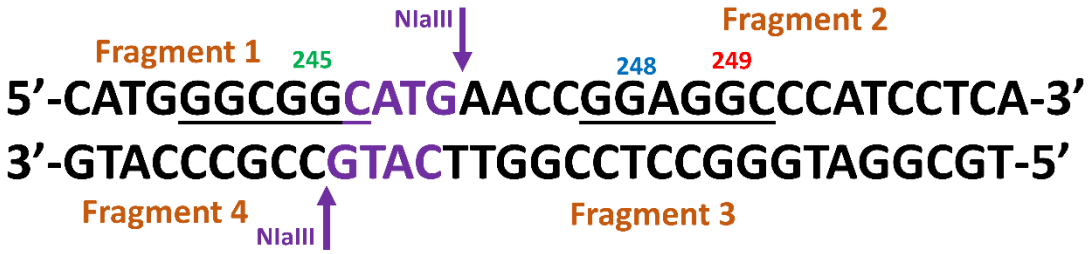

Scheme 4-1. Structure of 32 base pair (bp) exon 7 probe of the p53 gene extending from codon 242 to 253. Three mutation hotspot codons 245 (green), 248 (blue) and 249 (red) in various cancers[Error! Bookmark not defined.] are highlighted. The NlaIII restriction enzyme site, CATG, is shown in purple and four fragments obtained after restriction enzyme and heat and cool treatment are labeled in brown.

The present paper focuses on determining sequence specific DNA damage from in situ metabolized aflatoxin B1 on exon 7 probe of P53 gene (Scheme 1). Additional studies were done on nicotine-derived nitrosoamine ketone (NNK) and Styrene to demonstrate generality. Restrictions enzymes were used to cut the 34 bp p53 sequence into smaller fragments and LC-MS/MS sequencing was used to determine sequence specificity gene damage. Results for aflatoxin B1 show that it is efficiently converted to aflatoxin B1-8,9-epoxide, which reacts manly with N7 on the guanine in codon 249, then undergoes depurination (perhaps ralated to heating

during the protocol) to form an abasic site, which also results in a fraction of strand breaks adjacent to the abasic site.

4-3. Experimental

4-3-1. Chemicals & Reagents

Aflatoxin B1 (AFB1, MW=312.23), poly(diallyldimethylammonium chloride) (PDDA, average M_w= 100,000-200,000), poly(sodium 4-styrenesulfonate) (PSS, average M_W= 70000), calf thymus DNA, Triethyl ammonium bicarbonate and all other chemicals were from Sigma. 1μ carboxylated magnetic particles from Bangs Laboratories. Custom made 32 base pair exon 7 fragment from codon 242-253 was from Integrated DNA technologies (IDT). Restriction enzyme NIaIII was purchased from New England Biolabs. Pooled male human liver microsomes, HLM, Human lung micrososmes, Supersomes, 3A4, 2A6, 1B1, 3A5 and 1A2 were obtained from BD Gentest.

Caution. Aflatoxin B1 is a known chemical carcinogen. Protective measure like wearing eyewear and gloves were taken while doing experiment. All experiments were performed in a closed hood.

4-3-2. Magnetic Bio-colloid Methodology

A high throughput methodology was developed to screen multiple chemicals by multiple cytochrome P450 enzyme sources for their potential to cause DNA damage on P53 gene fragments. Carboxylated magnetic beads were used on to which layer by layer assembly of enzyme sources were made to facilitate simple and easy conversion of prodrugs/carcinogens to their reactive metabolites ad their subsequent reaction with P53 gene fragments. Layer by layer assembly of PDDA/enzymes was made on magnetic particles in a 96 well plate (Scheme 4-2).[22,23] Briefly 80 μL of 1μM carboxylated magnetic particles (128 mg) were taken and added to

120 µL of 10mM Tris buffer pH 7.4. To this 200 µL of 2 mg mL-1 PDDA in water was added and incubated on a temperature controlled shaker at 25°C for 20 minutes at 800 rpm speed. After 20 minutes magnetic particles were washed with 10 mM Tris buffer with 50mM NaCl, pH 7.4 three times. To this magnetic beads 340 µL of 10 mM Tris + 50 mM NaCl buffer, pH 7.4 was added to this suspension 60µL of enzyme was added slowly dropwise and incubated at 4°C for 30 minutes on a temperature controlled shaker at 800 rpm speed. After the incubation step the beads were washed with 10 mM Tris buffer with 50mM NaCl, pH 7.4 three times. These beads were incubated for 4 hours with 150 µM Aflatoxin B1 solution and 150 µg of ds-32 base pair

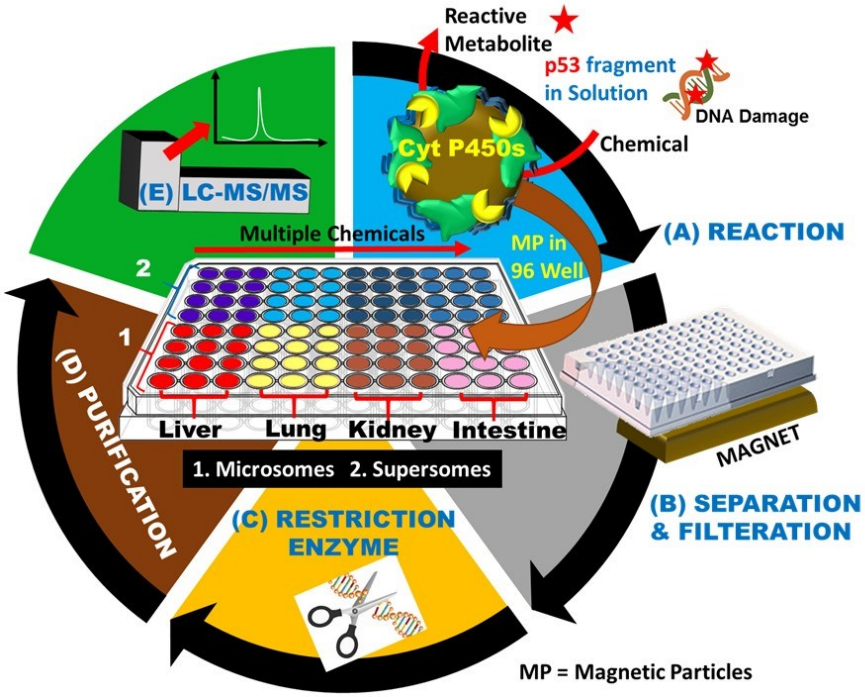

exon 7 fragment at 37°C in the presence of NADPH regeneration system[24] and 10 mM Phosphate buffer, pH 7.4.

Scheme 4-2. Schematic representation of experimental protocol for 96-well plate, magnetic biocolloid and restriction enzyme assisted analysis of P53 gene fragments. A) Cytrochrome P450 assisted conversion of carcinogen/prodrug to reactive metabolite that can cause DNA damage. B)

Separation of magnetic beads and filteration to remove small molecules. C) Restriction enzyme treatment to cut 53 gene fragments. D) Purification to remove proteins & Salts E) LC-MS/MS analysis.

After the reaction the beads were separated using a magnet and the supernatant containing the reacted 32 base pair exon 7 fragment and excess AFB1 was collected (Scheme 4-2B). 3000 da molecular weight cut off filters (from EMD Millipore, UFC500396) were used to remove the small molecules from DNA and small molecule mixture before restriction enzyme treatment.

4-3-3. Restriction Enzyme treatment, Protein separation & Desalting

Approximately 150 µg of ds-32 base pair DNA was incubated with 15 µL (150 units) of NIaIII enzyme in 20 µL of 10 X NE buffer (provided by New England Biolabs) and volume made up to 200 µL using water for 8 hours at 37 °C. After the reaction is complete, DNA fragments were extracted from restriction enzyme reaction mixture using a previously described protocol using phenol/chloroform/isoamylalcohol, 25/24/1 and chloroform/isoamylalcohol, 24/1 to remove proteins.[Error! Bookmark not defined.] Briefly mixture of DNA and RE enzymes was vortexed with equal volume of phenol/chloroform/isoamyl alcohol for 15 min followed by centrifugation for 10 min, organic phase discarded and aqueous phase was collected (for 3 times), and then repeated the same process with chloroform /isoamylalcohol (2 times). Before subjecting to LC-MS/MS analysis DNA samples were subjected desalting using solid phase extraction (SPE) cartridges (Waters Oasis HLB cartridges, WAT094226). Briefly the cartridges were first washed with methanol, followed by water then samples was added and washed with 5% methanol to remove salts. The DNA samples were eluted from the cartridges using 100 % methanol. Samples

were dried using a roto-vap and dissolved in 100 µL of distilled water. This sample was heated and cooled rapidly to convert ds-DNA to ss-DNA and stored at -20 °C until use. For small molecule analysis 7-methylguanosine was added to the reaction mixture as an internal standard with final concentration to be 0.2 µM.

4-3-4. LC-MS/MS Parameters

Ion pair reverse phase chromatography is used to separate the oligonucleotides using 25 mM Triethylammonium bicarbonate as ion pairing agent. A binary solvent system with 25 mM Triethylammoniun bicarbonate as buffer A and 100 % Methanol as Buffer B was used. Gemini C-18 column (0.5 mm ID, 3 µ particle size and 150 mm length was used along with Thermo Scientific Ultimate 3000 UPLC. Separation protocol was 0-3 % B (Methanol) for 3 min, then increased gradient from 3 to 27 % B (Methanol) for 24 min, then back to 3 % for 3 min. Between each run a wash is performed with gradient from 3% B isocratic for 2 min followed by 3-80 % B for 24 min followed by equilibrating back to 3 % for 4 min at 10 µL/min. Post column m-Nitrobenzylalcohol was used via syringe pump through three way connector to increase the intensity and charge states of oligonucleotide fragments.[25] Absciex QSTAR was used in negative mode. Product ion scanning was used for qualitative evaluation of site selective of modification of oligonucleotides. Ionization parameters for the AB Sciex QSTAR, -4500 ion spray voltage, ion source gas 1 at 30 units and ion source gas 2 at 25 units, -80 V declustering potential, -280 V focusing potential and 300°C temperature was used with collision energy from -42 to -50 eV for MS/MS analysis. All samples were run in triplicate. ThermoScientific, Hypersil gold column (C18, 100 mm X 0.3mm id and 3 µ particle size) was used for small molecule analysis. Reverse phase chromatography with binary solvent system containing 10 mM Ammonium acetate as

buffer A and Methanol as buffer B with 0.2 % Formic acid was used. Separation protocol involves 15 min with 5 % B (for 2 min) and %B increased to 70 % (2-12 min) and stabilized back to 5 % (12- 15min). Absciex Qtrap 4000 was used for quantitation in positive mode and Multiple reaction monitoring was used to quantitate the DNA adducts. Ionization conditions include 5000 ion spray voltage, curtain gas at 10 units, ion source gas 1 at 12 and ion source gas 2 at 5 units & temperature at 200°C with collision energy of 45 eV.

4-4. Results

A 96 well plate based high throughput methodology was developed to screen multiple chemicals under the influence of multiple CYT P450 enzyme sources for their biotransformation to their reactive metabolites that have potential to cause DNA damage on P53 gene fragments that can be correlated with organ specific cancer. CYT P450 enzyme sources from different tissue sources (both supersomes and microsomes) like liver, lung, intestine and kidney were used to see which of these enzyme sources play a major role in biotransformation of specific drugs. Aflatoxin B1, NNK and Styrene are the three carcinogens that are used in this study.

32 base pair exon 7 fragment of P53 gene was reacted with Aflatoxin B1 in the presence of CYT P450 enzymes and NADPH regeneration system. CYT P450 enzymes biotransform Aflatoxin B1 to Aflatoxin B1-8,9-epoxide in the presence of NADPH regeneration system. Aflatoxin B1-8,9-epoxide reacts with N-7 position of guanine to form covalent adducts, Scheme 4-3. These adducts are unstable and undergo depurination resulting in the formation of abasic site, Scheme 4-4.[26] These abasic sites can further undergo β-elimination resulting in strand breaks.[Error! Bookmark not defined.,27]

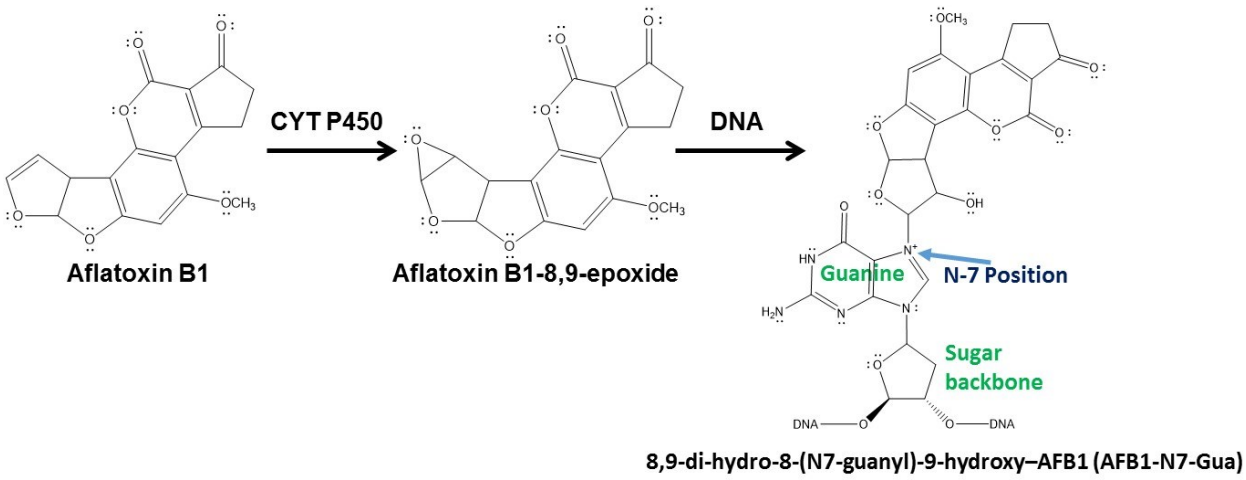

Scheme 4-3. Proposed metabolic pathway for conversion of Aflatoxin B1 to aflatoxin B1-8,9-epoxide and covalent adduction on N-7 position of guanine.

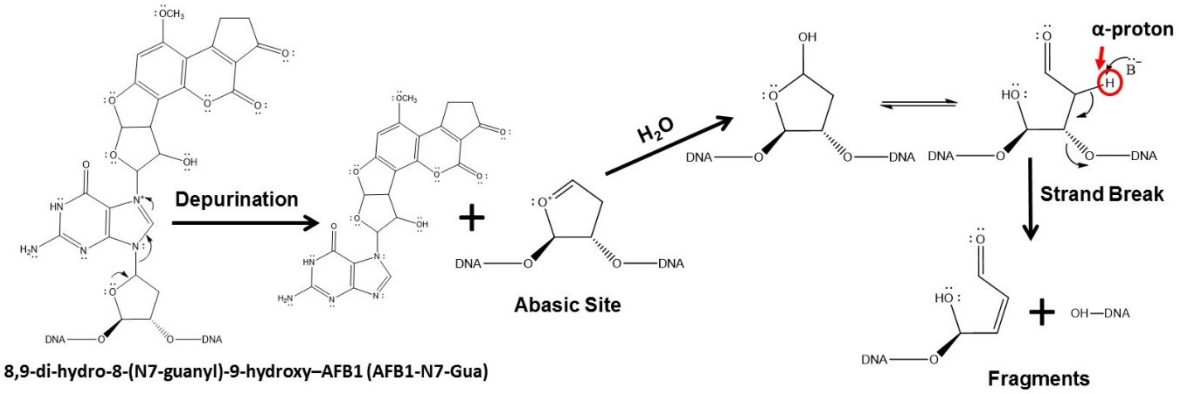

Scheme 4-4. Proposed mechanism of depurination/base loss from 8,9-dihydro-8-(7-guanyl)-9-hydroxy-AFB1 (AFB1-N7-Gua) and subsequent strand break via β elimination mechanism.

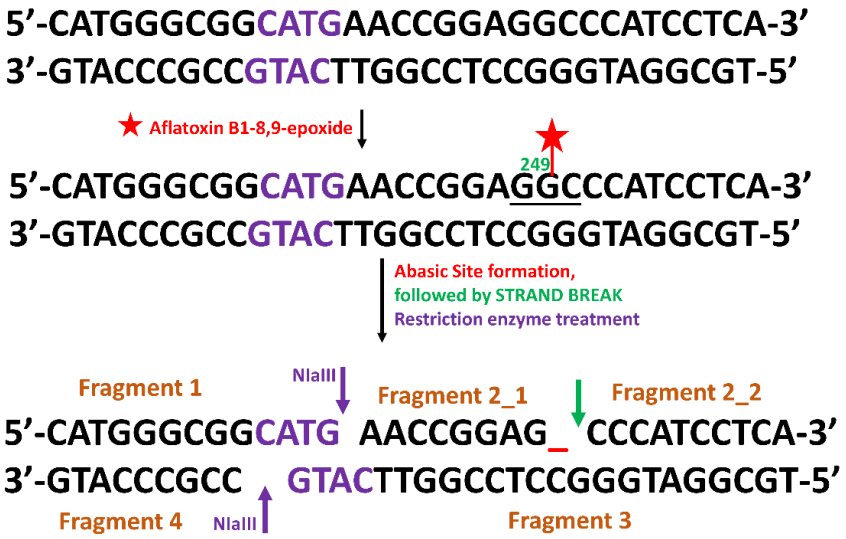

Scheme 4-5. Proposed mechanism of DNA damage effects of Aflatoxin B1 on 32 base pair exon 7 fragment.

Restriction enzyme treatment on 32 base pair exon 7 fragment will result in four fragments. Calculated m/z for all the fragments were as shown in Table 4-1. Aflatoxin B1 reacted 32 base pair exon 7 fragment of P53 gene in the present of cytochrome P450 enzymes and NADPH regeneration system includes both undamaged and damaged oligonucleotide fragments. Mass spec analysis of the reacted sample include undamaged fragment 1 (m/z=1002.6, z=-4), undamaged fragment 2 (m/z=1163.5 z=-5), undamaged fragment 4 (m/z=912.7, z=-3), undamaged fragment 3 (m/z=1421.3 z=-5), strand break on fragment 2 (Scheme 4-5) and abasic site on fragment 1.

Table 4-1. Calculated m/z for fragment 1, fragment 2, Damaged (Loss of guanine) Fragment 1, Damaged Fragment 2 and strand breaks from fragment 2.

Fragment 1, OH-CATGGGCGGCATG-OH		
Negative Charge	**Undamaged**	**Base loss,-G**

1.000	4014.656	3864.535
2.000	2006.824	1931.763
3.000	1337.546	1287.506
4.000	1002.908	965.377
5.000	802.124	772.100
6.000	668.269	643.249
7.000	572.658	551.212
8.000	500.950	482.184
9.000	445.176	428.460
10.000	400.558	385.546
11.000	364.052	350.405
12.000	333.630	321.120

Fragment 2, P-AACCGGAGGCCCATCCTCA-OH					
Negative Charge	**Undamaged**	**Base loss, -G**	**Strand break**		
			Fragment 2_1, P-AACCGGAGG-OH		**Fragment 2_2**
			Intact	**Base Loss, -G**	**Intact**
1.000	5821.771	5671.650	2851.847	2701.726	2986.931
2.000	2910.381	2835.321	1425.419	1350.359	1492.61
3.000	1939.918	1889.878	949.943	899.903	994.971
4.000	1454.686	1417.156	712.205	674.675	745.946
5.000	1163.547	1133.523	569.563	539.538	596.579
6.000	969.455	944.435	474.467	449.447	496.981
7.000	830.817	809.371	406.542	385.096	425.84
8.000	726.839	708.074	355.598	336.833	372.484
9.000	645.967	629.287	315.975	299.25	297.785

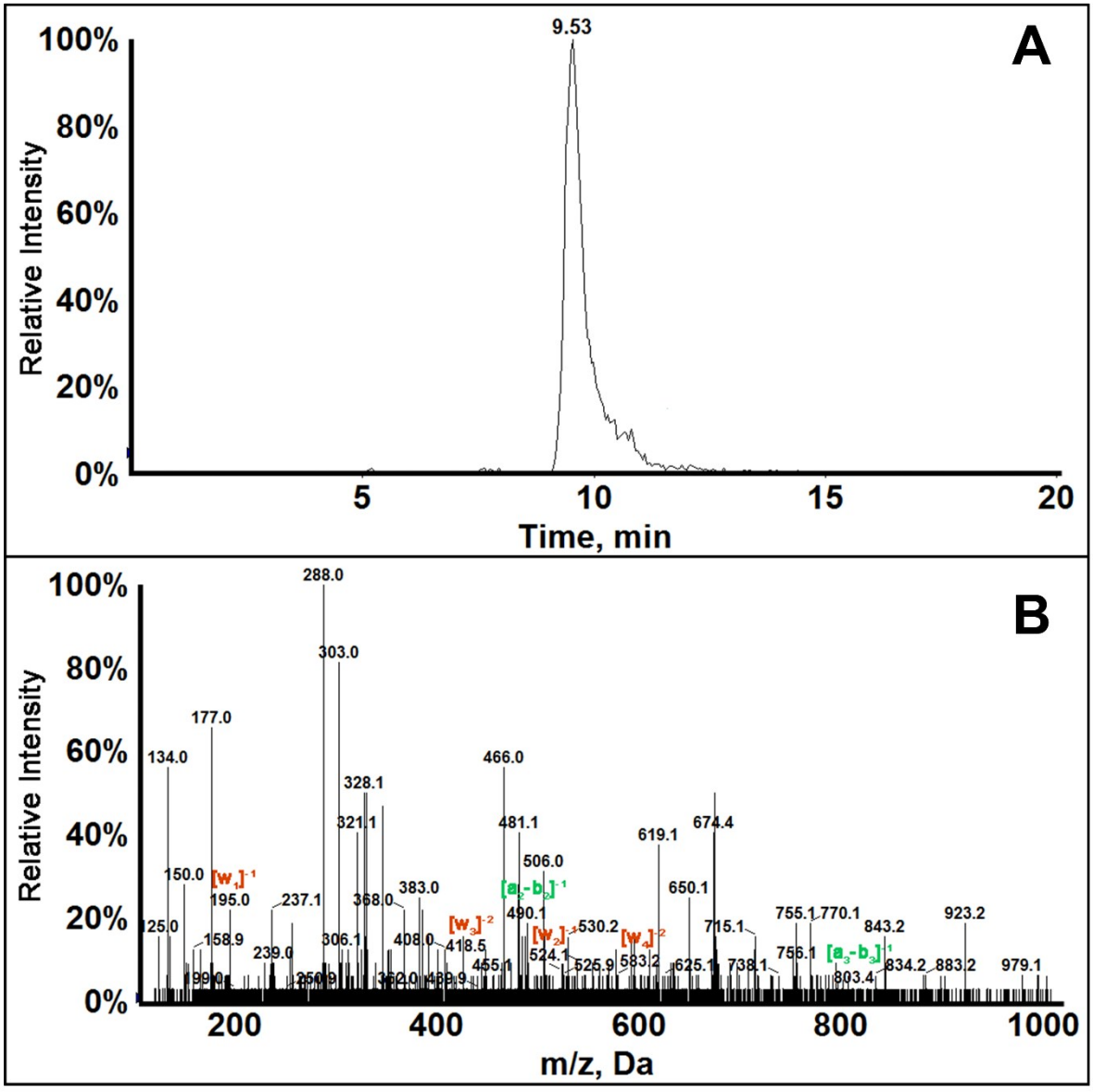

Figure 4-1. LC-MS of ds-32 bp exon 7 probe: (A) Extracted ion chromatogram of singly adducted fragment 2-1, m/z 674.4. (B) MSMS spectra of Fragment 2-2 showing the obtained a_n-b_n and w_n ions. Ions with m/z similar to standard are shown in green and ions with increased m/z shown in red.

A more detailed analysis on fragment 2 indicate two fragments of Fragment 2, Fragment 2_1 and Fragment 2_2, scheme 4-5. Fragment 2_1 m/z=674.4, z=-4. The fragment corresponding to this mass is AACCGGAGG with a guanine loss that is AACCGGAG_ difference in mass

between AACCGGAGG and AACCGGAG_ is ~151 daltons corresponding the guanine. Position of guanine loss determines by MS/MS analysis as shown in Figure 4-1. CID spectra of oligonucleotides give characteristic a_n-b_n and w_n ions, comparing the spectra of damaged/modifies fragments with that undamaged fragments gives us the exact position of DNA damage. For fragment 2_1 all w_n ions have m/z less than standard hence base lost is the terminal base.

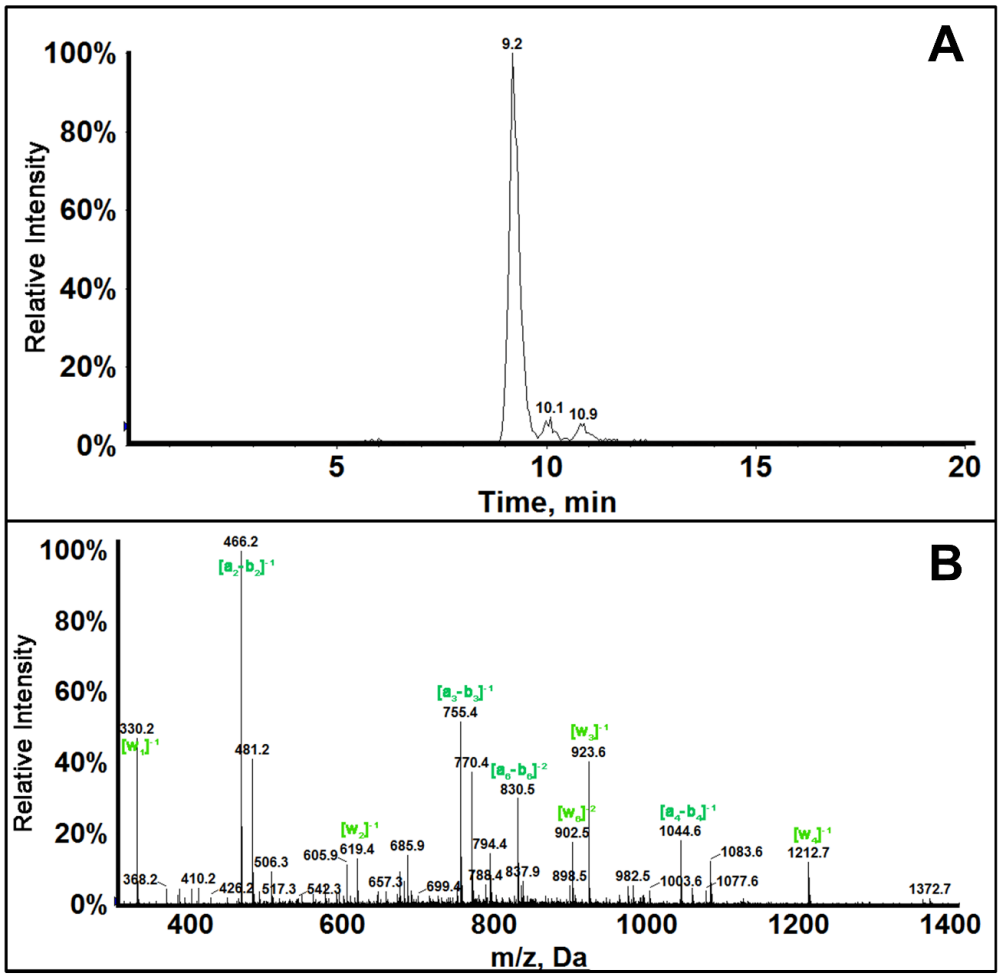

Figure 4-2. LC-MS of ds-32 bp exon 7 probe: (A) Extracted ion chromatogram of (CCCATCCTCA) fragment 2-1, m/z 674.4. (B) MSMS spectra of Fragment 2-2 showing the obtained a_n-b_n and w_n ions. Ions with m/z similar to standard are shown in green and ions with increased m/z shown in red.

Fragment 2_2 has an m/z of 994.9, z=-3. This fragment is intact without any base loss which is further confirmed by MS/MS analysis. MS/MS spectra of fragment 2-2 is as shown in figure 4-2. Presence on all a_n-b_n and w_n ions with m/z similar to that of standard CCCATCCTCA sequence indicate the depurination at codon 249 leading to a strand break between guanine and cytosine.

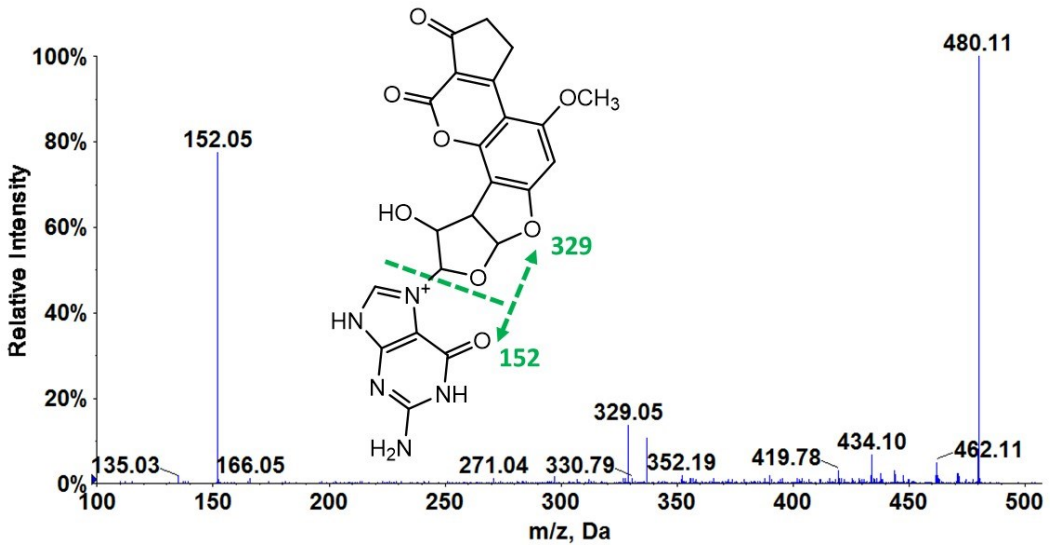

Figure 4-3. Product ion scan or MS/MS spectra of 8,9-dihydro-8-(7-guanyl)-9-hydroxy-AFB1 (AFB1-N7-Gua) adduct showing major peak 152 corresponding to protonated guanine.

In order to study the effect of different enzyme sources on the amount of DNA damage by Aflatoxin B1, 8 different CYT P450 enzyme sources are used namely Human liver microsomes (HLM), Human Lung Microsomes (HLuM), Human Kidney Microsomes (HKM) and Human Intestine microsomes (HIM). In addition to microsomes, supersomes that in rich in specific organs were selected namely 1A2 (Liver), 2A6 (Lung), 1B1 (Kidney) and 3A2 (Liver).[28,29,30] Relative amount of DNA damage was estimated by determining the amount 8,9-dihydro-8-(7-guanyl)-9-hydroxy-AFB1 (AFB1-N7-Gua) adduct formed when using different sources of CYT P450 enzymes.

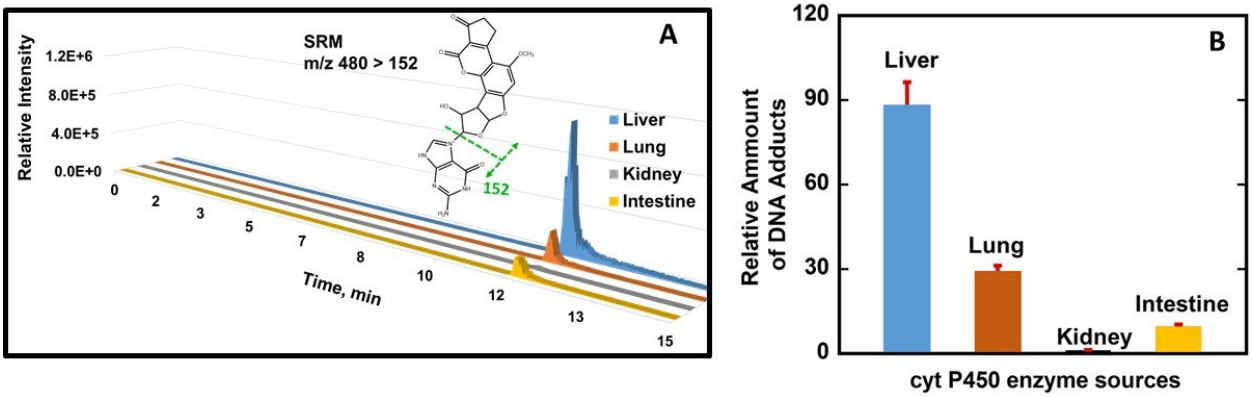

Figure 4-4. Quantitative estimation of amount of DNA damage through different enzyme sources estimated as a function of amount of N7 guanine adduct formed in the 96 well plate magnetic biocolloid reaction by microsomal enzyme sources. A) Selected reaction monitoring (SRM) transition chromatogram for 8,9-dihydro-8-(7-guanyl)-9-hydroxy-AFB1 (AFB1-N7-Gua) adduct (480 → 152) from magnetic bio-colloid reactors for microsomal enzyme sources (Liver, lung, kidney and intestine). B) Bar graph representing the relative amount adducts formed calculated as a ration of area under curve obtained from SRM transitions of Guanine adduct to that internal standard, 7-Methylguanosine.

Product ion scan of 8,9-dihydro-8-(7-guanyl)-9-hydroxy-AFB1 (AFB1-N7-Gua) adduct is as shown in figure 4-3. MS/MS spectra show two major fragments 152 and 329 corresponding to protonated guanine (152) and Aflatoxin B1 alcohol. Multiple reaction monitoring is used to quantify the amount of adduct formed using 7-methyl guanosine as an internal standard. MRM transitions selected are 480→ 152 for 8,9-dihydro-8-(7-guanyl)-9-hydroxy-AFB1 (AFB1-N7-Gua) adduct and 298→166 for 7-methylguanosine. Figure 4-4 shows the relative amount of 8,9-dihydro-8-(7-guanyl)-9-hydroxy-AFB1 (AFB1-N7-Gua) adducts obtained from the ratio of area under the curve from extracted ion chromatogram obtained for N7-Guanine adduct transition to that of internal standard transition.

Figure 4-5 shows the relative amount of 8,9-dihydro-8-(7-guanyl)-9-hydroxy-AFB1 (AFB1-N7-Gua) adducts obtained calculated as the ratio of area under the curve from extracted ion chromatogram obtained for N7-Guanine adduct transition to that of internal standard transition. Order of microsomal enzyme reactivity is HLM > HLuM > HIM > HKM. Order of relative amount N7 guanine adduct formed by supersomes is 3A5 > 2A6 > 1A2 > 1B1. Overall order of relative amount N7 gaunine adduct formation is HLM > 3A5 > HLuM > HIM > 2A6 > 1A2 > 1B1 > HKM.

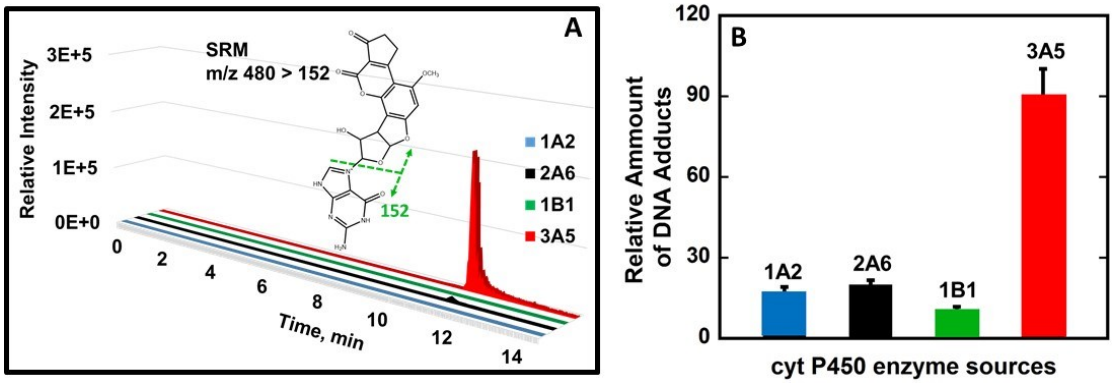

Figure 4-5. Quantitative estimation of amount of DNA damage through different enzyme sources estimated as a function of amount of N7 guanine adduct formed in the 96 well plate magnetic biocolloid reaction by supersomal enzyme sources. A) Selected reaction monitoring (SRM) transition chromatogram for 8,9-dihydro-8-(7-guanyl)-9-hydroxy-AFB1 (AFB1-N7-Gua) adduct (480 → 152) from magnetic bio-colloid reactors for supersomal enzyme sources (1A2, 2A6, 1B1, 3A5). B) Bar graph representing the relative amount adducts formed calculated as a ration of area under curve obtained from SRM transitions of Guanine adduct to that internal standard, 7-Methylguanosine.

Abasic site formed on fragment 1 was analyzed by comparing the MS/MS spectra of undamaged fragment 1 to that basic site formed fragment 1. Fragment 1 with basic site has an

m/z of 956.3, z=-4 which is approximately 151 Da less than undamaged fragment 1 indicating the loss of guanine. Comparison of a_n-b_n and w_n ions of undamaged vs the damaged fragment 1 indicate the presence of abasic site at codon 245. CATGGGCGGCATG (undamaged), CATGGGC_GCATG (damaged fragment with abasic site). Site of abasic site formed confirmed by decrease in a_9-b_9 and w_6 ions and also intact undamaged a_8-b_8 and w_5 ions.

Other chemicals were studied to expand the applicability of this study. Chemicals under study include styrene and Nicotine derive nitrosoamine ketoke (NNK). Mass spec analysis of NNK and Styrene indicate N7-guanine adducts and abasic site formation whereas benzo[a]pyrene-diolepoxide**Error! Bookmark not defined.** indicate covalent adduction of the exocyclic amine of guanine. Sequence specificity indicate possible DNA damage events at codon 248 and 244.

4-5. Discussion

Drug or environmental chemical induced toxicity is usually associated with either overdose or metabolism of the drug/chemical.[31] Metabolism plays major role in converting the lipophilic or nonpolar molecules to polar usually water soluble metabolites that are excreted out of the body. These metabolites are very reactive electrophiles sometime and might cause damage to biological molecules like DNA, protein and lipids.[32] In this current study magnetic bio-colloid based methodology in conjunction with LC-MS/MS has been developed to screen chemicals that require bio-activation to become reactive metabolites before causing adverse effects like genotoxicity. This methodology has advantages of being high throughput with capability of doing 96 reactions simultaneously with multiple enzymes sources and multiple carcinogens. Aflatoxin B1 is used as a model compound. Aflatoxin B1 requires metabolic activation to form

Aflatoxin B1-8,9-epoxide which forms adduct on the N7 position of guanine in DNA.[Error! Bookmark not defined.,Error! Bookmark not defined.,33] These N7 guanine adducts can either undergo depurination to form abasic site or rearrange to form a more stable formamidopyridine adduct.[34]

N-7 Position of guanine is the most nucleophilic site and hence the preferential site for DNA alkylation and adduct formation.[35,36] N7-Guanine adducts are unstable with half-life's ranging from 2 hours to 150 hours due to addition of positive formal charge on the guanine ring. Increase in size of adducts on the N7 position of the guanine decreases their half-life thus making them unstable and easier for depurination.[37] Abasic site formed can sometimes under strand breaks as shown in Scheme 4-3.[38] Mechanism of strand break is complex and might involve multiple pathways one them being loss of acidic α-proton that is adjacent to the carbonyl in the aldehydic form of abasic site leading to strand break via beta elimination of the phosphate group.[36,39] This reaction is catalyzed by strong nucleophile (ROS species formed by Aflatoxin B1) and heat. Aflatoxin B1 also known to cause CYT P450 mediated oxidative DNA damage in some cases.[34,40] by reactive oxygen species generation the exact mechanism is not known.[41]

Abasic site formed on fragment 2 of 32 base pair exon 7 fragment corresponds to codon 249 which is co-related with liver cancer according to the p53 data base.[Error! Bookmark not defined.] These results were further supported by our multi- enzyme reaction which shown high amount of 8,9-dihydro-8-(7-guanyl)-9-hydroxy-AFB1 (AFB1-N7-Gua) adducts formed when human liver microsomes were used as CYT P450 enzyme source. Among the supersomes 3A5 produced high amount of 8,9-dihydro-8-(7-guanyl)-9-hydroxy-AFB1 (AFB1-N7-Gua) adducts suggesting a high rate of Aflatoxin B1 biotransformation in liver and intestine.[42] Human kidney microsomes and 1B1 appear to have low capabilities of metabolite generation which is consistent with our previous ECL based assays.[Error! Bookmark not defined.]

Organ specific co-relation can be achieved using this methodology by comparing the damaged base within specific codon with tissue specific cancer already present in P53 database.[Error! Bookmark not defined.] Our previous study showed site specific covalent adduction at codon 248 for benzo[a]pyrenediolepoxide corresponding to lung, head and neck cancer. In our current study we established the sequence specific reactivity on codon 249 within the 32 base pair exon 7 fragment which is correlated with liver cancer for Aflatoxin B1. This is an exemplary in-vitro method that can differentiate sequence specific reactivity as close as one codon difference to determine the organ specific cancer.

This LC-MS/MS methodology in conjunction with 96 well plate magnetic bio-colloid technology is high throughput and has the capability to give greater insight on effect of chemicals or prodrugs that require metabolic activation to cause DNA damaging effect. In addition to being high throughput multiple DNA damaging events can be studied simultaneously like covalent adduction, abasic site formation, strand break, oxidative DNA damage, nucleobase adduct formation etc.,

4-6. Summary

In summary, our restriction enzyme aided LC-MS/MS methodology with magnetic biocolloid technology facilitates incorporation of CYT P450 enzyme for bioactivation of chemicals with lower reaction times to study the effect of genotoxic potential of chemical/prodrugs. We were able to differentiate organ specific cancer between Aflatoxin B1 and benzo[a]pyrenediolepoxide to be liver cancer and lung cancer respectively based on sequence specific DNA damage effects. This methodology can be used to predict the tissue specific cancer caused by unknown chemicals or environmental pollutants and also study the possible enzymes involved in their metabolic activation.

4-7. References

1. Guengerich, F. P. Mechanisms of drug toxicity and relevance to pharmaceutical development. *Drug metabolism and pharmacokinetics* **2011**, *26*, 3-14.

2. http://www.fda.gov/oc/initiatives/criticalpath/whitepaper.html last accessed December 9, 2016.

3. Hartun, T., Food for Thought Look Back in Anger – What Clinical Studies Tell Us About Preclinical Work, *ALTEX*. 2013 ; 30: 275–291.

4. Isabella WY Mak, Nathan Evaniew, Michelle Ghert. Lost in translation: animal models and clinical trials in cancer treatment, Am J Transl Res. 2014, 6, 114-118

5. Johnson, C. H.; Patterson, A. D.; Idle, J. R.; Gonzalez, F. J. Xenobiotic metabolomics: major impact on the metabolome. *Annu. Rev. Pharmacol. Toxicol.* **2012**, *52*, 37-56.

6 *Martin L. Stephens 1, Melvin Andersen 2, Richard A. Becker eta l.* Evidence-based Toxicology for the 21st Century: Opportunities and Challenges, ALTX, 30. 1/13; caat.jhsph.edu/CAATwalk/altex_2013_1_074_103_WR_Stephens.pdf, last accessed 12/09/2016

7. R. Judson, R. Kavlock, M. Martin et al. Perspectives on validation of high-throughput assays supporting 21st century toxicity testing. ALTEX. 2013;30(1):51-6. http://www.altex.ch/resources/altex_2013_1_051_066_Judson21.pdf, last accessed 12/09/2016

8. Hvastkovs, E. G.; Rusling, J. F. State-of-the-Art Metabolic Toxicity Screening and Pathway Evaluation. *Anal. Chem.* **2016**, *88*, 4584-4599.

9 (a) James F. Rusling, Eli G. Hvastkovs and John B. Schenkman, Screening for Reactive Metabolites using Genotoxicity Arrays and Enzyme/DNA Biocolloids, In A. Nassar, P. F.

Hollenburg and J. Scatina, Eds., *Drug Metabolism Handbook***,** J. Wiley, N. J. **2009,** pp. 307-340. (b) Eli G. Hvastkovs, John B. Schenkman and James F Rusling, Metabolic Toxicity Screening Using Electrochemiluminescence Arrays Coupled with Enzyme-DNA biocolloid reactors and LC-MS, *Annu. Rev. Anal. Chem*., **2012,** *5*, 79–105.

10 a) James F. Rusling and John B. Schenkman, High-throughput enzyme biocolloid systems for drug metabolism and genotoxicity profiling using LC-MS/MS. in Pablo Steinberg (ed.), High-Throughput Screening Methods in Toxicity Testing, John Wiley & Sons, Hoboken, NJ, **2013**, pp. 433-452. (b) James F. Rusling, Dhanuka P. Wasalathanthri, John B. Schenkman, Thin multicomponent films for functional enzyme devices and bioreactor particles (Review) *Soft Matter***, 2014**, **10,** 8145-8156 (c) Linlin Zhao, Besnik Bajrami, and James F. Rusling, Rapid LC-MS Drug Metabolite Profiling Using Bioreactor Particles, In Ian R. Phillips, Elizabeth A. Shephard, and Paul R. Ortiz de Montellano, *Cytochrome P450 Protocols*, 3rd Ed., Humana Press, Springer, NY, **2013**, pp. 129-134.

11. Malla, S.; Kadimisetty, K.; Fu, Y.; Choudhary, D.; Jansson, I.; Schenkman, J. B.; Rusling, J. F. Chemical selectivity of nucleobase adduction relative to in vivo mutation sites on exon 7 fragment of p53 tumor suppressor gene. *Chemical Science***2015***, 6*, 5554-5563.

12. Spundana Malla, Karteek Kadimisetty, You-Jun Fu, Dharamainder Choudhary, John B. Schenkman, and James F. Rusling, Methyl-Cytosine-Driven Structural Changes Enhance Adduction Kinetics of an Exon 7 fragment of the p53 Gene, *Sci Rep*., in press.

13. Levine, A. J. & Oren, M. The first 30 years of p53: growing ever more complex. *Nature Reviews Cancer* **9**, 749-758 (2009).

14. http://p53.free.fr/Database/p53_database.html, last accessed 9/12/2016.

15. http://p53.iarc.fr/TP53SomaticMutations.aspx, last accessed 9/12/2016.

16. http://p53.free.fr/Database/p53_cancer_db.html last accessed November 26, 2016.

17. Leroy, B.; Anderson, M.; Soussi, T. TP53 Mutations in Human Cancer: Database Reassessment and Prospects for the Next Decade. *Hum. Mutat.* **2014***, 35*, 672-688.

18. Baydar, T.; Engin, A. B.; Girgin, G.; Aydin, S.; Sahin, G. Aflatoxin and ochratoxin in various types of commonly consumed retail ground samples in Ankara, Turkey. *Annals of Agricultural and Environmental Medicine* **2005***, 12*, 193-197.

19. Wild, C. P.; Turner, P. C. The toxicology of aflatoxins as a basis for public health decisions. *Mutagenesis* **2002***, 17*, 471-481.

20. Xia, Q.; Huang, X.; Xue, F.; Zhang, J.; Zhai, B.; Kong, D.; Wang, C.; Huang, Z.; Long, X. Genetic polymorphisms of DNA repair genes and DNA repair capacity related to aflatoxin b1 (AFB1)-induced DNA damages. *New Research Directions in DNA Repair* **2013***, 1*, 377-412.

21. Aguilar, F.; Hussain, S. P.; Cerutti, P. Aflatoxin B1 induces the transversion of G-->T in codon 249 of the p53 tumor suppressor gene in human hepatocytes. *Proc. Natl. Acad. Sci. U. S. A.* **1993***, 90*, 8586-8590.

22. Zhao, L.; Schenkman, J. B.; Rusling, J. F. High-throughput metabolic toxicity screening using magnetic biocolloid reactors and LC− MS/MS. *Anal. Chem.* **2010***, 82*, 10172-10178.

23. Pan, S.; Zhao, L.; Schenkman, J. B.; Rusling, J. F. Evaluation of electrochemiluminescent metabolic toxicity screening arrays using a multiple compound set. *Anal. Chem.* **2011***, 83*, 2754-2760.

24. Meunier, B.; De Visser, S. P.; Shaik, S. Mechanism of oxidation reactions catalyzed by cytochrome P450 enzymes. *Chem. Rev.* **2004***, 104*, 3947-3980.

25. Brahim, B.; Alves, S.; Cole, R. B.; Tabet, J. Charge enhancement of single-stranded dna in negative electrospray ionization using the supercharging reagent meta-nitrobenzyl alcohol. *J. Am. Soc. Mass Spectrom.* **2013**, *24*, 1988-1996.

26. Gates, K. S. An overview of chemical processes that damage cellular DNA: spontaneous hydrolysis, alkylation, and reactions with radicals. *Chem. Res. Toxicol.* **2009**, *22*, 1747-1760.

27. Fortini, P.; Dogliotti, E. Base damage and single-strand break repair: mechanisms and functional significance of short-and long-patch repair subpathways. *DNA repair* **2007**, *6*, 398-409.

28. Ding, X.; Kaminsky, L. S. Human extrahepatic cytochromes p450: Function in Xenobiotic Metabolism and Tissue-Selective Chemical Toxicity in the Respiratory and Gastrointestinal Tracts*. *Annu. Rev. Pharmacol. Toxicol.* **2003**, *43*, 149-173.

29. Bieche, I.; Narjoz, C.; Asselah, T.; Vacher, S.; Marcellin, P.; Lidereau, R.; Beaune, P.; de Waziers, I. Reverse transcriptase-PCR quantification of mRNA levels from cytochrome (CYP)1, CYP2 and CYP3 families in 22 different human tissues. *Pharmacogenet Genomics* **2007**, *17*, 731-742.

30. Guengerich, F. P. Cytochromes P450. *Metabolism of Drugs and Other Xenobiotics* **2012**, 27-66.

31. Liebler, D. C.; Guengerich, F. P. Elucidating mechanisms of drug-induced toxicity. *Nature reviews Drug discovery* **2005**, *4*, 410-420.

32. Miller, J. A. Carcinogenesis by chemicals: an overview--G. H. A. Clowes memorial lecture. *Cancer Res.* **1970**, *30*, 559-576.

33. Denissenko, M. F.; Cahill, J.; Koudriakova, T. B.; Gerber, N.; Pfeifer, G. P. Quantitation and mapping of aflatoxin B1-induced DNA damage in genomic DNA using aflatoxin B1-8, 9-epoxide and microsomal activation systems. *Mutation Research/Fundamental and Molecular Mechanisms of Mutagenesis* **1999**, *425*, 205-211.

34. Bedard, L. L.; Massey, T. E. Aflatoxin B 1-induced DNA damage and its repair. *Cancer Lett.* **2006**, *241*, 174-183.

35. Reiner, B.; Zamenhof, S. Studies on the chemically reactive groups of deoxyribonucleic acids. *J. Biol. Chem.* **1957**, *228*, 475-486.

36. Gates, K. S.; Nooner, T.; Dutta, S. Biologically relevant chemical reactions of N7-alkylguanine residues in DNA. *Chem. Res. Toxicol.* **2004**, *17*, 839-856.

37. Boysen, G.; Pachkowski, B. F.; Nakamura, J.; Swenberg, J. A. The formation and biological significance of N7-guanine adducts. *Mutation Research/Genetic Toxicology and Environmental Mutagenesis* **2009**, *678*, 76-94.

38. Benasutti, M.; Ejadi, S.; Whitlow, M. D.; Loechler, E. L. Mapping the binding site of aflatoxin B1 in DNA: systematic analysis of the reactivity of aflatoxin B1 with guanines in different DNA sequences. *Biochemistry (N. Y.)* **1988**, *27*, 472-481.

39. Doetsch, P. W.; Cunningham, R. P. The enzymology of apurinic/apyrimidinic endonucleases. *Mutat. Res. /DNA Repair* **1990**, *236*, 173-201.

40. Yang, C.; Liu, J.; Shen, H.; Ong, C. Protective Effect of Ebselen on Aflatoxin B1-Induced Cytotoxicity in Primary Rat Hepatocytes. *Pharmacol. Toxicol.* **2000**, *86*, 156-161.

41. Mary, V. S.; Theumer, M. G.; Arias, S. L.; Rubinstein, H. R. Reactive oxygen species sources and biomolecular oxidative damage induced by aflatoxin B1 and fumonisin B1 in rat spleen mononuclear cells. *Toxicology* **2012**, *302*, 299-307.

42. Wang, H.; Dick, R.; Yin, H.; Licad-Coles, E.; Kroetz, D. L.; Szklarz, G.; Harlow, G.; Halpert, J. R.; Correia, M. A. Structure-function relationships of human liver cytochromes P450 3A: aflatoxin B1 metabolism as a probe. *Biochemistry (N. Y.)***1998***, 37*, 12536-12545.

CHAPTER 5

Biosensors for Multiple Prostate Cancer Biomarker Detection

5.1 Abstract

Point-of-care diagnostics based on multiplexed protein measurements face challenges of simple, automated, low cost, high throughput operation with high sensitivity. We developed an automated, microprocessor-controlled microfluidic immunoarray for simultaneous multiplexed detection of small protein panels in complex samples. A microfluidic sample/reagent delivery cassette was coupled to a 30 microwell detection array to achieve sensitive detection of 4 prostate cancer biomarker proteins in serum. The six-channel system is driven by integrated micropumps controlled by an inexpensive programmable microprocessor. An on-board microcontroller controls micropumps and reagent flow to the detection chamber according to a preset program. Detection employs tripropylamine, a sacrificial reductant, while applying 0.95 V vs Ag/AgCl. Resulting ECL light was measured by a CCD camera. Ultralow detection limits of 10-100 fg mL^{-1} were achieved in simultaneous detection of the four protein in 36 min. assays. While the described method can detect 4 biomarkers simultaneously and our method is one of the first reports where automated reagent handling using reagent chambers coupled was performed. There is still need for sensors that are inexpensive miniaturized that can be used in resource poor settings. Following project uses 3-D printing technology for inexpensive, mass production and miniaturized sensors for cancer diagnosis.

We developed low cost, sensitive, supercapacitor-powered electrochemiluminescent (ECL) protein immunoarray fabricated by an inexpensive 3-dimensional (3D) printer. The

immunosensor detects three cancer biomarker proteins in serum in 35 min. The 3D-printed device employs hand screen printed carbon sensors with gravity flow for sample and reagent delivery and washing. The supercapacitor was rapidly photo-recharged between assays using an inexpensive solar cell and used to apply voltage to Electro chemical sensor to generate ECL. Detection limits were 300-500 fg mL^{-1} for the 3 proteins in undiluted calf serum. This technology could provide sensitive onsite cancer diagnostic tests in resource-limited settings with the need for only moderate-level training.

5.2 Introduction

5.2.1 Prostate Cancer & Biomarkers

Prostate cancer is the most common cancer among men besides skin cancer with current annual mortality of more than 27,000 in the United States. About 1 in 7 men are currently diagnosed with prostate cancer during their lifetime with about 1 in 39 men will die of prostate cancer.[1] Current methods in detection of prostate cancer includes direct detection of prostate specific antigen (PSA) using gold standard enzyme linked immunosorbent assay (ELISA) commonly referred as PSA test, Digital rectal examination (DRE) and biopsy.[2] These current methods falls behind in terms of sensitivity, specificity and inability to distinguish between aggressive and non-aggressive forms of cancer. These imprecise assessments ask for needless treatment for the patient leading to deteriorated quality of life and mental health.

Biomarkers are any measurable or noticeable factors that can indicate a diseased or recovery state of a person.[3] Biomarkers can also indicate any biological processed or response to a treatment. Measuring single markers as in prostate cancer PSA test can lead to false positives and false negatives. These markers can be of any type like mutated DNA and RNAs, biological processes like cell death and cell proliferation, serum or urine secreted proteins, lipids, small molecules etc.[4,5] Measuring small panels of these biomarkers can hold tremendous potential in early cancer detection and staging of cancer patients for better treatment options.[6] In this current work we used generalized prostate cancer biomarkers as a panel that include prostate specific antigen (PSA), prostate specific membrane antigen (PSMA), platelet factor-4 (PF-4) and interlukin-6 (IL-6).

5.2.2 Electrochemiluminescence

Electrochemiluminescence (ECL) is referred as electrogenerated chemiluminescence that involves generation of light emitting species at electrode surfaces, where they involve series of electron transfer reactions to generate an excited state of the species that emits light as they reach to ground state.[7] In general a specified voltage is applied to electrode surface which initiates series of reaction where oxidation of the ECL luminophores like ruthenium bipyridine ($Ru(bpy)_3^{2+}$) that emits light at 610 nm and this light can be easily captures on a photomultiplier tube (PMT) or a charged couple device (CCD) camera.[8]

STEP 1: $TPrA \rightarrow TPrA^{\bullet+} + e^-$

STEP 2: $TPrA^{\bullet+} \rightarrow TPrA^{\bullet} + H^+$

STEP 3:

$TPrA^{\bullet} + [Ru\text{-}(bpy)_3]^{2+} \rightarrow [Ru\text{-}(bpy)_3]^{+} + Products$

STEP 4:

$[Ru\text{-}(bpy)_3]^{+} + TPrA^{\bullet+} \rightarrow [Ru\text{-}(bpy)_3]^{2+}{}^{*} + Products$

STEP 5:

$[Ru\text{-}(bpy)_3]^{2+}{}^{*} \rightarrow [Ru\text{-}(bpy)_3]^{2+} + h\upsilon\ (610\ nm)$

Scheme 5-1. ECL generation mechanism at 0.95 V vs Ag/AgCl when reacted with tripropylamine that in turn reacts with RuBPY. Direct oxidation of Tripropylamine (TPrA) on the electrode surface to TPrA cation radical which in return forms TPrA radical and H^+. TPrA radical reacts with $[[Ru\text{-}(bpy)_3]^{2+}]$ to generate $[[Ru\text{-}(bpy)_3]^{+}]$. This $[[Ru\text{-}(bpy)_3]^{+}]$ reacts with TPrA cation radical to generative photo excited $[[Ru\text{-}(bpy)_3]^{2+}]^*$ that readily generates ECL light at 610nm.

Usually ECL is generated by reduction of $[Ru\text{-}(bpy)_3]^{2+}$ mediated by oxidation of tripropylamine (TPrA) at electrode surface. $[Ru\text{-}(bpy)_3]^{2+}$ used as a label the measured light intensity from ECL generated at electrode surface is directly proportional to concentration of detecting species in our case it is directly proportional to protein under investigation.[9] From previous investigations in our lab to avoid direct oxidation $[Ru\text{-}(bpy)_3]^{2+}$ in the particles which might show signal from nonspecific binding, an alternative method where a voltage potential of 0.95 V vs SCE was chosen that causes indirect oxidation of $[Ru\text{-}(bpy)_3]^{2+}$ by TprA resulting in ECL,[10] See Scheme 5-1. The intensity of ECL light captured by CCD camera is proportional to concentration of protein being detected.

5.2.3 Reagent Delivery & Automation

Widespread use of diagnostic protein measurements at clinical point-of-care will require simple, cheap, fast, sensitive, automated assay devices.[11] Critical issues in these systems are cost, method complexity, and the need for technically trained operators and frequent maintenance.[12] Immunoassays in general suffer from multiple operations to load samples and add reagents to block non-specific binding, remove interferences, and detect target proteins. Significantly improved automation is needed to translate immunoassays to point-of-care use.[13] A major practical challenge involves integrating components into low cost, fully automated devices for clinical use. In this work we describe an inexpensive automated multiplexed protein immunoarray featuring an onboard microprocessor to control micropumps,[14] and a microfluidic sample/reagent cassette upstream of a microwell ECL immunoarray. Here we integrated electronics, microprocessor platforms, micropumps and microcontrollers with microfluidic

components that can handle sample and immunoassay reagents resulting in automated platforms for protein detection.

5.2.4 3-D Printing

The recent emergence of inexpensive 3D printers offers revolutionary low cost options for designing and constructing biosensor systems.[15] Generally 3D printing involves production of an object from a computer aided design. The production of an object is achieved by layer by layer deposition of material while precisely controlling the position of deposition to achieve shape of the object.[16] With recent advances there are multiple methods of fabrication techniques like fused deposition modeling (FDM)[17], stereo lithography (SLA)[18], laser sintering etc., that are available as desktop printers. Where are multiple varieties of materials are available like regular thermo plastics Acrylonitrile butadiene styrene, polylactic acid for food packing for FDM printers, acrylate flexible polymers and clear polymers in the form of resins for SLA printers.[19] The printing involves three simple steps 1. Designing a CAD file and transform into printable format (splicing format) 2. Uploading instructions to printer and preparing stage for object to print. 3. Post treatment steps to remove the object from the platform, smoothen to remove roughness, remove any supports used for printing. By using this simple approach, prototyping was made easy and scalability was achieved for rapid production of wide variety of prototypes. In this work, we reported FDM printer based 3D-printed, gravity flow microfluidic immunoarray for multiple protein detection.

5.3 Experimental – Automated Reagent Cassette Delivery

Microfluidic device. Figure 5-1 shows the automated microfluidic immunoarray featuring (i) printed-circuit board (PCB)-linked, microprocessor-controlled micropumps, (ii) 6-channel sample/reagent delivery cassette, and (iii) 6-channel microfluidic detection array. A PCB circuit design was constructed to serve 6 micropumps. Micropumps (Mp6, Bartels) featuring piezo-actuated membranes were optimized to 155 ± 1.5 µL min^{-1} by tuning potentiometers for each pump. An Arduino microcontroller was used to switch on and off micropumps according to a preset program to deliver sample and immunoreagents, and to stop flow for incubations.

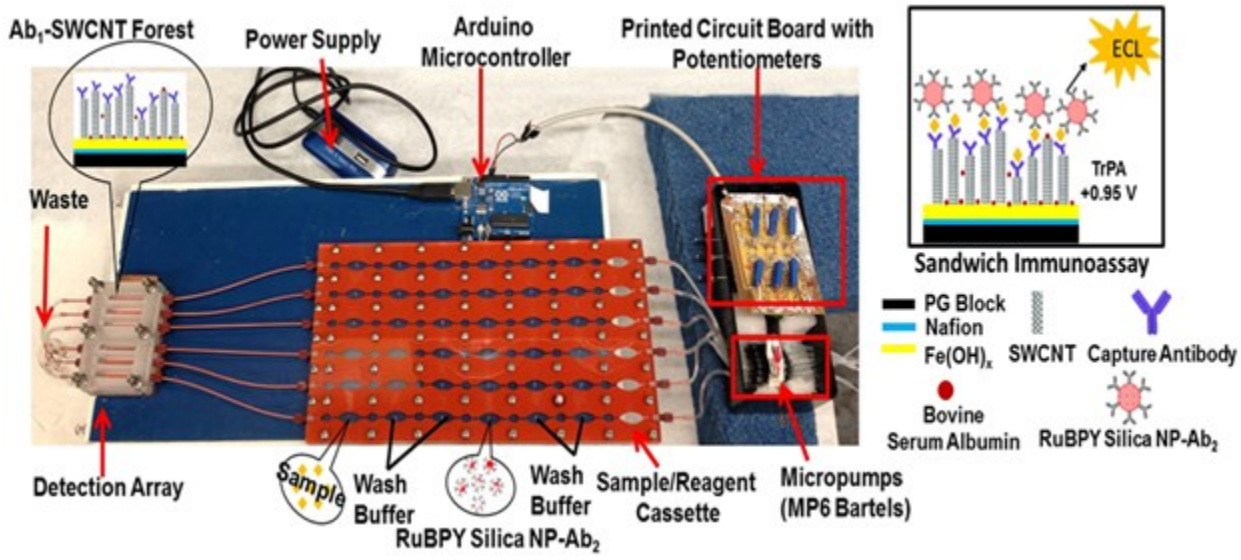

Figure 5-1. Automated microfluidic system featuring 30-microwell detection array connected to sample/reagent cassette and PCB-controlled micropumps. An onboard programmed Arduino microcontroller runs a micropump program to achieve the assay.

Sample/reagent delivery cassette was prepared by cutting silicone gaskets (Figure 5-2A) using a graft cutter and followed by placing between two machined hard PMMA plates (Figure 5-2B&C). All the components were assembled with screws to complete sample/reagent delivery cassette (Figure 5-2D). The final assembled sample/reagent delivery cassette was 11 in x 5.5

inches with six channels, each having 7 loading chambers separated individually by smaller air-filled channels to ensure delivery of reagents without mixing. The detection chamber also features 6 microfluidic channels (60 ± 2 µL) cut from a silicone gasket that is then placed on a thin 2 x 3 in PG wafer with computer-printed microwells (Figure 5-2E) made for patterned 6 channeled silicone gasket from the craft cutter (Figure 5-2F) which the placed on against PMMA plate (Figure 5-2G) with PG chip (Figure 5-2H)at the bottom making a sandwiched detection microfluidic array.

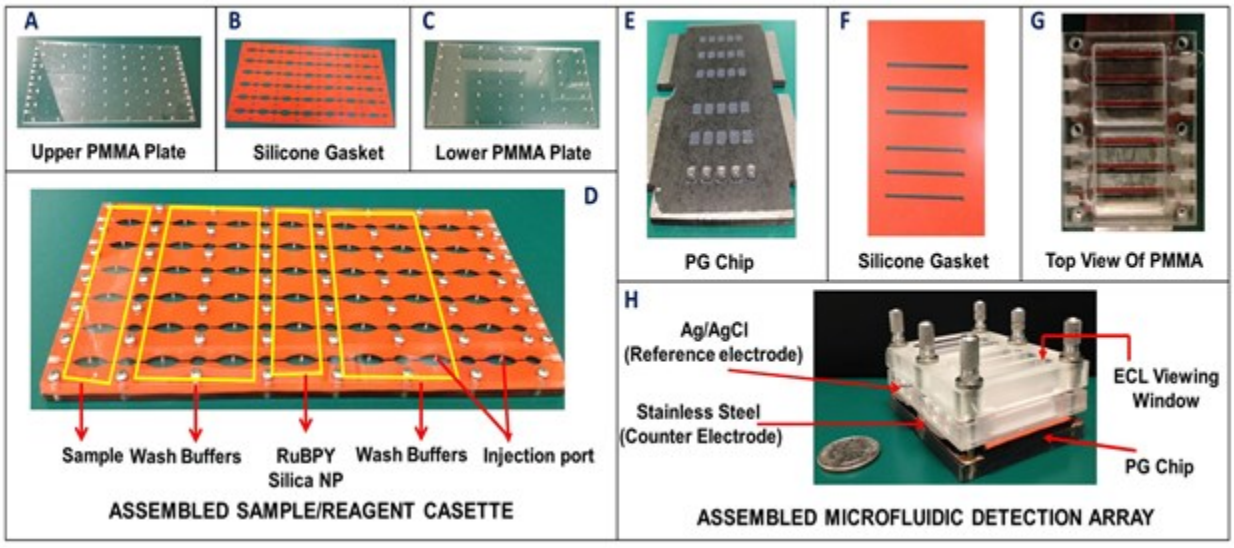

Figure 5-2. Immunoarray components: On left, sample/reagent delivery cassette consisting of (A) 0.8 mm silicon gasket cut to scale using a KNK cutter, (B) Upper hard PMMA plate machined with injection ports, (C) lower PMMA plate and (D) Assembled sample/reagent cassette shown with chambers for solutions, assembled with screws. Right panels show detection array consisting of (E) PG wafer with computer-printed microwells, (F) silicone gasket cut with 6 precision channels, (G) top PMMA plate showing attached stainless steel counter electrode on top with clear windows for ECL detection and Ag/AgCl reference electrode and (H) fully

assembled microfluidic detection array with clear windows in top PMMA plate positioned above microwells in each channel.

Dense SWCNT forests were grown in each microwell (volume 2 ± 0.5 μL)[20], Tapping-mode atomic force microscopy and Raman spectrum confirmed vertical aligned SWCNT forests in the microwells with surface roughness 17 ± 4 nm surrounded by the hydrophobic printed wall. Terminal carboxylic groups on SWCNTs were activated by freshly prepared 400 mM EDC + 100 mM NHSS to attach cognate primary antibodies (Ab_1) by amidization.

Once the sample/reagent cassette is loaded with sample, wash buffers, RuBPY-Si-Ab_2 nanoparticles and TPrA, micropumps turn on initially for 55 s to deliver sample to the detector. Second, flow is stopped for 20 min to allow analyte proteins in the sample to bind onto Ab_1's in microwells. Next, micropumps activate again for 220 s to deliver wash buffer to move sample solution and unbound target proteins out of the detection channels. Then, pumps deliver RuBPY-Si-Ab_2 nanoparticles to the detector, and a 900 s stopped-flow incubation follows. Flow then turns on to wash away unbound RuBPY-silica nanoparticles. Finally, with the detection chamber in a dark box, micropumps deliver TPrA co-reactant to the detection channels, and a potential of 0.95 V vs. Ag/AgCl is applied for 400 s to generate ECL from RuBPY-Si particles, while a CCD camera captures the ECL light.

5.4 Results – Automated Reagent Cassette Delivery

Relative ECL intensities for the immunoarray with controls (undiluted calf serum) showed spot to spot variability of <9 % for n=5 per channel. First and the last channels were used for controls and the inner 4 channels were used for detection of the four target proteins. Array to array reproducibility of background signals was measured by injecting undiluted calf serum into all six

channels giving array to array variability ~11 %. Initially single protein calibrations were developed after optimizing the capture and detection antibody concentrations. Calibration studies were done by dissolving the four target protein standards in calf serum, which serves as a human serum surrogate without human proteins. Channels 1 and 6 in the detection array were used as controls, and only undiluted calf serum was introduced into these channels. Channels 2 to 5 were assigned for detection of IL-6, PF4, PSMA and PSA, respectively. Simultaneous detection was achieved by using a mixture of the 2 RuBPY-Si-Ab_2 detection nanoparticles that were each decorated with antibodies for 2 of the 4 proteins.

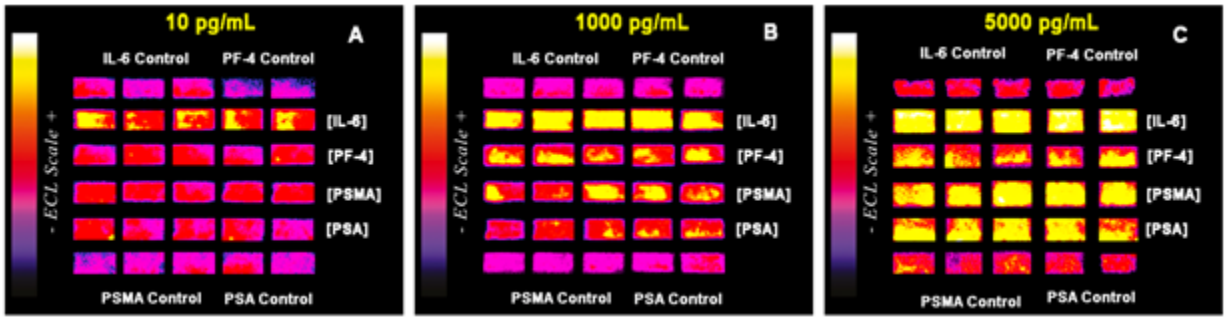

Figure 5-3. Recolourized CCD images of 3 microfluidic immunoarray experiments showing reproducibility in simultaneous detection of IL-6, PF-4, PSMA and PSA in calf with respective controls at protein concentrations: (A) 10 pg mL^{-1} (B) 1000 pg mL^{-1} (C) 5000 pg mL^{-1}.

Increased ECL light with increased concentrations of proteins in the mixture (Figure 5-3). Using the average ECL signal divided by the average blank on each chip, we achieved dynamic ranges for of 100 fg mL^{-1} to 1 ng mL^{-1} for PSA ,100 fg mL^{-1} to 10 ng mL^{-1} for PSMA, and 100 fg mL^{-1} to 5 ng mL^{-1} for IL-6 and PF-4. Nine serum samples from prostate cancer patients and two samples from cancer free patients were analyzed and compared with single protein ELISA (Figure 5-4). The immunoarray values gave good correspondence with ELISA values. Linear

correlation plots of the ELISA vs. immunoarray data gave slopes that were all close to 1.0 and intercepts of these plots were within one standard deviation of zero show excellent correlation confirming high selectivity and specificity of our assay

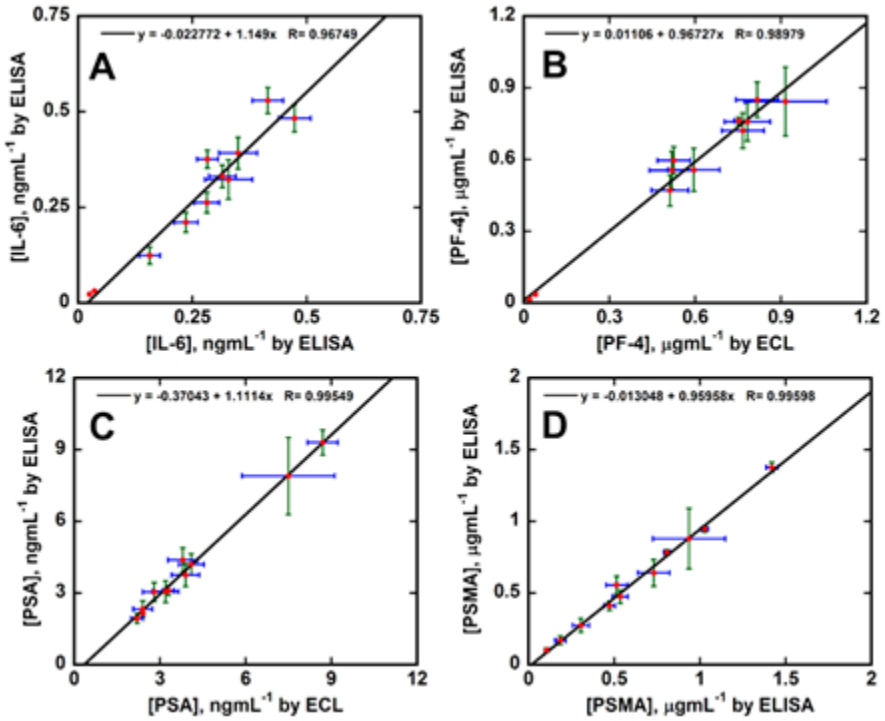

Figure 5-4. Correlation plots of ELISA vs. ECL immunoarray for human serum samples for (A) IL-6, (B) PF-4, (C) PSA, and (D) PSMA.

5.5 Discussion – Automated Reagent Cassette Delivery

The developed automated immunoarray showed need for minimal operator attention for sensitive, simultaneous quantitative measurements of up to 4 proteins. Once the sample/reagent cassette is filled, automated operation and detection takes less than 40 min. Ultrasensitive detection in serum was achieved down to concentrations of 10 fg mL^{-1} over dynamic ranges of 5 orders of magnitude in concentration. Automation of the methodology is under control of the Arduino microcontroller that turns micropumps on and off according to a preset program and

controls the flow of reagents completing immunoassay rapidly. Sample/reagent cassette and detection device made by this approach costs just 15$, whereas micropumps and other electronics cost 450$. All these components are reusable, making the cost per assay very economical. SWCNT forests in detector chip microwells provides a high-area nanostructured along multilabel RuBPY-Si-Ab_2 nanoparticle provides nearly ½ million RuBPY labels resulted in ultrasensitive detection of 4 markers simultaneously. The device is versatile and in principle can be reprogrammed for the detection of virtually any small protein panel.

5.6 Experimental – 3-D Printed Arrays

Commercial desktop 3D Fused Deposition Modeling (FDM) printer, MakerBot Replicator 2X, was used and microfluidic immunoarray was printed from polylactic acid (PLA). The printer instructions we optimized for optimal printing, heated platform was set to 60 ºC and extruder temperature was 230 ºC, with layer height 200 µm. Extruder speed while travelling was optimized at 80 mm s^{-1}, whereas speed while extruding was 40 mm s^{-1}.

Main array printed with 40 mm length x 30 mm width of the base. It has three reagent chambers connected to a common downstream microfluidic channel. The reagent chambers volume is 170 ± 5 µL that can fill 160 µL microfluidic channel downstream. Under hydrostatic pressure the channels were filled with reagents from the reservoirs when in horizontal position. The reservoirs are prefilled with sample or reagents through port holes located in custom fit 3D-printed inserts (Figure. 5-5 A) with rods that seal the outlets of the reservoirs. Flow of sample and reagents is controlled by placing the insert to seal the reservoir, or removing it to drain the reservoir into the detection channel in a horizontal position. All reagents are prefilled on the array, and the operator needs only to release reagents sequentially by removing the inserts.

Figure. 5-5 B shows the add-on wash reservoir designed to work with a lever-assisted moving platform device that accommodates the sensor array, wash reservoirs and a waste collector at the bottom. The wash reservoir was designed to align with reagent reservoirs of the main array and is 68 mm length x 44 mm width x 26 mm height with capacity of ~1.6 mL buffer. Wash buffer in these reservoirs is used to wash off excess sample/reagent from the main array microfluidic channels after the immunoassay. Wash reservoirs employ custom fit inserts to turn flow on and off similar to the reagent chambers. Normal load position has the detection channel with the sensors horizontal. Changing the lever on the wash reservoir to wash position provides a 25º tilt angle to the sensor array (Figure. 5-5 B), which enables washing of the immunoreagents to a waste chamber at the bottom of the detection channel.

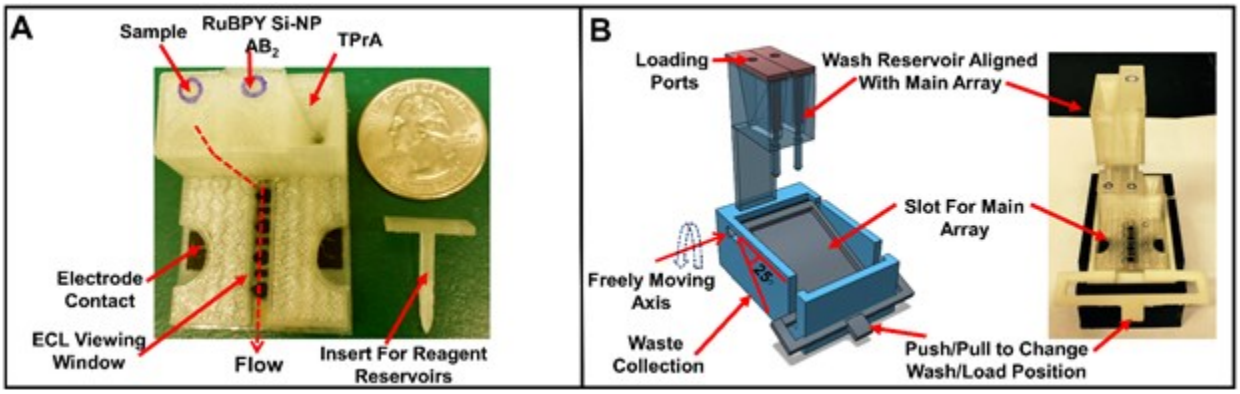

Figure 5-5. 3D-printed main array and wash reservoir module. (A) Basic array showing three reagent reservoirs equipped with inserts along with flow path for reagents to reach microfluidic channel. (B) Wash reservoir module (5-5B Left) 3D model showing freely moving lever to change between wash and load position along with wash reservoirs aligned with main array, (5-5 B Right) assembled immunoarray setup with both main array and wash module.

Supercapacitors (Cellergy, 2.1 V, 80 mF) used to power ECL arrays were low equivalent series resistance (ESR) aqueous state electrolyte, high output electrochemical double layer capacitors (EDLC's). A solar panel (Sparkfun, 0.45 W, 94 mA) was used to charge the supercapacitor to 1.5 V under ambient room, sun, or iPhone light. Voltage was checked with a digital multimeter prior to every experiment to ensure accuracy. ECL was generated by electrochemical oxidation of both tripropylamine (TPrA) and RuBPY on the sensors when 1.5 V was applied.

Assay Procedure: Delivery of sample/reagents from prefilled reservoirs of the main array is accomplished by removing the insert top. The reagents flow downstream to fill the detection channel. Prefilled wash buffers from wash reservoirs flush the detection channel when the wash module lever is adjusted to 25º tilt angle. Individual assay steps are: (1) Release sample from its reservoir to fill the detection channel and incubate for 20 min (Figure. 5-6 A) in horizontal load position (Figure. 5-6 B). This allows analyte proteins to be captured on Ab_1-coated sensors. (2) Move platform to wash position (25º tilt) by pushing the lever down, then release wash buffer from its reservoir (Figure. 5-6 C). Buffer from the larger wash reservoir passes through the sample reservoir into the detection channel and flushes unbound protein to waste (Figure. 5-6 D). (3) The platform lever is then returned to the load position, followed by release of Ab_2-RuBPY-SiNPs into the horizontal detection chamber, and incubation for 15 min is allowed to bind to previously captured proteins. (4) Wash unbound silica nanoparticles to waste by placing the lever in wash position. (5) TPrA solution is released from its reservoir into the horizontal detection channel, the array is placed under the CCD camera in a dark box and potential of 1.5 V vs. Ag/AgCl is applied with the supercapacitor to generate ECL for 60 s. Acquired ECL images are then processed by software to estimate light intensities from each microwell on the array.

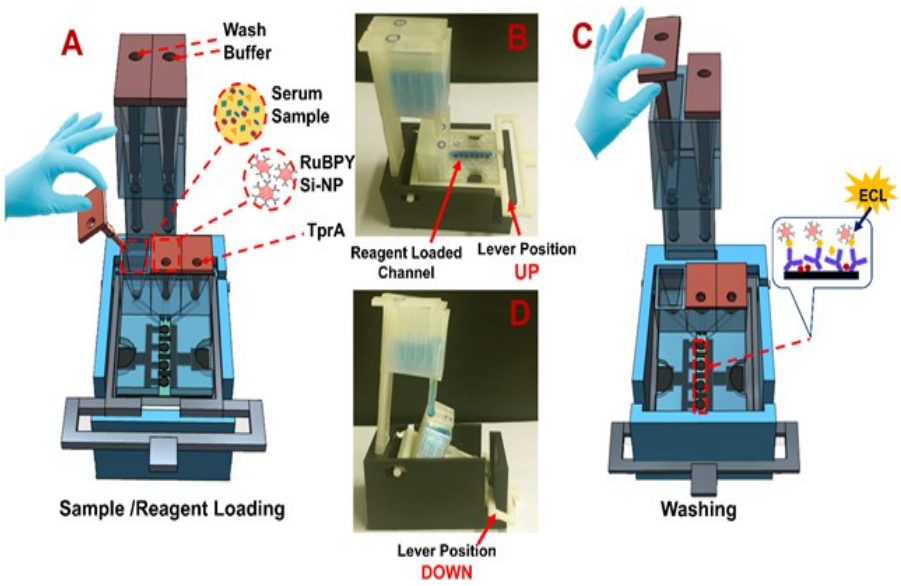

Figure 5-6. Details of the assay procedure: (A) Cartoon showing removal of insert for sample delivery from reservoir by gravity flow. (B) Load position shown with blue food color solution filling the horizontal detection channel with lever up. (C) Cartoon showing buffer delivery from wash reservoir to detection channel for washing away unbound proteins (inset shows sandwich immunoassay on sensors). (D) Wash position showing blue food color solution delivered from wash reservoir to main array when lever is down for 25º tilt of detection channel.

5.6 Results – 3-D Printed Arrays

Reproducibility of array sensors was evaluated at 0 and 500 pg mL^{-1} for the 3 protein analytes. Variation in relative ECL intensities was ≤ 7 % (n=3) array-to-array and ≤10 % spot-to-spot (n=9). Out of four sensors on the array, sensors 1, 3 and 4 were used for specific protein detection. Sensor 2 at the center was used to measure background for each array, and was coated with 1 % casein only. Calibrations were done for all 3 proteins individually in calf serum, with relative standard deviations ≤ 13 %. supercapacitor mounted on a printed circuit board (PCB), connected to the array inside a dark box to generate ECL showed increase in ECL response with increase in concentration of proteins (Figure 5-7 A). Multiplexed calibration curves were

obtained by assigning sensor 1 to detect PSA (Figure. 5-7 B), 2 to background, 3 to PSMA (Figure. 5-7C) and 4 to PF-4 (Figure. 5-7 D).

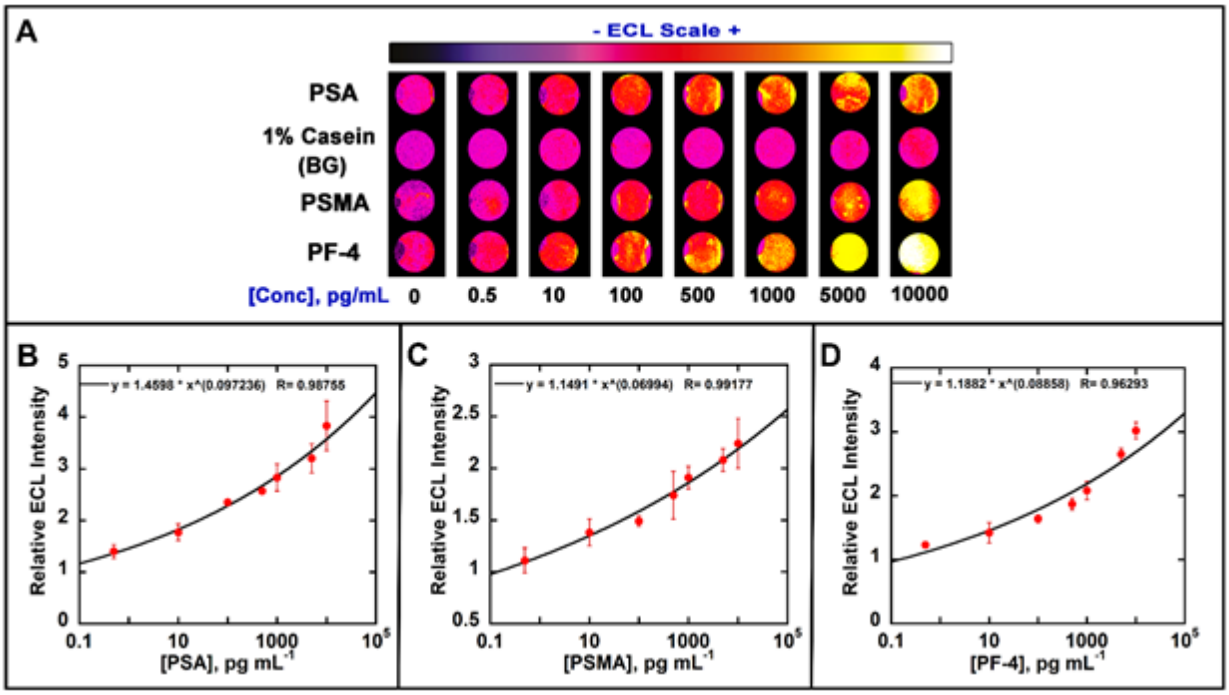

Figure 5-7. Calibration data in undiluted calf serum showing influence of biomarker protein concentration on ECL response: (A) Recolorized ECL images of 8 arrays with showing increase in ECL intensity with increased concentration. ECL signals digitized for (B) PSA, (C) PSMA and (D) PF-4 in calf serum. Error bars show standard deviation for n = 4.

Dynamic ranges were from 500 fg mL^{-1} to 10 ng mL^{-1} for all protiens and detection limits as 3 times the standard deviations of zero protien controls were 300 fg mL^{-1} for PSA, 535 fg mL^{-1} for PSMA and 420 fg mL^{-1} for PF-4. Assay validation was done using 4 prostate cancer patient serum samples and 2 cancer free human samples using the calibration curves. Linear correlation plots obtained for ELISA vs. ECL immunoarray data had slopes close to 1.0 & intercepts of these plots were close to zero consistent with good correlation (Figure 5-8).

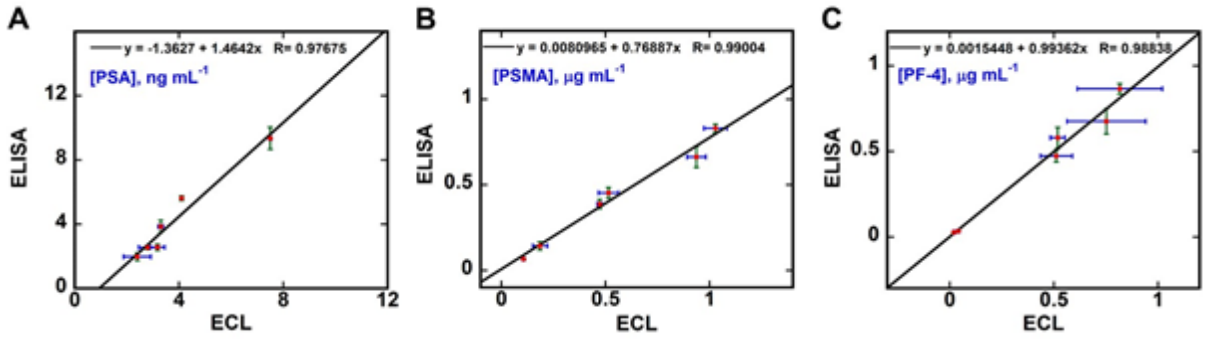

Figure 5-8. Linear correlation plots of ECL vs. ELISA validation studies for (A) PSA, (B) PSMA and (C) PF-4.

5.7 Discussion – 3-D Printed Arrays

Developed inexpensive, portable, 3D-printed ECL immunoarray capable of measuring three proteins simultaneously. The cost per assay is ~€0.50 when the arrays are re-used with the replaceable sensor chip. The platform utilizes simple steps to complete the immunoassay in 35 min without external equipment except a CCD camera. Excellent correlation between ELISA and the ECL arrays along with relatively small array-to-array standard deviations indicates potential for future clinical applications. Considering all costs for immunoreagents, a single immunoassay costs ~$1.20, considering the entire platform ($0.90) to be disposable, or ~$0.50 if the wash module is reused. Solar panels allowed rapid light-driven charging to 1.5 V of the supercapacitor power source to drive the ECL generation step. Integration of this small power source on the immunoarray helps make it portable, avoids potentiostatic equipment, and makes the assay simpler for the operator.

5-8. References

1. http://www.cancer.org/cancer/prostatecancer/detailedguide/prostate-cancer-key-statistics

2. Catalona, W. J.; Smith, D. S.; Wolfert, R. L.; Wang, T. J.; Rittenhouse, H. G.; Ratliff, T. L.; Nadler, R. B. Evaluation of percentage of free serum prostate-specific antigen to improve specificity of prostate cancer screening. *JAMA* **1995**, *274*, 1214-1220.

3. Kulasingam, V.; Diamandis, E. P. Strategies for discovering novel cancer biomarkers through utilization of emerging technologies. *Nature clinical practice Oncology* **2008**, *5*, 588-599.

4. Hanash, S. M.; Pitteri, S. J.; Faca, V. M. Mining the plasma proteome for cancer biomarkers. *Nature* **2008**, *452*, 571-579.

5. Hawkridge, A. M.; Muddiman, D. C. Mass spectrometry-based biomarker discovery: toward a global proteome index of individuality. *Annu. Rev. Anal. Chem. (Palo Alto Calif)* **2009**, *2*, 265-277.

6. Rusling, J. F.; Kumar, C. V.; Gutkind, J. S.; Patel, V. Measurement of biomarker proteins for point-of-care early detection and monitoring of cancer. *Analyst* **2010**, *135*, 2496-2511.

7. Richter, M. M. Electrochemiluminescence (ecl). *Chem. Rev.* **2004**, *104*, 3003-3036.

8. Zanarini, S.; Rampazzo, E.; Ciana, L. D.; Marcaccio, M.; Marzocchi, E.; Montalti, M.; Paolucci, F.; Prodi, L. Ru (bpy) 3 covalently doped silica nanoparticles as multicenter tunable structures for electrochemiluminescence amplification. *J. Am. Chem. Soc.* **2009**, *131*, 2260-2267.

9. Miao, W.; Choi, J.; Bard, A. J. Electrogenerated Chemiluminescence 69: The Tris (2, 2'-bipyridine) ruthenium (II),(Ru (bpy) 32)/Tri-n-propylamine (TPrA) System Revisited A New Route Involving TPrA Cation Radicals. *J. Am. Chem. Soc.* **2002**, *124*, 14478-14485.

10. Sardesai, N.; Pan, S.; Rusling, J. Electrochemiluminescent immunosensor for detection of protein cancer biomarkers using carbon nanotube forests and [Ru-(bpy) 3] 2 -doped silica nanoparticles. *Chemical Communications* **2009**, 4968-4970.

11. Giljohann, D. A.; Mirkin, C. A. Drivers of biodiagnostic development. *Nature* **2009**, *462*, 461-464.

12. Rusling, J. F. Multiplexed electrochemical protein detection and translation to personalized cancer diagnostics. *Anal. Chem.* **2013**, *85*, 5304-5310.

13. Chin, C. D.; Linder, V.; Sia, S. K. Commercialization of microfluidic point-of-care diagnostic devices. *Lab on a Chip* **2012**, *12*, 2118-2134.

14. http://arduino.cc

15. Gross, B. C.; Erkal, J. L.; Lockwood, S. Y.; Chen, C.; Spence, D. M. Evaluation of 3D printing and its potential impact on biotechnology and the chemical sciences. *Anal. Chem.* **2014**, *86*, 3240-3253.

16. Bishop, G. W.; Satterwhite-Warden, J. E.; Kadimisetty, K.; Rusling, J. F. 3D-printed bioanalytical devices. *Nanotechnology* **2016**, *27*, 284002.

17. Zein, I.; Hutmacher, D. W.; Tan, K. C.; Teoh, S. H. Fused deposition modeling of novel scaffold architectures for tissue engineering applications. *Biomaterials* **2002**, *23*, 1169-1185.

18. Hockaday, L.; Kang, K.; Colangelo, N.; Cheung, P.; Duan, B.; Malone, E.; Wu, J.; Girardi, L.; Bonassar, L.; Lipson, H. Rapid 3D printing of anatomically accurate and mechanically heterogeneous aortic valve hydrogel scaffolds. *Biofabrication* **2012**, *4*, 035005.

19. O'Neill, P.; Azouz, A. B.; Vazquez, M.; Liu, J.; Marczak, S.; Slouka, Z.; Chang, H. C.; Diamond, D.; Brabazon, D. Advances in three-dimensional rapid prototyping of microfluidic devices for biological applications. *Biomicrofluidics* **2014**, *8*, 052112.

20. Yu, X.; Munge, B.; Patel, V.; Jensen, G.; Bhirde, A.; Gong, J. D.; Kim, S. N.; Gillespie, J.; Gutkind, J. S.; Papadimitrakopoulos, F. Carbon nanotube amplification strategies for highly sensitive immunodetection of cancer biomarkers. *J. Am. Chem. Soc.* **2006**, *128*, 11199-11205.